DMD Fast Forward. Published on May 16, 2018 as DOI: 10.1124/dmd.118.081547
This article has not been copyedited and formatted. The final version may differ from this version.

DMD # #81547

PBDEs Altered Gut Microbiome and Bile Acid Homeostasis in Male C57BL/6 Mice

Cindy Yanfei Li, Joseph L. Dempsey, Dongfang Wang, Soowan Lee, Kris M. Weigel, Qiang Fei, Deepak Kumar Bhatt, Bhagwat Prasad, Daniel Raftery, Haiwei Gu, and Julia Yue Cui

Department of Environmental and Occupational Health Sciences, University of Washington, Seattle, WA 98105, USA (CYF, JLD, KMW, SL, and JYC); Northwest Metabolomics Research Center, Department of Anesthesiology and Pain Medicine, University of Washington, 850 Republican St., Seattle, WA 98109, USA (DW, QF, and DR); Arizona Metabolomics Laboratory, Center for Metabolic and Vascular Biology, School of Nutrition and Health Promotion, College of Health Solutions, Arizona State University, Phoenix, AZ 85004, USA (HG); Department of Pharmaceutics, University of Washington, Seattle, WA 98105, USA (DKB, BP); Department of Laboratorial Science and Technology, School of Public Health, Peking University, Beijing 100191, P. R. China (DF); Department of Chemistry, Jilin University, Changchun, Jilin Province 130061, P. R. China (QF).

DMD Fast Forward. Published on May 16, 2018 as DOI: 10.1124/dmd.118.081547
This article has not been copyedited and formatted. The final version may differ from this version.

DMD # #81547

Running title: Effect of PBDEs on gut microbiome and bile acid homeostasis

Address correspondence to:

Julia Yue Cui, PhD

Department of Environmental and Occupational Health Sciences, University of Washington

Email: juliacui@uw.edu

AND:

Haiwei Gu, PhD

Arizona Metabolomics Laboratory, Center for Metabolic and Vascular Biology, School of Nutrition and Health Promotion, College of Health Solutions, Arizona State University

Email: haiweigu@asu.edu

Number of Text Page:	46
Number of Tables:	0
Number of Figures:	10
Number of References:	64
Number of Words in Abstract:	256
Number of Words in Introduction:	667
Number of Words in Discussion:	2600

Abbreviations

ACN, acetonitrile; aldo-keto reductase, Akr1c14; Baat, bile acid CoA:amino acid N-acyltransferase; bai, BA-inducible operons; Bal, bile acid-CoA ligase; BAs, bile acids; BDE-47, 2, 2', 4, 4'-tetrabromodiphenyl ether; BDE-99, 2, 2', 4, 4', 5-pentabromodiphenyl ether; BSA, bovine serum albumin; Bsep, bile salt export pump; bsh, bile salt hydrolase; CA-D4, cholic acid-2,2,4,4-D4; CAR, constitutive androstane receptor; CV, conventional; CV CO, corn oil-exposed

CV; Cyp, cytochrome P450; DCA-D4, deoxycholic acid-2,2,4,4-D4; ddCq, delta-delta cycle value of the quantitative PCR; DTT, dithiothreitol; GCA-D4, glycocholic acid-2,2,4,4-D4; GCDCA-D4, glycochenodeoxycholic acid-2,2,4,4-D4; GF, germ-free; GF CO, corn oil-exposed GF; IS, internal standard; LCA-D4, lithocholic acid-2,2,4,4-D4; LC-MS/MS, LiquidChromatography-Tandem Mass Spectrometry; LIC, large intestinal content; LOD, limit of detection; MRM, multiple-reaction-monitoring; Ntcp, sodium taurocholate cotransporting polypeptide; Oatp, organic anion transporting polypeptide; OTU, Operational Taxonomy Unit; PBDEs, polybrominated diphenyl ethers; PCoA, principle coordinates analysis; PICRUSt, Phylogenetic Investigation of Communities by Reconstruction of Unobserved States; PTS, phosphotransferase system; PXR, pregnane X receptor; qPCR, quantitative polymerase chain reaction; Quantitative Insights Into Microbial Ecology, QIIME; RSD, relative standard deviation; SE, standard error; SIC, small intestinal content; T-αMCA, tauro-α muricholic acid; UGTs, uridine 5'-diphospho-glucuronosyltransferases

DMD Fast Forward. Published on May 16, 2018 as DOI: 10.1124/dmd.118.081547
This article has not been copyedited and formatted. The final version may differ from this version.

ABSTRACT

Polybrominated diphenyl ethers (PBDEs) are persistent environmental contaminants with well-characterized toxicities in host organs. Gut microbiome is increasingly recognized as an important regulator of xenobiotic biotransformation; however, little is known about its interactions with PBDEs. Primary bile acids (BAs) are metabolized by the gut microbiome into more lipophilic secondary BAs that may be absorbed and interact with certain host receptors. The goal of this study was to test our hypothesis that PBDEs cause dysbiosis and aberrant regulation of BA homeostasis. Nine-week-old male C57BL/6 conventional (CV) and germ-free (GF) mice were orally gavaged with corn oil (10 mg/kg), BDE-47 (100 μmol/kg), or BDE-99 (100 μmol/kg) once daily for 4-days (n=3-5/group). Gut microbiome was characterized using 16S rRNA sequencing of the large intestinal content in CV mice. Both BDE-47 and BDE-99 profoundly decreased the alpha diversity of gut microbiome and differentially regulated 45 bacterial species. Both PBDE congeners increased *Akkermansia muciniphila* and *Erysipelotrichacea Allobaculum spp.*, which have been reported to have anti-inflammatory and anti-obesity functions. Targeted metabolomics of 56 BAs was conducted in serum, liver, and small and large intestinal content of CV and GF mice. BDE-99 increased many unconjugated BAs in multiple bio-compartments in a gut microbiota-dependent manner. This correlated with an increase in microbial 7α-dehydroxylation enzymes for secondary BA synthesis and increased expression of host intestinal transporters for BA absorption. Targeted proteomics showed that PBDEs down-regulated host BA-synthesizing enzymes and transporters in livers of CV but not GF mice. In conclusion, there is a novel interaction between PBDEs and the endogenous BA-signaling through modifying the “gut-liver axis”.

DMD Fast Forward. Published on May 16, 2018 as DOI: 10.1124/dmd.118.081547
This article has not been copyedited and formatted. The final version may differ from this version.

INTRODUCTION

PBDEs are flame retardants that are commonly used in a variety of consumer products, such as plastics, rubbers, textiles, furniture, and electronic devices. Health concerns from PBDE exposures have increased significantly in recent years as their presence has been detected in environmental samples and in human tissues (Frederiksen et al., 2009). PBDEs have been shown to cause developmental neurotoxicity, reproductive toxicity, thyroid hormone disruption, liver toxicity, and potential cancer development in rodent studies (Gascon et al., 2011; Linares et al., 2015). Among the 209 PBDE congeners, 2, 2', 4, 4'-tetrabromodiphenyl ether (BDE-47) and 2, 2', 4, 4', 5-pentabromodiphenyl ether (BDE-99) are the most predominant congeners detected in the environment and in human samples (Erratico et al., 2011). BDE-47 and BDE-99 activate the major xenobiotic-sensing nuclear receptors pregnane X receptor (PXR/Nr1i2) and constitutive androstane receptor (CAR/Nr1i3) in both rodents and human hepatocytes, leading to induced expression of cytochrome P450s (Cyps), which may cause adverse drug reactions or drug-drug reactions (Pacyniak et al., 2007; Sueyoshi et al., 2014). Using RNA-Seq, we recently demonstrated that BDE-47 and BDE-99 differentially regulated many other phase-I drug-metabolizing enzymes (i.e. enzymes involved in oxidation, reduction, and hydrolysis), phase-II enzymes (i.e. enzymes involved in conjugation) as well as transporters in mouse liver. We also demonstrated that the lack of gut microbiota in GF mice altered the oxidative metabolites of BDE-47 and BDE-99, and profoundly modified the PBDE-mediated transcriptomic responses in liver (Li et al., 2017). This provided the first evidence that there is a novel interaction between gut microbiota and PBDEs that influence the host hepatic xenobiotic biotransformation. However, very little is known regarding the interactions between PBDEs and gut microbiota on intermediary metabolism.

Gut microbiome communicates with the host liver to modify hepatic xenobiotic biotransformation and nutrient homeostasis (Shreiner et al., 2015; Fu and Cui, 2017). Disruptions in the

DMD Fast Forward. Published on May 16, 2018 as DOI: 10.1124/dmd.118.081547
This article has not been copyedited and formatted. The final version may differ from this version.

composition of gut microbial communities and altered microbiota-host interactions have been linked to several diseases, such as cancer and metabolic disorders (Jumpertz et al., 2011). Bile acids (BAs), which are a group of steroids produced in liver from cholesterol, are important signaling molecules for intermediary metabolism within the gut-liver axis and in extrahepatic organs, such as brown adipose tissue and muscle (Broeders et al., 2015). The primary BAs are secreted across the canalicular membrane of hepatocytes via the bile salt export pump (Bsep) into bile for release into the lumen of the duodenum. In intestine, gut microbiota converts primary BAs to secondary BAs via dehydroxylation, deconjugation, and epimerization. The intestinal microbiota contains enzymes that metabolize BAs such as bile salt hydrolases (Bsh), which removes glycine or taurine from conjugated BAs. The bacteria *Clostridia* contain hydroxysteroid dehydrogenases and 7-dehydratases that produce BA intermediates and secondary BAs (Ridlon et al., 2006). Ninety-five percent of BAs undergo reabsorption from the intestinal lumen via active transport and recirculates to liver by the portal blood (Chiang, 2003). Upon reaching the liver, BAs are taken up across the sinusoidal membrane of hepatocytes via sodium taurocholate cotransporting polypeptide (*Ntcp/Slc10a1*) and organic anion transporting polypeptide 1b2 (*Oatp1b2/Slco1b2*) transporters (Russell, 2003; Klaassen and Cui, 2015). Accumulation of BAs in hepatocytes or the biliary tract may lead to oxidative stress, inflammation, and cholestatic liver injury (Perez and Briz, 2009).

Clinically, many therapeutic drugs have been shown to produce cholestatic liver injury by elevating hepatic BA levels (Padda et al., 2011). In laboratory animals, activation of the xenobiotic sensor CAR by phenobarbital decreased BAs in mouse liver, but increased fecal excretion of muricholic acids (Sberna et al., 2011; Lickteig et al., 2016). Lack of gut microbiota in GF mice resulted in higher BA concentrations in serum, liver, bile, and ileum than that in conventional (CV) mice with a microbiome (Selwyn et al., 2015b). To investigate to what extent PBDEs modulate host BA homeostasis and the potential involvement of the “gut-liver axis,” the

DMD Fast Forward. Published on May 16, 2018 as DOI: 10.1124/dmd.118.081547
This article has not been copyedited and formatted. The final version may differ from this version.

present study utilized a multi-omics approach, to test our working hypothesis that the gut microbiome serves as a critical interface in modulating the crosstalk between PBDEs and BA synthesis and metabolism pathways (Figure 1).

MATERIALS AND METHODS

Chemicals

BDE-47 was purchased from Chem Service, Inc. (Part #: N-10522-10MG, CAS: 5436-43-1, West Chester, PA) (PubChem CID: 95170; link to chemical structure: https://pubchem.ncbi.nlm.nih.gov/compound/95170#section=Top), and BDE-99 (PubChem CID: 36159; link to chemical structure: https://pubchem.ncbi.nlm.nih.gov/compound/36159) was purchased from AccuStandard, Inc. (Catalog #: FF-BDE-099N-80MG, New Haven, CT). Phosphate-buffered saline (PBS, 10x, pH 7.4, PubChem CID: 24978514), LC-MS grade methanol, water, and acetonitrile were purchased from Thermo Fisher Scientific (Grand Island, NY). Bile acid standards and deuterated internal standards (IS) lithocholic acid-2,2,4,4-D4 (LCA-D4) (PubChem CID of LCA: 9903), deoxycholic acid-2,2,4,4-D4 (DCA-D4) (PubChem CID of DCA: 222528), cholic acid-2,2,4,4-D4 (CA-D4) (PubChem CID of CA: 221493), glycochenodeoxycholic acid-2,2,4,4-D4 (GCDCA-D4) (PubChem CID of GCDCA: 12544), and glycocholic acid-2,2,4,4-D4 (GCA-D4) (PubChem CID of GCA: 10140) were purchased from Steraloids, Inc. (Newport, RI). All other chemicals and reagents, unless indicated otherwise, were purchased from Sigma-Aldrich (St. Louis, MO).

Animals and Procedures

Eight-week-old male C57BL/6 CV mice were purchased from The Jackson Laboratory (Bar Harbor, ME) and were acclimated to the animal facility at University of Washington for one week prior to experiments. The initial breeding colony of GF mice in the C57BL/6 background was established with mice purchased from the National Gnotobiotic Rodent Resource Center

DMD Fast Forward. Published on May 16, 2018 as DOI: 10.1124/dmd.118.081547
This article has not been copyedited and formatted. The final version may differ from this version.

(University of North Carolina, Chapel Hill). All mice were housed according to the Association for Assessment and Accreditation of Laboratory Animal Care International guidelines, and the animal studies were approved by the Institutional Animal Care and Use Committee at the University of Washington. The CV and GF mice were exposed to the same diet (laboratory autoclaved rodent diet #5010, LabDiet, St. Louis, MO), water (non-acidified autoclaved water), and bedding (autoclaved Enrich-N'Pure). All chemical solutions were sterilized using the Steriflip Vacuum-driven Filtration System with a 0.22 μM Millipore Express Plus Membrane (EMD Millipore, Temecula, CA). All gavage needles and syringes were sterilized by autoclave. As described in Figure 1, at 9 weeks of age, male CV and GF mice were randomly allocated for the exposure of vehicle (corn oil, 10 ml/kg), BDE-47 (100 μmol/kg), or BDE-99 (100 μmol/kg) via oral gavage once daily for 4 consecutive days between 8:00 am and noon (n = 3~5 per group). On the 5th day (24 hours after the final dose), various tissues were collected. Blood was collected via cardiac puncture and centrifuged at 1500*g* for 10 min at 4 °C to obtain serum. Livers were removed and immediately frozen in liquid nitrogen. Small and large intestinal contents (SIC and LIC) were flushed using PBS containing 10 mM dithiothreitol (DTT) (Sigma Aldrich, St. Louis, MO) and centrifuged at 20,000*g* for 30 min at 4 °C to isolate the solid intestinal content pellet. The intestinal tissues were separated into duodenum, jejunum, ileum, and large intestine (colon and cecum). All samples were stored at -80 °C until further analysis.

Quantification of Bacterial DNA and 16S rRNA Gene Sequencing

Total DNA was extracted from the LIC of CV mice using OMEGA E.Z.N.A. DNA Stool Kit (Omega Bio-tek, Inc., Norcross, GA) according to the manufacturer's instructions. The concentration of DNA was determined using a Qubit 2.0 Fluorometer (Life Technologies, Grand Island, NY), and the integrity and quality of DNA samples were confirmed using an Agilent 2100 Bioanalyzer (Agilent Technologies Inc., Santa Clara, CA). The V4 region of 16S rRNA gene

was amplified and sequenced using a HiSeq 2500 platform (250bp paired-end) (Beijing Genome Institute Americans Corporation, Cambridge, MA) (n=3 per group). The paired-end sequence reads were merged, de-multiplexed, and chimera-filtered using QIIME version 1.9.1 (Quantitative Insights Into Microbial Ecology) (Caporaso et al., 2010). Operational Taxonomy Unit (OTU) clustering and taxonomy classification were performed using open-reference operational taxonomic unit picking method (UCLUST version 1. 2. 22q) against the 99% representative databases for Greengenes (version 13.8) (DeSantis et al., 2006; Wang et al., 2007; Edgar, 2010). Functional profiles of microbial communities were predicted using PICRUSt (Phylogenetic Investigation of Communities by Reconstruction of Unobserved States) (Langille et al., 2013). Differentially enriched pathways were plotted as two-way hierarchical clustering dendrograms using JMP Genomics (SAS Institute, Inc., Cary, NC). Selected differentially regulated bacteria were validated by quantitative polymerase chain reaction (qPCR) using Bio-Rad CFX384 Real-Time PCR Detection System (Hercules, CA). The 16S rRNA primers for the detection of *Akkermansia muciniphila*, *Erysipelotrichaceae Allobaculum spp.*, and *Clostridium scindens* were designed based on the 16S rRNA sequences of these bacteria (Supplemental Table 1). The primers recognizing the universal bacterial 16S rRNA sequences were provided by the University of North Carolina Gnotobiotic core facilities (Supplemental Table 1) (Packey et al., 2013). All primers were synthesized by Integrated DNA Technologies (Coralville, IA). The abundances of the genomic DNA were expressed as mean delta-delta cycle value of the quantitative PCR (ddCq) as compared to the universal bacteria.

Targeted Metabolomics of Bile Acids using Liquid Chromatography-Tandem Mass Spectrometry

A standard stock solution of each individual BA and deuterated IS were prepared at a concentration of 2 mg/ml in methanol. IS (10 μM of LCA-D4, DCA-D4, CA-D4, GCDCA-D4, and GCA-D4) were added to the samples, and BAs were extracted from the serum, liver, SIC, and

DMD Fast Forward. Published on May 16, 2018 as DOI: 10.1124/dmd.118.081547
This article has not been copyedited and formatted. The final version may differ from this version.

LIC using methods reported previously (Zhang and Klaassen, 2010). Fifty-six BAs were quantified using liquid chromatography-tandem mass spectrometry (LC-MS/MS) as listed in Supplemental Table 2. Among them, tauro-α muricholic acid (T-αMCA) and T-βMCA were summed together and expressed as T-α/βMCA. The concentrations of individual BAs were analyzed relative to their corresponding internal standards.

For serum BA extraction, 50 µl serum samples were spiked with 25 µl of the mixed internal standard solution. The samples were vortexed and put on ice for 5 min. Cold methanol (500 µl) was added for protein precipitation, and samples were vortexed 3 x 10s and maintained on ice for 10 min. After centrifugation at 12,000*g* for 10 min at 4 °C, supernatants were transferred to clean tubes. The residues were reconstituted in 500 µl methanol, vortexed for 10 min, and centrifuged at 12,000*g* for 10 min at 4 °C. The two extraction supernatants were pooled and dried under vacuum. The residue was then reconstituted by adding 100 µl methanol solution (methanol: water = 50:50, v/v), and centrifuged at 20,000 *g* for 10 min at 4 °C. The supernatants were transferred to individual glass vials for MS analysis.

For liver BA extraction, approximately 60 mg frozen liver were accurately weighed and homogenized in 5 volumes of water (300 µl for 60 mg). For each 300 µl homogenate (50 mg of liver in 250 ul of water), 1.5 ml of acetonitrile (ACN) with 5% ammonia hydroxide (NH_4OH) and 25 µl of IS solution was added. Tubes were vortexed and shaken for 1 h at room temperature. The mixtures were centrifuged at 12,000*g* for 15 min at 4 °C, and supernatants were transferred to clean tubes. A second BA extraction was performed with 750 µl methanol, shaking for 20 min, sonicating for 5~10 min, and centrifuging at 15,000*g* for 20 min. Finally, the two extraction supernatants were pooled and dried under vacuum. The residue was then reconstituted by adding 100 µl 50% MeOH, vortexed, transferred onto the 0.22 µm Costar Spin-X centrifuge tube filter (Sigma-Aldrich, St. Louis, MO), and centrifuged at 20,000 *g* for 10 min before injection.

DMD Fast Forward. Published on May 16, 2018 as DOI: 10.1124/dmd.118.081547
This article has not been copyedited and formatted. The final version may differ from this version.

For BA extraction from SIC and LIC, approximately 60 mg frozen pellets that were isolated by centrifuging the flushed intestinal contests at 20,000 *g* for 30 minutes at 4°C were accurately weighed and homogenized in 5 volumes of water (300 µl). For each 280 µl homogenate (46.667 mg of liver in 233.333 ul of water), 1.5 ml ACN with 5% NH_4OH and 20 µl IS were added. The remaining procedures were same as the liver BA extraction.

For BAs measurements, 2 µL of each prepared sample was injected into a LC-MS/MS system (Waters Acquity I-Class UPLC TQS-micro MS, Waters, Milford, MA) for analysis using negative ionization mode. The LC-MS/MS system was equipped with an electrospray ionization source. Chromatographic separation was achieved on a Waters XSelect HSS T3 column (2.5 µm, 2.1 × 150 mm). The mobile phase A was 5 mM ammonium acetate in H_2O with 0.1% acetic acid, and the mobile phase B was acetonitrile with 0.1% acetic acid. After 1 min of isocratic elution of 75% of solvent A, the mobile phase composition changed to 5% A at t=15 min. It was then maintained at 5% A for 10 min, followed by a rapid increase at t=25 min to 75% A to prepare for the next injection. The total experimental time for each injection was 40 min. The flow rate was 0.3 mL/min, the auto-sampler temperature was 4 °C, and column compartment temperature was 40 °C. The targeted LC-MS/MS data was acquired using multiple-reaction-monitoring (MRM) mode. The experimental parameters for all the 56 BAs and five ISs, such as MRM transitions and retention times, were validated by spiking mixtures of standard compounds into a pooled study sample. TargetLynx software (Waters, Milford, MA) was used to integrate extracted MRM peaks. To determine absolute BA concentrations, calibration curves were first constructed for all the BAs standards in reference to their corresponding internal standard (Supplementary Table 2). Concentrations of the BAs in the study samples were then calculated from the peak areas and the slopes of the calibration curves. Inter-subject differences were normalized by the volume of serum (50 ul) and mass of liver (50 mg) or frozen intestinal pellet (46.667 mg).

DMD Fast Forward. Published on May 16, 2018 as DOI: 10.1124/dmd.118.081547
This article has not been copyedited and formatted. The final version may differ from this version.

Total RNA Isolation

Total RNA was isolated from liver and intestinal tissue sections using RNA-Bee reagent (Tel-Test Inc., Friendswood, TX). The concentration of total RNA was quantified using NanoDrop 1000 Spectrophotometer (Thermo Scientific, Waltham, MA) at 260 nm. The quality of RNA was evaluated by formaldehyde-agarose gel electrophoresis with visualization of 18S and 28S rRNA bands under ultraviolet light and was confirmed using an Agilent 2100 Bioanalyzer (Agilent Technologies Inc. Santa Clara, CA). Liver samples with RNA integrity number (RIN) above 8.0 were used for RNA-sequencing.

Messenger RNA quantification

The mRNA of *Cyp7a1* (Figure 12A) as well as the mRNAs of other BA-processing genes in liver were retrieved from our previously published RNA-Seq dataset (Li et al., 2017) and are accessible though the NCBI Gene Expression Omnibus Series accession number GSE101650. Intestinal mRNAs of various BA-processing genes were determined using RT-qPCR. Briefly, total RNA from intestinal tissue sections was transcribed to cDNA using a High Capacity cDNA Reverse Transcription Kit (Applied Biosystems, Foster City, CA). The cDNAs were amplified by PCR using SsoAdvanced Universal SYBR Green Supermix in a BioRad CFX384 Real-Time PCR Detection System (Bio-Rad, Hercules, CA). The PCR primers were synthesized by Integrated DNA Technologies (Coralville, IA) and the primer sequences are listed in Supplemental Table 1. The ddCq values were calculated for each target gene and were normalized to the expression of the housekeeping gene β-actin.

Targeted Proteomics by LC-MS/MS

The procedure is similar to a previous publication with a few modifications (Selwyn et al., 2015a; Li et al., 2017). Briefly, the membrane proteins of the mouse livers were isolated using a Mem-

DMD Fast Forward. Published on May 16, 2018 as DOI: 10.1124/dmd.118.081547
This article has not been copyedited and formatted. The final version may differ from this version.

PER plus membrane protein extraction kit (Pierce Biotechnology, Rockford, IL). Eighty µl of the tissue extract (2 mg/ml total protein) was mixed with 10 µl DTT (250 mM), 20 µl of 0.2 mg/ml bovine serum albumin, 10 µl of 10 mg/ml human serum albumin, and 40 µl ammonium bicarbonate buffer (100 mM, pH 7.8), and incubated at 95 °C for 5 min (denaturation and reduction). Subsequently, 20 µl iodoacetamide (500 mM) was added and the sample was incubated for 30 min at ambient temperature in the dark (alkylation). Ice-cold methanol (0.5 ml), chloroform (0.1 ml) and water (0.4 ml) were added to each sample. After centrifugation at 16,000*g* for 5 min at 4 °C, the upper and lower layer were removed, and the pellet was washed with ice-cold methanol (0.5 ml) and centrifuged at 8,000*g* for 5 min at 4 °C. The pellet was re-suspended with 60 µl 50 mM ammonium bicarbonate buffer. Trypsin (20 µl) was added at a 1:80 trypsin:protein ratio (w/w), and samples were incubated for 16 h at 37 °C. Trypsin digestion was stopped by adding 10 µl of chilled quenching solvent (80% acetonitrile with 0.5% formic acid) followed by 20 µl heavy peptide internal standard. Samples were centrifuged for 5 min at 4,000*g* under 4 °C, and supernatant was collected into a LC-MS vial. The stable isotope-labeled heavy peptides were used as internal standards (Thermo Fisher Scientific, Rockford, IL). LC-MS/MS consisted of an Acquity LC (Waters Technologies, Milford, MA) coupled to an AB Sciex Triple Quadrupole 6500 MS system (Framingham, MA). One to three surrogate peptides per protein were designed for the quantification of selected proteins (Supplemental Table 3) according to a previously published protocol (Prasad and Unadkat, 2014). The peptide separation was achieved on an Acquity UPLC column (HSS T3 1.8 µm, 2.1x100 mm, Waters, Hertfordshire, UK). Mobile phase A (water with 0.1% formic acid; v/v) and mobile phase B (ACN with 0.1% formic acid; v/v) were used with a flow rate of 0.3 ml/min in a gradient manner. Peak integration and quantification were performed using Analyst (Version 1.6, Mass Spectrometry Toolkit v3.3, Framingham, MA, USA). A robust strategy was used to ensure optimal reproducibility when quantifying these proteins (Bhatt and Prasad, 2017). For example, ion suppression was addressed by using heavy peptide. Bovine serum albumin (BSA) was

DMD Fast Forward. Published on May 16, 2018 as DOI: 10.1124/dmd.118.081547
This article has not been copyedited and formatted. The final version may differ from this version.

used as an exogenous internal standard, which was added to each sample to correct for protein loss during processing and digestion efficiency. In total, three-step data normalization was used; first average peak areas of light peptides were divided by corresponding average heavy peptide peak areas. This ratio was then divided by BSA light/heavy peak area ratio. Finally, the data were normalized to average quality control values (pooled representative sample). Specific peptides targeting these proteins are listed in Supplemental Table 3. Due to instrument sensitivity, bile acid synthesis genes with an FPKM for mRNA expression greater than 20 were selected for targeted proteomics.

Statistical Analysis

Data are presented as mean ± standard error (SE). Statistically significant differences were determined by Analysis of Variance (ANOVA) followed by Duncan's post-hoc test ($p<0.05$). Asterisks (*) represent statistically significant differences between corn oil- and PBDE-exposed groups within CV or GF mouse colonies. Pounds (#) represent significant differences between CV and GF mice under the same exposure. A hierarchical clustering dendrogram (Ward's minimum variance method, distance scale) of the differentially enriched pathways was generated by JMP Genomics software (SAS Institute, Inc., Cary, NC). Pearson's correlations between BAs and bacterial species were performed with R (corrplot).

RESULTS

Effect of PBDEs on gut microbiome using 16S rRNA sequencing

To determine the effect of oral exposure to PBDEs on gut microbiome, 16S rRNA sequencing targeting V4 region was performed in the LIC of CV mice exposed to corn oil, BDE-47 (100 μmol/kg), or BDE-99 (100 μmol/kg) (n=3 per group). The sequence analysis yielded a total of 104,282 ± 3,574 reads per sample (Supplemental Table 4). Rarefaction analysis (QIIME) was performed from 0 to 80,000 reads with an increment of 10,000 reads. The alpha diversity (Chao

DMD Fast Forward. Published on May 16, 2018 as DOI: 10.1124/dmd.118.081547
This article has not been copyedited and formatted. The final version may differ from this version.

1 Index), which describes species richness, demonstrated that both BDE-47 and BDE-99 profoundly decreased microbial richness compared to corn oil-exposed control group in the LIC of CV mice (Figure 2A). The beta diversity, which describes the species differences among different samples, was calculated using weighted UniFrac distance matrix and visualized with EMPeror by principle coordinates analysis (PCoA) (Vazquez-Baeza et al., 2013). As shown in Figure 2B, there was a clear separation between PBDE-exposed samples and control samples. The BDE-47 exposed samples were clustered separately from BDE-99 exposed samples at PC2 direction in the PCoA plot (Figure 2B).

The majority of OTUs were assigned to the phyla *Firmicutes*, *Bacteroidetes*, and *Verrucomicrobia* (Supplemental Figure 1); *Actinobacteria*, *Tenericutes*, *Fusobacteria*, *Proteobacteria*, *Acidobacteria*, *Deferribacteres*, *Chlorobi*, *Planctomycetes*, *Crenarchaeota*, *Fibrobacteres*, *Nitrospirae*, and *Chloroflexi* were detected at levels <1%. In addition, 2.5 ± 0.4% of sequences were not assigned to any bacterial phylum (Supplemental Figure 1). At class level (Figure 2C), BDE-99 decreased the abundance of *Actinobacteria* in the *Actinobacteria* phylum. *Coriobacteriia* in *Actinobacteria* phylum and *Bacilli* in *Firmicutes* phylum were decreased by both BDE-47 and BDE-99. Conversely, *Erysipelotrichi* in *Firmicutes* phylum, *Gammaproteobacteria* in *Proteobacteria* phylum, and *Verrucomicrobiae* in *Verrucomicrobia* phylum were profoundly increased by both BDE-47 and BDE-99 exposure (Figure 2C). Analysis conducted at the species level identified 154 bacterial taxa, of which 41 were differentially regulated by PBDEs as compared to corn oil-exposed control group (Figure 3A). These bacterial species partitioned into three distinct patterns: Pattern I include 4 taxa that were increased by both BDE-47 and BDE-99; Pattern II included 6 taxa that were decreased by BDE-47 but increased by BDE-99; Pattern III included 31 taxa that were consistently decreased by both BDE-47 and BDE-99. The relative abundance of bacterial species was determined across all exposure groups with Figure 3B showing the top 9 most abundant bacterial species and all

other summed and labeled as "other taxa" in the 10th category. On average, across all exposure groups, the predominant species were *S24-7* in *Bacteroidetes* phylum and *Clostridiales* in *Firmicutes* phylum. Most notably, *Akkermansia muciniphila* in *Verrucomicrobia* phylum and *Erysipelotrichaceae Allobaculum spp*. in *Firmicutes* phylum were minimally present in corn oil exposed control group, but were markedly increased after PBDE exposure (Figure 3B). The elevated levels of *Akkermansia muciniphila* and *Erysipelotrichaceae Allobaculum spp.* by PBDEs were further confirmed by qPCR (Figure 3C).

To further examine the effect of PBDEs on BA-metabolizing bacteria and microbial enzymes, qPCR was performed on *Clostridium scindens*, which is a bacterium with known 7α de-hydroxylation functions (Ridlon et al., 2006); the BA-inducible operons *baiCD* and *baiJ*, which are microbial enzymes involved in BA dehydroxylation (i.e. secondary BA synthesis); as well as bile salt hydrolase (*bsh*), which performs BA deconjugation. Interestingly, although PBDEs did not alter the abundance of *C. scindens, baiCD* was increased by BDE-99 and *baiJ* was increased by both BDE-47 and BDE-99. *Bsh* appeared to be increased by BDE-99 although a statistical significance was not achieved (Figure 3C). Together these data indicate that bacteria other than *C. scindens*, which are likely from Pattern I and Pattern II may be responsible for the up-regulation of microbial BA-metabolizing enzymes.

Predicted functional composition of gut microbiome with PICRUSt

The metagenomic functional content of gut microbiota was predicted by PICRUSt (Langille et al., 2013) across all three exposure groups. A total of 39 differentially enriched KEGG pathways by PBDEs were identified and plotted using the mean value for each exposure (Figure 4). These pathways were grouped into four categories: bacteria-specific processes (Figure 4A), xenobiotic biodegradation and metabolism (Figure 4B), basal cellular processes (Figure 4C), and intermediary metabolism (Figure 4D). For bacteria-specific processes, BDE-99 increased the

abundance of five KEGG pathways, namely penicillin and cephalosporin biosynthesis; lipopolysaccharide biosynthesis; beta-lactam resistance; stilbenoid, diarylheptanoid and gingerol biosynthesis; and phosphotransferase system (PTS, a bacterial-specific pathway for carbohydrate metabolism). BDE-47 also increased the stilbenoid, diarylheptanoid and gingerol biosynthesis and the PTS pathways (Figure 4A). These data indicate that there may be a compensatory mechanism to up-regulate these microbial processes to fight against PBDE-induced dysbiosis.

For xenobiotic biodegradation and metabolism (Figure 4B), BDE-99 up-regulated four KEGG pathways: caffeine metabolism; fluorobenzoate degradation; geraniol degradation; and chlorocyclohexane and chlorobenzene degradation. Conversely, both BDE-47 and BDE99 decreased the KEGG pathways related to dioxin degradation, xylene degradation, drug metabolism, and ethylbenzene degradation. These data suggest that the microbial biotransformation of PBDEs may interact and influence the metabolism of other xenobiotics.

Regarding basal cellular functions (Figure 4C), BDE-47 increased the KEGG pathway of ion channels, but decreased the KEGG pathways involved in cell division, glycan biosynthesis and metabolism, glycosphingolipid biosynthesis, electron transfer carriers, basal transcription factors, and G protein-coupled receptors. BDE-99 increased the KEGG pathways involved in cell motility and secretion, transcription related proteins, glycosaminoglycan degradation, ubiquitin system, non-homologous end-joining, and ion channels, but decreased the KEGG pathways involved in apoptosis, cell division, glycan biosynthesis and metabolism, electron transfer carriers, and basal transcription factors. These data further suggest that there is a compensatory mechanism of bacterial functions to fight against the PBDE-induced insult on the basal functions of the gut microbiota.

DMD Fast Forward. Published on May 16, 2018 as DOI: 10.1124/dmd.118.081547
This article has not been copyedited and formatted. The final version may differ from this version.

Within intermediary metabolism pathways (Figure 4D), BDE-47 decreased the KEGG pathways involved in ether lipid metabolism, mineral absorption, α-linolenic acid metabolism and cyanoamino acid metabolism, but increased arachidonic acid metabolism. BDE-99 showed a similar trend in regulating these pathways. In addition, BDE-99 decreased the KEGG pathways involved in carbohydrate digestion and absorption, nicotinate and nicotinamide metabolism, but increased arachidonic acid metabolism, fatty acid elongation in mitochondria, steroid and steroid hormone biosynthesis, ubiquinone and other terpenoid-quinone biosynthesis, and carotenoid biosynthesis. Because of the decrease in the anti-inflammatory α-linolenic metabolism pathway and an increase in the pro-inflammatory arachidonic acid metabolism pathway, these data suggest that PBDEs may lead to a pro-inflammatory stage in the GI tract and perturb the absorption and biotransformation of essential micronutrients.

BAs in serum, liver, SIC, and LIC of CV mice

To determine how oral exposure to PBDEs affects BA homeostasis, targeted metabolomics analysis of BAs was performed in serum, liver, SIC, and LIC of CV mice exposed to corn oil, BDE-47 (100 μmol/kg), or BDE-99 (100 μmol/kg) (n=3 per group). Abbreviations for all BAs are in Supplemental Table 2.

We estimated relative standard deviation (RSD) values from the QC samples that were injected multiple times during the experiment runs. For serum samples, the detected BAs had a median RSD of 7.3%, ranging from 0.2-16.6% (0.2% for CA, and 16.6% for T-UDCA). For liver tissue, the median RSD was 5.9%, ranging from 0.1-28.0% (0.1% for MCA, and 28.0% for ωMCA). For SIC and LIC samples, the median RSD was 8.7%, ranging from 2.5-35.7% (2.5% for G-CDCA, and 35.7% for 9(11), (5β)-Cholenic Acid-3α-ol-12-one). We obtained acceptable recovery rates between 80.0-112.1% (80.0% for T-DCA, and 112.1% for AlloLCA) with a median of 98.1% for detected BAs in all samples. The limit of detection (LOD) is different for each BA. The median

LOD of each BA is $4.5x10^{-4}$ nmol, ranging from $1.1x10^{-4}$ ~ $3.2x10^{-3}$ nmol ($1.1x10^{-4}$ nmol for T-UDCA, and $3.2x10^{-3}$ nmol for HDCA).

To evaluate the overall changes in the regulation of BA pool, the sum of all BAs for each compartment (serum, liver, SIC, and LIC) were summed and categorized by group (Figure 5A). Overall, total BAs, primary BAs, secondary BAs, and unconjugated BAs did not change due to BDE-99 or BDE-47. Conjugated BAs were decreased by BDE-47 exposure, but remained unchanged by BDE-99 exposure. Conversely, in the liver, BDE-99 exposure increased total BAs, primary BAs, secondary BAs, and unconjugated BAs, but conjugated BAs were not altered by BDE-99 or BDE-47 (Figure 5B).

In serum, 12 BAs were detectable in CV mice, including four unconjugated BAs (Figure 6A) and eight taurine (T)- or glycine (G)-conjugated BAs (Supplemental Figure 2A). In general, PBDEs did not markedly alter the primary or secondary conjugated BAs in serum, except for a moderate decrease in G-CA by BDE-99 and an apparent decrease in T-α/βMCA by BDE-47 (Supplemental Figure 2A). Regarding the unconjugated BAs in serum, BDE-99 increased the primary BA βMCA and also tended to increase the primary BA CA and the secondary BA ωMCA; conversely, BDE-47 decreased the secondary BA 3-DHCA and tended to decrease the primary BAs CA, βMCA, and the secondary BA ωMCA.

In the liver, 23 BAs were detected in CV mice, including 12 unconjugated BAs (Figure 6B) and 11 T- or G-conjugated BAs (Supplemental Figure 2B). In general, PBDEs had less effect on the conjugated BA profiles, except for an increase in the primary BA G-CA and the secondary BA T-DCA by BDE-99. In contrast, BDE-99 markedly increased most unconjugated primary BAs, including CA, αMCA, and βMCA, as well as most unconjugated secondary BAs, including

ωMCA, MCA, HDCA, 12-DHCA, 5β-Cholanic Acid-3α, 6α-diol-7-one, and 5 β-Cholanic Acid-3β, 12α-diol (Figure 6B).

In the SIC, 24 BAs were detected in CV mice, including 14 unconjugated BAs (Figure 7A) and 10 T- or G-conjugated BAs (Supplemental Figure 3A). For conjugated BAs, PBDEs in general decreased many primary and secondary BAs in SIC: BDE-47 and BDE-99 decreased T-UDCA, G-CA, T-LCA, and T-HDCA. BDE-47 also decreased T-α/βMCA, whereas BDE-99 decreased T-HCA. Conversely, BDE-99 increased unconjugated primary BAs such as the primary BAs βMCA and UDCA and most unconjugated secondary BAs, including ωMCA, DCA, HCA, 3-DHCA, 3α-OH-12 Ketolithocholic Acid, 8(14), (5β)-Cholenic Acid-3α, 12α-diol, and 9(11), (5β)-Cholenic Acid-3α-ol-12-one. BDE-47 also increased several unconjugated secondary BAs, including ωMCA, HCA, 3 DHCA, and 9(11), (5β)-Cholenic Acid-3α-ol-12-one (Figure 7A).

In the LIC, 25 BAs were detected in CV mice, including 14 unconjugated BAs (Figure 7B) and 11 T- or G-conjugated BAs (Supplemental Figure 3B). For conjugated BAs, BDE-47 increased the primary BA T-α/βMCA and the secondary BA T-DCA, whereas BDE-99 increased the primary BA G-CDCA and the secondary BA T-HDCA (Supplemental Figure 3B). Among unconjugated BAs, BDE-47 increased the primary BA αMCA, as well as the secondary BAs LCA, HCA, HDCA, 3-DHCA, AlloLCA, IsoLCA, and 3-Ketocholanic acid. BDE-99 decreased the primary BA CDCA, but increased UDCA, as well as increased the secondary BAs DCA and AlloLCA (Figure 7B).

Pearson's correlation between secondary BAs and bacterial species

Because secondary BAs were exclusively produced by gut microbiota, to determine which bacterial species may contribute to altered total secondary BA pool in CV mice, individual secondary BAs from all four compartments of CV mice were summed and then correlated with

41 bacterial species that were differentially regulated by PBDEs (Figure 8). Both unconjugated secondary BAs (which were exclusively produced by gut microbiota) and conjugated secondary BAs (which were produced by bacteria and then conjugated in liver) were considered. Pearson's correlation analysis revealed that 32 out of 41 bacterial species were positively correlated with taurine-conjugated secondary BAs (including T-ωMCA, T-HCA, T-HDCA, and T-LCA), but negatively correlated with many unconjugated secondary BAs. Conversely, 4 taxa, namely *Bacteroidales* other, *Anaerofustis*, *Allobaculum spp.*, and *A. muciniphila*, were in general negatively correlated with conjugated secondary BAs, but in general positively correlated with unconjugated secondary BAs, suggesting that may directly or indirectly contribute to BA deconjugation.

Comparison of PBDE-mediated changes in BA compositions in serum, liver, SIC, and LIC between CV and GF mice

To determine the BA compositional changes caused by PBDEs and the necessity of gut microbiota in modulating the basal and PBDE-regulated BA profiles, the proportions of individual BAs in serum, liver, SIC, and LIC of CV and GF mice were analyzed across all 3 exposure groups (Supplemental Figures 4-7).

In serum (Supplemental Figure 4), compared to corn oil-exposed CV (CV CO) mice with more diversified BA profiles, the BA profiles in corn oil-exposed GF (GF CO) mice were predominated by the primary BAs T-α/βMCA and T-CA, whereas other BAs were minimally detected. Following PBDE exposure, BDE-99 had a more prominent effect on BA compositional changes than BDE-47 in CV mice, namely an apparent increase in the proportion of major primary conjugated BA T-α/βMCA. In PBDE-exposed GF mice, serum BA profiles were still predominated by T-α/βMCA and T-CA. In particular, BDE-47 exposure led to an apparent

increase in the proportion of T-α/βMCA, whereas BDE-99 exposure led to an apparent increase in the proportions of T-HDCA and T-UDCA.

In liver (Supplemental Figure 5), under CV control conditions, T-α/βMCA and T-CA were the predominant BAs detected, whereas lack of gut microbiota increased the proportion of T-α/βMCA, but decreased the proportion of T-CA; in addition, there was an increase in the proportion of hepatic βMCA in control GF mice. Following PBDE exposure in CV mice, both BDE-47 and BDE-99 increased the proportions of T-CA, and doubled the proportions of the major secondary BAs T-DCA and ωMCA. BDE-99 also doubled the proportions of the primary unconjugated BAs βMCA and CA in livers of CV mice. In livers of GF mice, PBDEs had less effect, except for an apparent decrease in the proportions of T-α/βMCA by BDE-99.

In SIC (Supplemental Figure 6), in general, BA profiles were more diverse in CV mice than in GF mice. Under CV control conditions, CA in its unconjugated form became a major BA in this compartment, in addition to other major BAs including T-α/βMCA and T-CA, suggesting extensive deconjugation reactions converting T-CA to CA in the presence of gut microbiota. In contrast, in control GF mice, the predominant BAs were T-α/βMCA and T-CA, whereas other BAs were minimal. Following PBDE exposure, the proportions of BAs remained relatively constant in GF mice. Conversely, in CV mice, there was a marked increase in the proportion of CA (from 25% in controls to 42% by BDE-47 and to 35% by BDE-99), and correspondingly, the proportion of the primary BA T-CA was reduced by BDE-99 in CV mice. In addition, the proportion of T-α/βMCA was reduced by both BDE-47 and BDE-99. These data suggested that PBDEs further enhanced the BA deconjugation reactions in a microbiota-dependent manner.

In LIC (Supplemental Figure 7), under CV control conditions, the BA profiles were more diverse than those in GF mice, and the most predominant BAs were T-α/βMCA and ωMCA. In GF mice,

DMD Fast Forward. Published on May 16, 2018 as DOI: 10.1124/dmd.118.081547
This article has not been copyedited and formatted. The final version may differ from this version.

the LIC BAs were predominated by T-α/βMCA, followed by T-CA, with all other BA levels minimal. Following PBDE exposure, BAs in GF mice remained relatively constant; in contrast, in CV mice, both PBDEs increased the proportion of T-α/βMCA, but decreased the proportions of ωMCA and βMCA. BDE-99 exposure also led to an apparent increase in the proportions of the secondary BAs DCA and T-HDCA, as well as the primary BA UDCA.

Host BA-processing gene expression in livers of CV and GF mice

To determine to what extent BA-metabolizing enzymes and transporters are affected by PBDEs and gut microbiota interactions, the expression of major BA-processing genes involved in BA biosynthesis (Cyp8b1, Cyp27a1, Cyp7b1, Hsd3b7, Akr1c14), conjugation (Slc27a5 [also known as bile acid ligase]), and transport (Ntcp, Oatp1b2, Bsep) were quantified using targeted proteomics; Cyp7a1 was below the detection limit, and therefore, the mRNA level is shown.

Cyp7a1 and Cyp8b1 are involved in the classical pathway of BA synthesis. Under control conditions, the mRNA of the rate-limiting enzyme Cyp7a1 was higher in CV mice than GF mice (Figure 9A). Following PBDE exposure, Cyp7a1 mRNA was increased by BDE-47 and BDE-99 in CV mice. However, in GF mice, Cyp7a1 mRNA was not altered by BDE-47, but increased 4.2-fold by BDE-99, suggesting that the BDE-47 mediated increase in Cyp7a1 mRNA was dependent on gut microbiota. Cyp8b1 protein was lower in GF mice than CV mice under control conditions, whereas BDE-99 decreased Cyp8b1 protein expression in CV mice, and the PBDE-mediated decrease in Cyp8b1 was completely abolished in livers of GF mice. Cyp27a1 and Cyp7b1 are key enzymes in the alternative pathway of BA synthesis. The Cyp27a1 protein was lower in control GF mice as compared to control CV mice, whereas both BDE-47 and BDE-99 decreased Cyp27a1 protein in livers of CV mice but not in GF mice, suggesting that the down-regulation of Cyp27a1 protein by PBDEs is gut microbiota-dependent. The Cyp7b1 protein was not altered by either PBDEs or gut microbiota. The proteins of the downstream BA-synthetic

DMD Fast Forward. Published on May 16, 2018 as DOI: 10.1124/dmd.118.081547
This article has not been copyedited and formatted. The final version may differ from this version.

enzymes, namely Hsd3b7, which catalyzes the inversion of 3β-hydroxyl group of cholesterol to the 3α-hydroxyl group of bile acids, and Akr1c14 (aldo-keto reductase), were also determined. Both enzymes were lower in control GF mice as compared to control CV mice and were decreased by BDE-47 and BDE-99 in CV mice. This down-regulation in their protein expression was absent in livers of GF mice. Regarding BA conjugation, Slc27a5 is a bile acid-CoA ligase (Bal) that mediates the conjugation of primary BAs with glycine or taurine before excretion into bile canaliculi. The Slc27a5 protein was decreased by BDE-47 in CV mice but not in GF mice.

Regarding BA transporters, the proteins of the major basolateral uptake transporter for conjugated BAs, namely sodium taurocholate cotransporting polypeptide (Ntcp/Slc10a1), as well as the major basolateral uptake transporter for unconjugated BAs, namely organic anion transporting polypeptide (Oatp/Slco) 1b2, were both lower in control GF mice than those in control CV mice. Both BDE-47 and BDE-99 decreased the proteins of Ntcp and Oatp1b2 in a gut microbiota-dependent manner. The protein of the rate-limiting canalicular BA efflux transporter Bsep was similar between livers of CV and GF mice under control conditions, whereas both BDE-47 and BDE-99 decreased its expression in livers of CV mice. This down-regulation was dampened by the lack of gut microbiota, since there was no change in Bsep protein expression by BDE-47 and decrease by BDE-99 in livers of GF mice (Figure 9B).

The mRNA expression of several other genes involved in BA homeostasis was also quantified in livers of CV and GF mice, including the BA-synthetic enzymes Cyp39a1 and Akr1d1, the BA-conjugation enzyme Baat (bile acid CoA:amino acid N-acyltransferase), the basolacteral BA-efflux transporters Ostα (Slc51a) and Ostβ (Slc51b), the cholesterol efflux transporter Abca1, the lipid uptake transporter Atp8b1, the BA-efflux transporter Asbt (Slc10a2), as well as various transcription factors Nr1h4 (or FXR), Nr0b2 (or Shp), Mafg (Musculoaponeurotic fibrosarcoma

DMD Fast Forward. Published on May 16, 2018 as DOI: 10.1124/dmd.118.081547
This article has not been copyedited and formatted. The final version may differ from this version.

oncogene homolog G), Crip2 (cysteine-rich intestinal protein 2), Zfp385a (Zinc-finger protein 385a), Nr1h2 (or LXRβ), and Nr1h3 (or LXRα) (Supplemental Figure 4). The mRNAs of Abcb4, Abcg5, and Abcg8 were not altered by lack of gut microbiota or PBDEs (data not shown). Under control conditions, lack of gut microbiome moderately decreased Cyp39a1 mRNA. Following PBDE exposure, many of the mRNAs in CV mice were not affected. However, in GF mice, BDE-47 increased the mRNAs of Cyp39a1 and Slc51b, and BDE-99 increased Akr1d1, Slc51b, Abca1, Atp8b1, Slc10a2, and Mafg. Conversely, the mRNAs of the majority of transcription factors were decreased by BDE-99 in GF mice, including Nr0b2, Crip2, Zfp385a, Nr1h2, and Nr1h3 (Supplemental Figure 8).

BA-transporters and Fgf15 gene expression in various parts of the intestine

The mRNA expression of major intestinal transporters involved in enterohepatic circulation of BAs was determined in four intestinal sections of CV and GF mice, including the uptake transporter Asbt and efflux transporters Ostα, Ostβ, and Mrp4. The intestinal hormone Fgf15, which regulates the hepatic BA-synthesis, was also determined (Figure 9C).

Asbt brings BAs from the intestinal lumen into enterocytes. In ileum, where the peak basal expression of Asbt was observed, both BDE-47 and BDE-99 markedly increased Asbt mRNA in CV mice; however, in GF mice, only BDE-47 increased Asbt mRNA. Asbt mRNA was not affected by either lack of gut microbiota or PBDE exposure in other sections of intestine. The basolateral BA efflux transporters Ostα and Ostβ transport the reabsorbed BAs from enterocytes to portal blood. The mRNA expression of Ostα was not affected by lack of gut microbiota under control conditions, and PBDE exposure did not affect Ostα in CV mice. In GF mice, BDE-47 increased Ostα mRNA in jejunum, and BDE-99 increased Ostα mRNA in colon. The basal mRNA expression of Ostβ was lower in jejunum and ileum of GF mice. In CV mice, BDE-99 moderately increased Ostβ in duodenum. For the basolateral efflux transporter Mrp4,

its basal expression in duodenum was higher in GF mice, and interestingly, Mrp4 mRNA was consistently up-regulated by BDE-99 in all four sections of intestine of CV mice in a gut microbiota-dependent manner. The mRNA of the intestinal hormone Fgf15 was not altered by lack of gut microbiota under control conditions, and remained unchanged following PBDE exposure in CV mice. However, in GF mice, BDE-47 increased Fgf15 mRNA in duodenum and BDE-99 increased Fgf15 mRNA in colon.

DISCUSSION

Taken together, the present study provides the first evidence of the effect of PBDEs on gut microbiota and BA homeostasis. Specifically, PBDEs decreased the bacterial richness and differentially regulated various bacterial species in the large intestine of mice. Most notably, *Akkermansia muciniphila* and *Erysipelotrichaceae Allobaculum spp.,* which have been shown to have anti-obesogenic effects, were overwhelmingly increased by PBDEs and suggests that there may be a novel interaction between environmental PBDEs and nutrition. Regarding BA profiles, PBDEs, in particular BDE-99, increased the unconjugated BAs in serum, liver, SIC, and LIC of CV mice but not in GF mice. The lack of gut microbiome was associated with a shift in BA composition toward an increase in conjugated muricholic acids in all four compartments of GF mice.

As the human intestinal microbiota is dominated by strict anaerobic bacteria, there is limited information regarding how GI bacteria respond to PBDE exposure. The present study provided the first evidence of the effect of PBDEs on bacterial community in the GI tract. At class level, we found oral exposure to BDE-47 or BDE-99 decreased *Actinobacteria*, *Coriobacteriia*, and *Bacilli*, but increased *Erysipelotrichi*, *Gammaproteobacteria*, and *Verrucomicrobiae* in LIC of CV mice. The elevated abundances of *Erysipelotrichi* and *Gammaproteobacteria* in the present study is similar to previous findings from sediment samples. Using an *in vitro* culture approach,

previous studies have reported positive correlation of five bacterial classes (*Clostridia*, *Bacilli*, *Betaproteobacteria*, *Alphaproteobacteria*, and *Gammaproteobacteria*) *with* anaerobic degradation of BDE-209 and BDE-28 in the sediment (Robrock et al., 2008; Yang et al., 2017). Another study also demonstrated a positive relationship between bacteria (*Actinobacteria* and *Erysipelotrichi*) and biodegradation of lesser-brominated PBDE congeners, tri-BDE, and tetra-BDE (Xu et al., 2012). Therefore, the increased *Erysipelotrichi* and *Gammaproteobacteria* following PBDE exposure suggests that these two bacterial classes may be involved in debromination of BDE-47 and BDE-99 *in vivo*. Although *Bacilli* and *Actinobacteria* have been reported to be positively correlated with degradation of PBDEs (BDE-209 and BDE-28) in sediment, we observed decreased abundances of *Bacilli*, *Actinobacteria,* and *Coriobacteriia* (which is also from *Actinobacteria* phylum) by PBDEs. It is possible that these bacterial classes are more sensitive and susceptible to BDE-47 and BDE-99-mediated insults, since tetra- and penta-BDEs are considered to be more toxic and bio-accumulative than higher brominated congeners such as BDE-209 (Siddiqi et al., 2003).

The present study provides the first evidence linking *A. muciniphila* and *E. Allobaculum* with exposure to PBDEs. *A. muciniphila* is a mucin-degrading bacteria that resides in the mucus layer of the human intestinal tract and helps to maintain the gut barrier and can be found is present is found in the colon of health human subjects at 1-4% of the bacterial population (van Passel et al., 2011; Zhao et al., 2017). Studies have shown that *A. muciniphila* may have anti-inflammatory effects in humans, and inverse relationships have been observed between *A. muciniphila* colonization and inflammatory conditions, such as irritable bowel syndrome (Png et al., 2010). Reduced levels of *A. muciniphila* have also been found in patients with metabolic disorders such as diabetes and obesity, suggesting *A. muciniphila* may also have anti-obesogenic properties (Derrien et al., 2017). Similarly, *Allobaculum spp.* has also been shown to have anti-obesogenic effects. Lower abundances of *Allobaculum spp.* was found in mice fed

with high-fat diet compared to mice fed with control diet, and *Allobaculum spp.* was enriched in the weight reduced mice (Ravussin et al., 2012). Moreover, both *A. muciniphila* and *Allobaculum spp.* were found negatively correlated with circulating leptin concentrations in obese mice (Ravussin et al., 2012). The mechanisms underlying the effects of *A. muciniphila* and *Allobaculum spp.* in inflammation and metabolic disorders are not understood, and no studies have linked these two bacterial species with environmental chemical exposure in the literature. The involvement of PBDEs in modulating the nutrition response by altering these two bacteria is worth investigating in future studies.

In the present study, the bacterial species that were differentially regulated by PBDEs have been linked with multiple pathways: bacteria-specific processes, basal cellular processes, xenobiotic metabolism, and intermediary metabolism (Figure 4). The increased bacteria-specific processes by BDE-47 and BDE-99 suggest that there may be a compensatory mechanism to up-regulate these microbial processes to fight against PBDE-induced dysbiosis. Conversely, many xenobiotic metabolism-related pathways were decreased by both BDE-47 and BDE99, suggesting that the microbial biotransformation of PBDEs may affect the metabolism of other xenobiotics. In addition, predictive analysis by PICRUSt showed that BDE-99 may increase cell motility and secretion, transcription related proteins, glycosaminoglycan degradation, ubiquitin system, non-homologous end-joining, and ion channels. These data further suggested that there is a compensatory mechanism of bacterial functions to fight against the PBDE-induced insult on the basal functions of the gut microbiota. Regarding intermediary metabolism, both BDE-47 and BDE-99 decreased ether lipid metabolism, mineral absorption, alpha-linolenic acid metabolism (which is anti-inflammatory), and cyanoamino acid metabolism; whereas BDE-99 markedly increased arachidonic acid metabolism, fatty acid elongation in mitochondria, steroid and steroid hormone biosynthesis, ubiquinone and other terpenoid-quinone biosynthesis, and carotenoid biosynthesis. These data suggest that PBDEs may lead

to a pro-inflammatory stage in the GI tract and perturb the absorption and biotransformation of essential micronutrients. The BDE-99-mediated increase in steroid/steroid hormone synthesis also coincides with increased microbial biotransformation of BAs (Figure 3C), which are part of the steroid hormone signaling.

The increased unconjugated secondary BAs by PBDEs correlated with the increased abundance of bacteria (*Clostridiales* and *Clostridiaceae*) and the increased expression of microbial enzymes (*baiCD* and *baiJ*) that are involved in BA metabolism (Figure 3A and 3C). The microbial enzymes *baiCD* and *baiJ* convert primary BAs to secondary BAs via dihydroxylation and *Bsh* removes glycine or taurine conjugates via deconjugation. *Bsh* activity is widely present in bacteria present in the large and small intestines, including *Clostridium, Enterococcus, Bifidobacterium, Lactobacillus, and Bacteroides (Ridlon et al., 2006)*. In the present study, we found a slight increase of *Bsh* following BDE-99 exposure although a statistical significance was not achieved. In addition to the bacterial species that are mentioned above, there are also many other bacterial species involved in BA metabolism, including genera *Bacteroides, Clostridium, Lactobacillus, Bifidobacterium, Enbacterium*, and *Escherichia (Ridlon et al., 2006)*. Therefore, future studies discovering novel bacteria and microbial enzymes involved in BA deconjugation and dehydroxylation will help us further understand the connection between the gut microbiome and BA homeostasis.

The BA profiles of GF mice differ markedly from those of CV mice under both control and PBDE exposed conditions. As expected, GF mice have increased conjugated BAs and decreased secondary BAs. Under control condition, the proportion of T-α/βMCA is much higher in GF mice than that in CV mice in all four compartments (Supplemental Figures 4-7). These findings are consistent with previous studies (Sayin et al., 2013; Hu et al., 2014; Miyata et al., 2015; Selwyn et al., 2015b). T-CA was increased in all compartments, except in the liver. In contrast, the

unconjugated BAs were decreased in all four compartments of GF mice compared with those of CV mice.

Many enzymes and transporters that are involved in BA synthesis, conjugation and transport were decreased by PBDEs, in a gut microbiome dependent manner. It is well known that BAs can regulate their own synthesis by activating farnesoid X receptor (FXR) in liver and in intestine. In the liver, activation of FXR induces the expression of Shp, which subsequently decreases the BA-processing genes for BA synthesis. However, the hepatic mRNA expression of Shp was not induced by PBDEs in the present study. In the ileum, activation of FXR by BAs induces the secretion of Fgf15, which could also decrease the transcription of BA-synthesis genes such as Cyp7a1 (Chiang, 2004). However, we did not observe increased Fgf15 in the ileum of CV mice, suggesting that mechanisms other than FXR signaling are responsible for the reduced expression of BA-processing genes in liver. Since BDE-47 and BDE-99 are known activators of human and mouse PXR, and activation of human PXR by its prototypical ligand rifampicin have shown reduced hepatic BA cholestatic patients (Geenes et al., 2015), it is possible that PBDE exposure may affect PXR signaling to modulate the BA pathway in CV mice with a minor effect from FXR activation.

In the present study, we found that the mRNA of Asbt was up-regulated by both BDE-47 and BDE-99 in the ileum. The ileal BA uptake transporter Asbt is responsible for the reabsorption of most of the BAs from the intestine. Combined with the decreased total BAs in SIC and increased total BAs in serum and liver following BDE-99 exposure (Supplemental Table 5), these results suggest that there is an increase in the reabsorption of BAs. In addition, the mRNA of basolateral efflux transporter Mrp4, which actively transports BAs from enterocytes to portal circulation, was also increased by BDE-99 in all four sections of intestine in CV mice

(Figure 12C). This also correlated with the increased total BAs in serum and liver and suggests more BAs are retrieved back from the gut.

In the present study, we dosed CV and GF mice with 100 μmol/kg of PBDEs (which is 48.5 mg/kg body weight for BDE-47 and 56.5 mg/kg boday weight for BDE-99) for four consecutive days in a similar exposure scheme used to induce Cyps in adult mice (Pacyniak et al., 2007). Another study showed that a single oral exposure of BDE-99 at 20 mg/kg resulted in serum concentrations of 3.6 pg/g serum two days later (Lundgren et al., 2013). These acute doses are higher than environmental exposure to humans. In the United States, human serum concentrations for BDE-47 was from 3.9-1000 pg/g serum and the concentration range for BDE-99 was 1.3-290 pg/g serum (Makey et al., 2016). Therefore, the circulating levels of PBDEs in this study were at concentrations similar to humans.

The vehicle used in the present study was corn oil, which contains a variety of saturated, monounsaturated, and polyunsaturated fatty acids, and is especially high in linoleic acid (42-56%). This was consistent with the observation that linoleic acid metabolism pathway was high in differentially regulated microbial taxa from large intestinal content of vehicle-exposed CV mice (Figure 4D), indicating that this was likely due to vehicle-effect. For the present study, we did not quantify the bacterial profiles between vehicle and naïve (unexposed) mice because the goal of the study was to determine the effect of PBDEs, which were dissolved in corn oil, and the effect of corn oil itself should be similar between the vehicle and PBDE-exposed groups. In the literature, it has been demonstrated that certain fatty acids are associated with dysbiosis (Alcock and Lin, 2015), and certain fatty acids themselves can also regulate bile acid metabolism by altering the serum cholesterol levels (Liu et al., 2017). Therefore, results from the present study should be interpreted as the effects from a combination of PBDEs and corn oil.

Prior to our work, there were no studies in the literature investigating the association between PBDE exposure and perturbation of the gut microbiome. Our study is the first showing that PBDEs can cause dysbiosis in the large intestinal content of mice, and this also leads to disrupted BA metabolism. Previous studies on PBDEs have focused primarily on the host effect such as thyroid toxicity, neurodevelopmental disorders, and oxidative stress. However, considering that the gut microbiome conducts the majority of the reduction reactions of the body, and also contribute to de-conjugation reactions (such as reversing the glucuronidation of toxic chemicals including PBDEs), it is critical to unveil such novel interactions between PBDE exposure and gut microbiome, so as to take a first step in further understanding idiosyncratic adverse reactions to chemicals in humans. One particular example is that we identified that PBDEs preferably increased unconjugated BAs in multiple biological compartments in mice (Figure 6-7). Especially in small and large intestinal contents, there were increases in multiple unconjugated secondary BAs (Figure 7), which are positively associated with colon cancer (Imray et al., 1992). Because secondary BAs can be carcinogens (Ajouz et al., 2014), it is possible that people at a higher risk of PBDE exposure, in particular BDE-47 exposure (Figure 7B), may also have increased risks of developing colon cancer. Indeed, brominated compounds tend to induce colon cancer in rodents (Dunnick et al., 1997) and transcript patterns following PBDE exposure in rodents is similar to human colon cancer gene expression profiles (Dunnick et al., 2012). More studies are needed to understand the potential PBDE-induced colon cancer mediated by unconjugated BAs. In addition, it has been shown in mice that unconjugated BAs are substrates for the major basolateral xenobiotic uptake transporter Oatp1b2, which is the mouse ortholog to human OATP1B1/1B3 (Csanaky et al., 2011). Genetic polymorphisms of OATP1B1/1B3 are implicated in altered pharmacokinetics of many clinical drugs such as statins and the subsequent adverse drug reactions (Akaike et al., 1991). Because PBDEs increased the endogenous Oatp1b2/OATP1B1/1B3 substrates (i.e. the

DMD Fast Forward. Published on May 16, 2018 as DOI: 10.1124/dmd.118.081547
This article has not been copyedited and formatted. The final version may differ from this version.

unconjugated BAs), it is possible that PBDEs may interfere with the hepatic uptake of many drugs that are OATP substrates. Further studies are necessary to determine the potential inhibitory effects of PBDE-induced increases in OATP-substrate BAs may alter the disposition and efficacy of drugs. In summary, in addition to their well characterized toxicities, PBDEs may produce additional adverse effects on human health through interfering with gut microbiome and bile acid metabolism as well as competing with hepatic uptake of other chemicals.

In general, unconjugated BAs are thought to be more toxic than their conjugated counterparts at excessive concentrations, evidenced by impaired liver functions and cholestasis (Fischer et al., 1996; Perez and Briz, 2009). In this study, unconjugated BAs were increased by PBDE exposure (Figures 6 and 7), suggesting that increased exposure to PBDEs could be a risk factor for liver injury. In particular, unconjugated BAs were increased almost 3-fold in liver (Figure 5B). This fold increase is similar to cholestatic liver injury observed in male adult mice exposed to oleanolic acid (Liu et al., 2013). The bacterial deconjugation enzyme *Bsh* had an increasing trend following BDE-99 exposure, although a statistical significance was not achieved; furthermore, among the 41 differentially regulated taxa, 5 were positively correlated with unconjugated secondary BAs, indicating that deconjugation of BAs by gut microbiota may not be the only mechanism for increased unconjugated BAs. A minor portion of BAs are conjugated to glucuronic acid in the liver by uridine 5'-diphospho-glucuronosyltransferases (UGTs) to decrease the toxicity and urinary excretion of unconjugated BAs (Barbier et al., 2009; Perreault et al., 2013; Chatterjee et al., 2014). Using human liver microsomes, it was shown that hydroxylated PBDEs can be glucuronidated by hepatic UGTs to increase urinary excretion (Erratico et al., 2015). However, in rat liver microsomes, glucuronidation of PBDEs inhibited the glucuronidation of 17β-estradiol (Lai et al., 2012). Therefore, the increased concentration of unconjugated BAs may be due to competitive inhibition by the glucorindation of hydroxylated PBDEs.

In conclusion, the present study using multi-omics approaches is among the first to show that oral exposure to PBDEs altered the gut microbiome and BA homeostasis (Figure 10). The key findings are: 1) PBDEs decreased bacterial diversity, but increased the taxa *A. muciniphila* and *Allobaculum spp*.; 2) PBDEs, and especially BDE-99, increased unconjugated BAs in the serum, liver, SIC, and LIC of CV mice; 3) the lack of gut microbiome mediated a shift in BA composition toward an increase in T-α/βMCA in GF mice; 4) PBDEs down-regulated enzymes and transporters involved in BA metabolism, in a gut microbiome dependent manner. The present study focused on the correlative rather than causal relationship between PBDE exposure and gut microbiome. It remains to be determined which specific bacteria are responsible for intestinal degradation of PBDEs. In addition, further research should be carried out to investigate the mechanism of *A. muciniphila* and *Allobaculum spp*. in host metabolism.

ACKNOWLEDGMENTS

The authors would like to thank the GNAC technical support for the germ-free mouse experiment, Dr. Debbie Nickerson's laboratory at UW Genome Sciences for sequencer access and support for the RNA-Seq experiments, Matt Karasu from UW School of Pharmacy for the proteomics data analysis, and other members of Dr. Cui laboratory for their help in tissue collection and revising the manuscript.

AUTHOR CONTRIBUTIONS

Participated in research design: Li, Gu, and Cui

Conducted experiments: Li, Wang, Lee, Dempsey, Weigel, Fei, Bhatt, Prasad, Gu, and Cui

Performed data analysis: Li, Wang, Lee, Dempsey, Weigel, Bhatt, Fei, Prasad, Gu, and Cui

Wrote or contributed to editing the manuscript: Li, Dempsey, Weigel, Raftery, Prasad, Gu, and Cui

REFERENCES

Ajouz H, Mukherji D, and Shamseddine A (2014) Secondary bile acids: an underrecognized cause of colon cancer. *World J Surg Oncol* **12:**164.

Akaike T, Kobayashi A, Tobe S, Takei Y, Goto M, and Kobayashi K (1991) [A preview of the practical application of hybrid artificial liver]. *Nihon Geka Gakkai Zasshi* **92:**1272-1275.

Alcock J and Lin HC (2015) Fatty acids from diet and microbiota regulate energy metabolism. *F1000Res* **4:**738.

Barbier O, Trottier J, Kaeding J, Caron P, and Verreault M (2009) Lipid-activated transcription factors control bile acid glucuronidation. *Mol Cell Biochem* **326:**3-8.

Bhatt DK and Prasad B (2017) Critical Issues and Optimized Practices in Quantification of Protein Abundance Level to Determine Interindividual Variability in DMET Proteins by LC-MS/MS Proteomics. *Clin Pharmacol Ther*.

Broeders EP, Nascimento EB, Havekes B, Brans B, Roumans KH, Tailleux A, Schaart G, Kouach M, Charton J, Deprez B, Bouvy ND, Mottaghy F, Staels B, van Marken Lichtenbelt WD, and Schrauwen P (2015) The Bile Acid Chenodeoxycholic Acid Increases Human Brown Adipose Tissue Activity. *Cell Metab* **22:**418-426.

Caporaso JG, Kuczynski J, Stombaugh J, Bittinger K, Bushman FD, Costello EK, Fierer N, Pena AG, Goodrich JK, Gordon JI, Huttley GA, Kelley ST, Knights D, Koenig JE, Ley RE, Lozupone CA, McDonald D, Muegge BD, Pirrung M, Reeder J, Sevinsky JR, Turnbaugh PJ, Walters WA, Widmann J, Yatsunenko T, Zaneveld J, and Knight R (2010) QIIME allows analysis of high-throughput community sequencing data. *Nat Methods* **7:**335-336.

Chatterjee S, Bijsmans IT, van Mil SW, Augustijns P, and Annaert P (2014) Toxicity and intracellular accumulation of bile acids in sandwich-cultured rat hepatocytes: role of glycine conjugates. *Toxicol In Vitro* **28:**218-230.

Chiang JY (2003) Bile acid regulation of hepatic physiology: III. Bile acids and nuclear receptors. *Am J Physiol Gastrointest Liver Physiol* **284:**G349-356.

Chiang JY (2004) Regulation of bile acid synthesis: pathways, nuclear receptors, and mechanisms. *J Hepatol* **40:**539-551.

Csanaky IL, Lu H, Zhang Y, Ogura K, Choudhuri S, and Klaassen CD (2011) Organic anion-transporting polypeptide 1b2 (Oatp1b2) is important for the hepatic uptake of unconjugated bile acids: Studies in Oatp1b2-null mice. *Hepatology* **53:**272-281.

Derrien M, Belzer C, and de Vos WM (2017) Akkermansia muciniphila and its role in regulating host functions. *Microb Pathog* **106:**171-181.

DeSantis TZ, Hugenholtz P, Larsen N, Rojas M, Brodie EL, Keller K, Huber T, Dalevi D, Hu P, and Andersen GL (2006) Greengenes, a chimera-checked 16S rRNA gene database and workbench compatible with ARB. *Appl Environ Microbiol* **72:**5069-5072.

Dunnick JK, Brix A, Cunny H, Vallant M, and Shockley KR (2012) Characterization of polybrominated diphenyl ether toxicity in Wistar Han rats and use of liver microarray data for predicting disease susceptibilities. *Toxicol Pathol* **40:**93-106.

Dunnick JK, Heath JE, Farnell DR, Prejean JD, Haseman JK, and Elwell MR (1997) Carcinogenic activity of the flame retardant, 2,2-bis(bromomethyl)-1,3-propanediol in rodents, and comparison with the carcinogenicity of other NTP brominated chemicals. *Toxicol Pathol* **25:**541-548.

Edgar RC (2010) Search and clustering orders of magnitude faster than BLAST. *Bioinformatics* **26:**2460-2461.

Erratico C, Zheng X, Ryden A, Marsh G, Maho W, and Covaci A (2015) Human hydroxylated metabolites of BDE-47 and BDE-99 are glucuronidated and sulfated in vitro. *Toxicol Lett* **236:**98-109.

Erratico CA, Moffatt SC, and Bandiera SM (2011) Comparative oxidative metabolism of BDE-47 and BDE-99 by rat hepatic microsomes. *Toxicol Sci* **123:**37-47.

Fischer S, Beuers U, Spengler U, Zwiebel FM, and Koebe HG (1996) Hepatic levels of bile acids in end-stage chronic cholestatic liver disease. *Clin Chim Acta* **251:**173-186.

Frederiksen M, Vorkamp K, Thomsen M, and Knudsen LE (2009) Human internal and external exposure to PBDEs--a review of levels and sources. *Int J Hyg Environ Health* **212:**109-134.

Fu ZD and Cui JY (2017) Remote Sensing between Liver and Intestine: Importance of Microbial Metabolites. *Curr Pharmacol Rep* **3:**101-113.

Gascon M, Vrijheid M, Martinez D, Forns J, Grimalt JO, Torrent M, and Sunyer J (2011) Effects of pre and postnatal exposure to low levels of polybromodiphenyl ethers on neurodevelopment and thyroid hormone levels at 4 years of age. *Environ Int* **37:**605-611.

Geenes V, Chambers J, Khurana R, Shemer EW, Sia W, Mandair D, Elias E, Marschall HU, Hague W, and Williamson C (2015) Rifampicin in the treatment of severe intrahepatic cholestasis of pregnancy. *Eur J Obstet Gynecol Reprod Biol* **189:**59-63.

Hu X, Bonde Y, Eggertsen G, and Rudling M (2014) Muricholic bile acids are potent regulators of bile acid synthesis via a positive feedback mechanism. *J Intern Med* **275:**27-38.

Imray CH, Radley S, Davis A, Barker G, Hendrickse CW, Donovan IA, Lawson AM, Baker PR, and Neoptolemos JP (1992) Faecal unconjugated bile acids in patients with colorectal cancer or polyps. *Gut* **33:**1239-1245.

Jumpertz R, Le DS, Turnbaugh PJ, Trinidad C, Bogardus C, Gordon JI, and Krakoff J (2011) Energy-balance studies reveal associations between gut microbes, caloric load, and nutrient absorption in humans. *Am J Clin Nutr* **94:**58-65.

Klaassen CD and Cui JY (2015) Review: Mechanisms of How the Intestinal Microbiota Alters the Effects of Drugs and Bile Acids. *Drug Metab Dispos* **43:**1505-1521.

Lai Y, Lu M, Lin S, and Cai Z (2012) Glucuronidation of hydroxylated polybrominated diphenyl ethers and their modulation of estrogen UDP-glucuronosyltransferases. *Chemosphere* **86:**727-734.

Langille MG, Zaneveld J, Caporaso JG, McDonald D, Knights D, Reyes JA, Clemente JC, Burkepile DE, Vega Thurber RL, Knight R, Beiko RG, and Huttenhower C (2013) Predictive functional profiling of microbial communities using 16S rRNA marker gene sequences. *Nat Biotechnol* **31:**814-821.

Li CY, Lee S, Cade S, Kuo LJ, Schultz IR, Bhatt DK, Prasad B, Bammler TK, and Cui JY (2017) Novel Interactions between Gut Microbiome and Host Drug-processing Genes Modify the Hepatic Metabolism of the Environmental Chemicals PBDEs. *Drug Metab Dispos*.

Lickteig AJ, Csanaky IL, Pratt-Hyatt M, and Klaassen CD (2016) Activation of Constitutive Androstane Receptor (CAR) in Mice Results in Maintained Biliary Excretion of Bile Acids Despite a Marked Decrease of Bile Acids in Liver. *Toxicol Sci*.

Linares V, Belles M, and Domingo JL (2015) Human exposure to PBDE and critical evaluation of health hazards. *Arch Toxicol* **89:**335-356.

Liu J, Lu YF, Zhang Y, Wu KC, Fan F, and Klaassen CD (2013) Oleanolic acid alters bile acid metabolism and produces cholestatic liver injury in mice. *Toxicol Appl Pharmacol* **272:**816-824.

Liu Y, Zhang Y, Zhang X, Xu Q, Yang X, and Xue C (2017) Medium-chain fatty acids reduce serum cholesterol by regulating the metabolism of bile acid in C57BL/6J mice. *Food Funct* **8:**291-298.

Lundgren M, Darnerud PO, and Ilback NG (2013) The flame-retardant BDE-99 dose-dependently affects viral replication in CVB3-infected mice. *Chemosphere* **91:**1434-1438.

Makey CM, McClean MD, Braverman LE, Pearce EN, He XM, Sjodin A, Weinberg JM, and Webster TF (2016) Polybrominated Diphenyl Ether Exposure and Thyroid Function Tests in North American Adults. *Environ Health Perspect* **124:**420-425.

Miyata M, Hayashi K, Yamakawa H, Yamazoe Y, and Yoshinari K (2015) Antibacterial drug treatment increases intestinal bile acid absorption via elevated levels of ileal apical

sodium-dependent bile acid transporter but not organic solute transporter alpha protein. *Biol Pharm Bull* **38:**493-496.

Packey CD, Shanahan MT, Manick S, Bower MA, Ellermann M, Tonkonogy SL, Carroll IM, and Sartor RB (2013) Molecular detection of bacterial contamination in gnotobiotic rodent units. *Gut Microbes* **4:**361-370.

Pacyniak EK, Cheng X, Cunningham ML, Crofton K, Klaassen CD, and Guo GL (2007) The flame retardants, polybrominated diphenyl ethers, are pregnane X receptor activators. *Toxicol Sci* **97:**94-102.

Padda MS, Sanchez M, Akhtar AJ, and Boyer JL (2011) Drug-induced cholestasis. *Hepatology* **53:**1377-1387.

Perez MJ and Briz O (2009) Bile-acid-induced cell injury and protection. *World J Gastroenterol* **15:**1677-1689.

Perreault M, Bialek A, Trottier J, Verreault M, Caron P, Milkiewicz P, and Barbier O (2013) Role of glucuronidation for hepatic detoxification and urinary elimination of toxic bile acids during biliary obstruction. *PLoS One* **8:**e80994.

Png CW, Linden SK, Gilshenan KS, Zoetendal EG, McSweeney CS, Sly LI, McGuckin MA, and Florin TH (2010) Mucolytic bacteria with increased prevalence in IBD mucosa augment in vitro utilization of mucin by other bacteria. *Am J Gastroenterol* **105:**2420-2428.

Prasad B and Unadkat JD (2014) Optimized approaches for quantification of drug transporters in tissues and cells by MRM proteomics. *AAPS J* **16:**634-648.

Ravussin Y, Koren O, Spor A, LeDuc C, Gutman R, Stombaugh J, Knight R, Ley RE, and Leibel RL (2012) Responses of gut microbiota to diet composition and weight loss in lean and obese mice. *Obesity (Silver Spring)* **20:**738-747.

Ridlon JM, Kang DJ, and Hylemon PB (2006) Bile salt biotransformations by human intestinal bacteria. *J Lipid Res* **47:**241-259.

Robrock KR, Korytar P, and Alvarez-Cohen L (2008) Pathways for the anaerobic microbial debromination of polybrominated diphenyl ethers. *Environ Sci Technol* **42:**2845-2852.

Russell DW (2003) The enzymes, regulation, and genetics of bile acid synthesis. *Annu Rev Biochem* **72:**137-174.

Sayin SI, Wahlstrom A, Felin J, Jantti S, Marschall HU, Bamberg K, Angelin B, Hyotylainen T, Oresic M, and Backhed F (2013) Gut microbiota regulates bile acid metabolism by reducing the levels of tauro-beta-muricholic acid, a naturally occurring FXR antagonist. *Cell Metab* **17:**225-235.

Sberna AL, Assem M, Gautier T, Grober J, Guiu B, Jeannin A, Pais de Barros JP, Athias A, Lagrost L, and Masson D (2011) Constitutive androstane receptor activation stimulates faecal bile acid excretion and reverse cholesterol transport in mice. *J Hepatol* **55:**154-161.

Selwyn FP, Cheng SL, Bammler TK, Prasad B, Vrana M, Klaassen C, and Cui JY (2015a) Developmental Regulation of Drug-Processing Genes in Livers of Germ-Free Mice. *Toxicol Sci* **147:**84-103.

Selwyn FP, Csanaky IL, Zhang Y, and Klaassen CD (2015b) Importance of Large Intestine in Regulating Bile Acids and Glucagon-Like Peptide-1 in Germ-Free Mice. *Drug Metab Dispos* **43:**1544-1556.

Shreiner AB, Kao JY, and Young VB (2015) The gut microbiome in health and in disease. *Curr Opin Gastroenterol* **31:**69-75.

Siddiqi MA, Laessig RH, and Reed KD (2003) Polybrominated diphenyl ethers (PBDEs): new pollutants-old diseases. *Clin Med Res* **1:**281-290.

Sueyoshi T, Li L, Wang H, Moore R, Kodavanti PR, Lehmler HJ, Negishi M, and Birnbaum LS (2014) Flame retardant BDE-47 effectively activates nuclear receptor CAR in human primary hepatocytes. *Toxicol Sci* **137:**292-302.

van Passel MW, Kant R, Zoetendal EG, Plugge CM, Derrien M, Malfatti SA, Chain PS, Woyke T, Palva A, de Vos WM, and Smidt H (2011) The genome of Akkermansia muciniphila, a dedicated intestinal mucin degrader, and its use in exploring intestinal metagenomes. *PLoS One* **6:**e16876.

Vazquez-Baeza Y, Pirrung M, Gonzalez A, and Knight R (2013) EMPeror: a tool for visualizing high-throughput microbial community data. *Gigascience* **2:**16.

Wang Q, Garrity GM, Tiedje JM, and Cole JR (2007) Naive Bayesian classifier for rapid assignment of rRNA sequences into the new bacterial taxonomy. *Appl Environ Microbiol* **73:**5261-5267.

Xu M, Chen X, Qiu M, Zeng X, Xu J, Deng D, Sun G, Li X, and Guo J (2012) Bar-coded pyrosequencing reveals the responses of PBDE-degrading microbial communities to electron donor amendments. *PLoS One* **7:**e30439.

Yang CW, Huang HW, and Chang BV (2017) Microbial communities associated with anaerobic degradation of polybrominated diphenyl ethers in river sediment. *J Microbiol Immunol Infect* **50:**32-39.

Zhang Y and Klaassen CD (2010) Effects of feeding bile acids and a bile acid sequestrant on hepatic bile acid composition in mice. *J Lipid Res* **51:**3230-3242.

Zhao S, Liu W, Wang J, Shi J, Sun Y, Wang W, Ning G, Liu R, and Hong J (2017) Akkermansia muciniphila improves metabolic profiles by reducing inflammation in chow diet-fed mice. *J Mol Endocrinol* **58:**1-14.

FOOTNOTES

Cindy Yanfei Li and Joseph Dempsey contributed equally to this work.

Funding Information

This work was supported by National Institutes of Health (NIH) grants [GM111381, ES019487, ES025708, T32 ES007032], the University of Washington Center for Exposures, Diseases, Genomics, and Environment [P30 ES0007033], and the Murphy Endowment.

DMD Fast Forward. Published on May 16, 2018 as DOI: 10.1124/dmd.118.081547
This article has not been copyedited and formatted. The final version may differ from this version.

FIGURE LEGENDS

Figure 1. A diagram illustrating the experimental design and dosing regimen of mice. Briefly, 9-week-old C57BL/6 CV and GF mice were exposed to vehicle (corn oil, 10ml/kg, oral gavage), BDE-47 (100 μmol/kg, oral gavage) or BDE-99 (100 μmol/kg, oral gavage) once daily for 4 consecutive days. Tissues were collected 24h after the final dose (n = 3-5 per group). The expression of genes involved in BA synthesis, conjugation, and transport was determined by RNA-Seq and targeted proteomics using LC-MS/MS. The gut microbiota from LIC of CV mice was determined by 16S rRNA sequencing. BAs in serum, liver, SIC and LIC were determined by targeted metabolomics. A total of 56 BAs was quantified (as listed in Supplemental Table 1), including primary and secondary BAs in either conjugated or unconjugated form.

Figure 2. Alpha diversity (**A**) and beta diversity (**B**) of gut microbiota in LIC of CV mice exposed to corn oil, BDE-47 (100 μmol/kg, oral gavage), or BDE-99 (100 μmol/kg, oral gavage) (n=3 per group). Data were analyzed using QIIME as described in Materials and Methods. Asterisks represent statistically significant differences as compared to corn oil-treated group (t-test, $p<0.05$). (**C**) The differentially regulated taxa at class level by BDE-47 and BDE-99 compared with corn oil-exposed group. Data were presented as mean percentage of operational taxonomical units (OTUs) ± SE. Asterisks represent statistically significant differences as compared to corn oil-exposed group (ANOVA, Duncan's post hoc test, $p<0.05$).

Figure 3. Differentially regulated taxa at the species level by PBDEs in LIC of CV mice. (**A**) A two-way hierarchical clustering dendrogram of the differentially regulated taxa at the species level (41 in total). Data were analyzed using JMP Genomics as described in Materials and Methods. Red represents relatively high abundance and blue represents relatively low abundance. (**B**) The top 10 most abundant bacterial species that were differentially regulated by PBDEs in LIC of CV mice. The taxa that were lower than the top 9 were summed and

presented as "other taxa" as the 10th category. (**C**) QPCR quanification of *Akkermansia muciniphila*, *Erysipelotrichaceae Allobaculum spp.* and *Clostridium scindens*, as well as microbial enzymes involved in secondary BA synthesis (*baiJ*, *baiCD*, and *bsh*) in LIC of CV mice (n=3 per group). Asterisks represent statistically significant differences as compared to corn oil-exposed group (ANOVA, Duncan's post hoc test, $p<0.05$).

Figure 4. Hierarchical clustering dendrograms of differentially regulated KEGG pathways predicted by PICRUSt, as described in Materials and Methods. (**A**) Bacteria-specific processes. (**B**) Xenobiotic biodegradation and metabolism. (**C**) Basal cellular processes. (**D**) Intermediary metabolism. Data were analyzed using JMP Genomics as described in Materials and Methods. Red represents relatively high expression, and blue represents relatively low expression. Asterisks (*) represent statistically significant differences as compared to corn oil-exposed group (ANOVA, Duncan's post hoc test, $p<0.05$).

Figure 6. Concentrations of unconjugated primary and secondary BAs in serum (**A**) and liver (**B**) of CV mice exposed to corn oil, BDE-47 (100 μmol/kg), or BDE-99 (100 μmol/kg). BAs were quantified using LC-MS/MS as described in Materials and Methods. Data were presented as mean ± SE (n=3 per group). Asterisks (*) represent statistically significant differences as compared to corn oil-exposed group by ANOVA (Duncan's post hoc test, $p<0.05$).

Figure 7. Concentrations of unconjugated primary and secondary BAs in SIC (**A**) and LIC (**B**) of CV mice exposed to corn oil, BDE-47(100 μmol/kg), or BDE-99 (100 μmol/kg). BAs were quantified using LC-MS/MS as described in Materials and Methods. Data were presented as mean ± SE (n= 3 per group). Asterisks (*) represent statistically significant differences as compared to corn oil-exposed group by ANOVA (Duncan's post hoc test, $p<0.05$).

Figure 8. Pearson's correlation between secondary BAs (including both taurine-conjugated and unconjugated BAs) and bacterial species that were differentially regulated by PBDE exposure (n=3). Each individual secondary BAs from all four compartments of CV mice were summed and used as an input (unit: nmol/ml). Each column represents one bacterial species (unit: operational taxonomical unit). Red represents positively correlated, and blue represents negatively correlated.

Figure 9. Messenger RNA and protein expression of various BA-processing genes in liver and intestine of CV and GF mice exposed to corn oil, BDE-47 (100 μmol/kg), or BDE-99 (100 μmol/kg). (**A**) Hepatic mRNA of Cyp7a1 and protein expression of other genes involved in BA synthesis (*Cyp8b1, Cyp27a1, Cyp7b1, Hsd3b7,* and *Akr1c14*) and conjugation (Slc27a5). Cyp7a1 mRNA expression was substituted for protein expression because the proteomics method cannot accurately detect proteins with an FPKM less than 20. (**B**) Hepatic protein expression of uptake transporters Ntcp and Oatp1b2, as well as the efflux transporter Bsep. (**C**) Messenger RNA expression of *Asbt, Ostα, Ostβ, Mrp4,* and *Fgf15* in intestine of CV and GF mice. Asterisks (*) represent statistically significant differences between corn oil- and PBDE-exposed groups within CV or GF mouse colonies. Pounds (#) represent statistically significant differences between CV and GF mice under the same exposure ($p<0.05$).

Figure 10. A diagram illustrating the major findings of the present study. Briefly, 1) PBDEs decreased bacterial diversity, but increased the taxa *A. muciniphila* and *Allobaculum spp.*; 2) PBDEs increased unconjugated BAs in the serum, liver, SIC, and LIC of CV mice; 3) the lack of gut microbiome led to a shift in BA composition toward an increase in T-α/βMCA in GF mice; 4) PBDEs down-regulated host enzymes and transporters involved in BA metabolism in a gut microbiota-dependent manner.

DMD Fast Forward. Published on May 16, 2018 as DOI: 10.1124/dmd.118.081547
This article has not been copyedited and formatted. The final version may differ from this version.

Figure 1

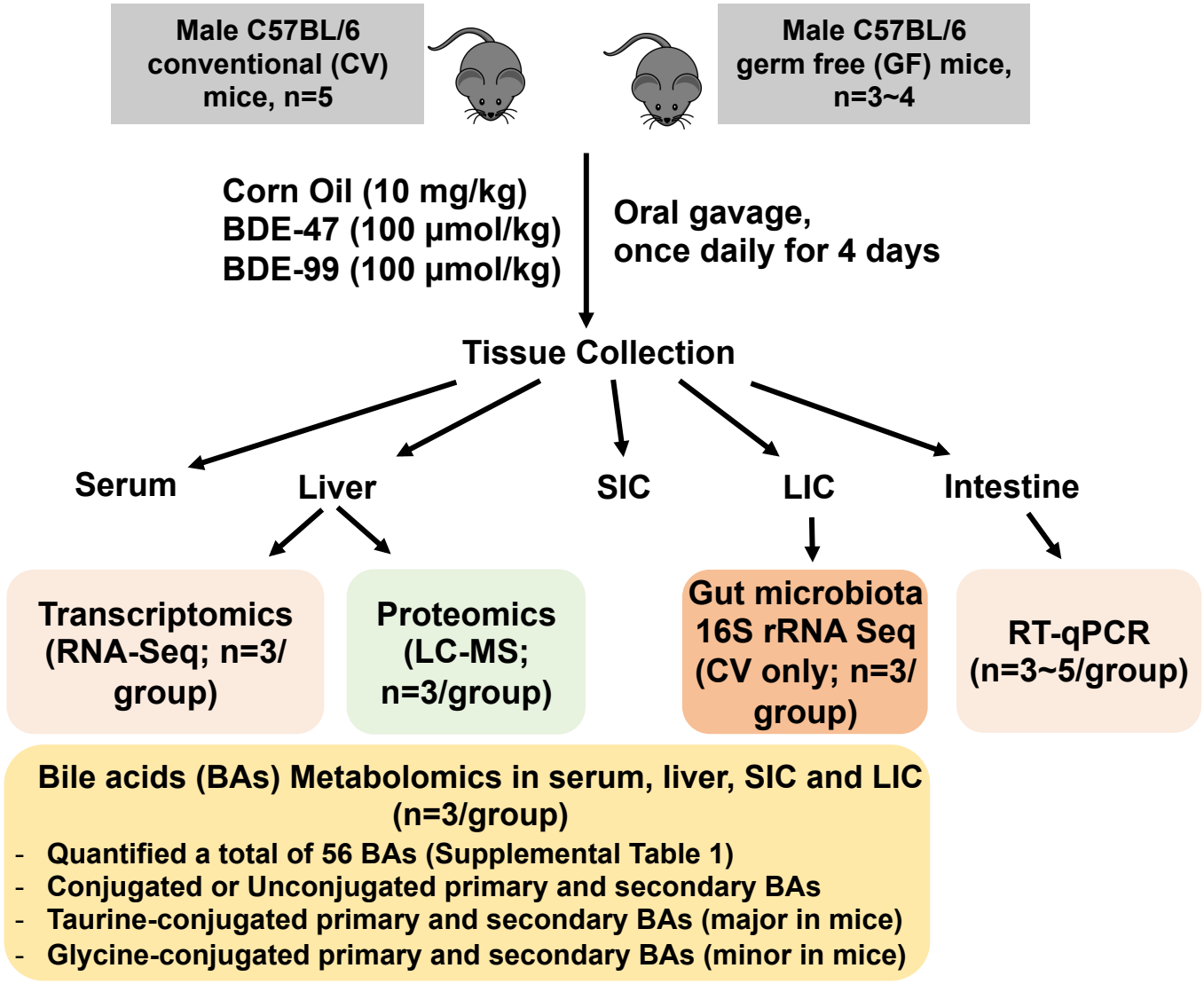

DMD Fast Forward. Published on May 16, 2018 as DOI: 10.1124/dmd.118.081547
This article has not been copyedited and formatted. The final version may differ from this version.

Figure 2

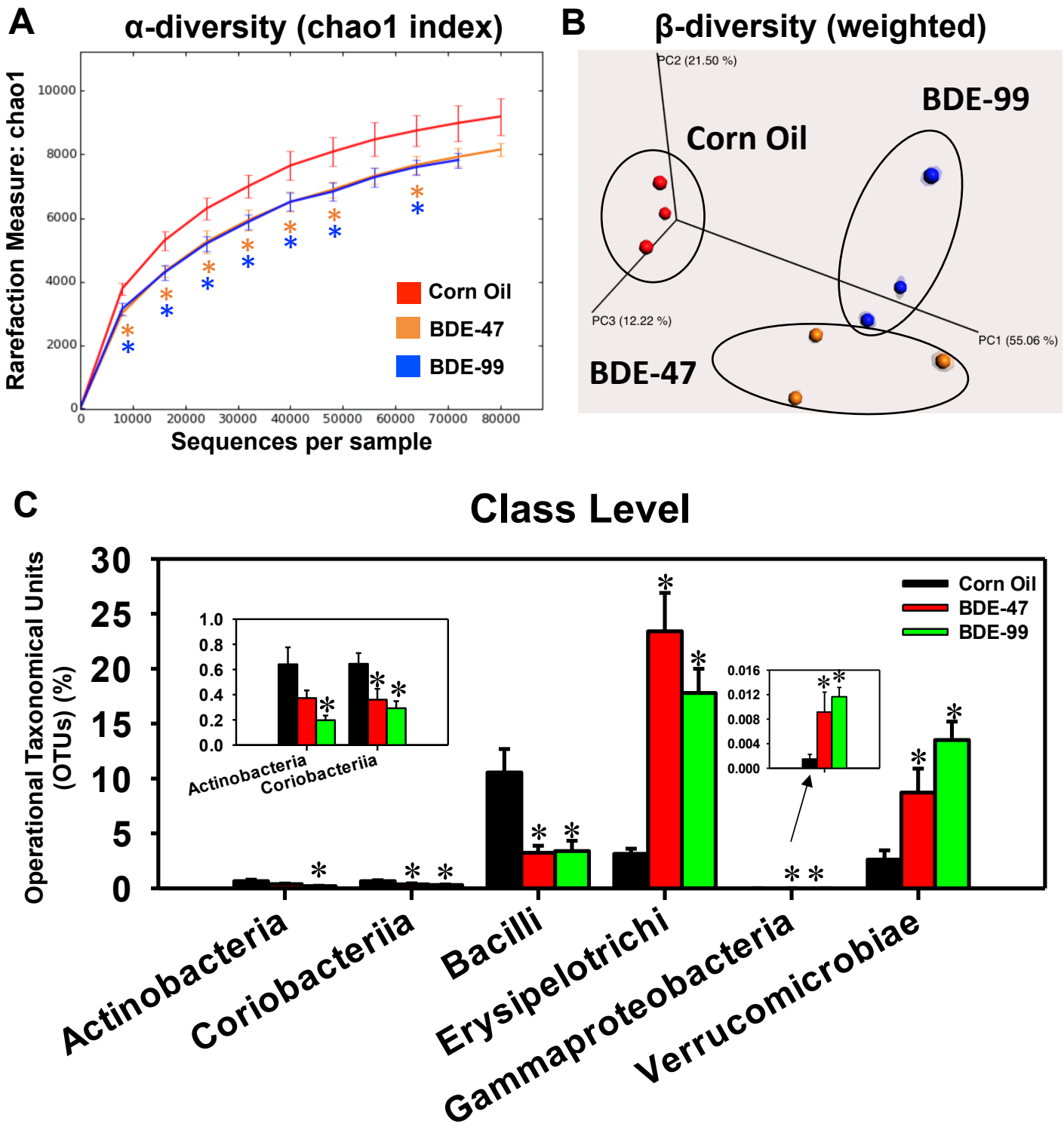

Figure 3

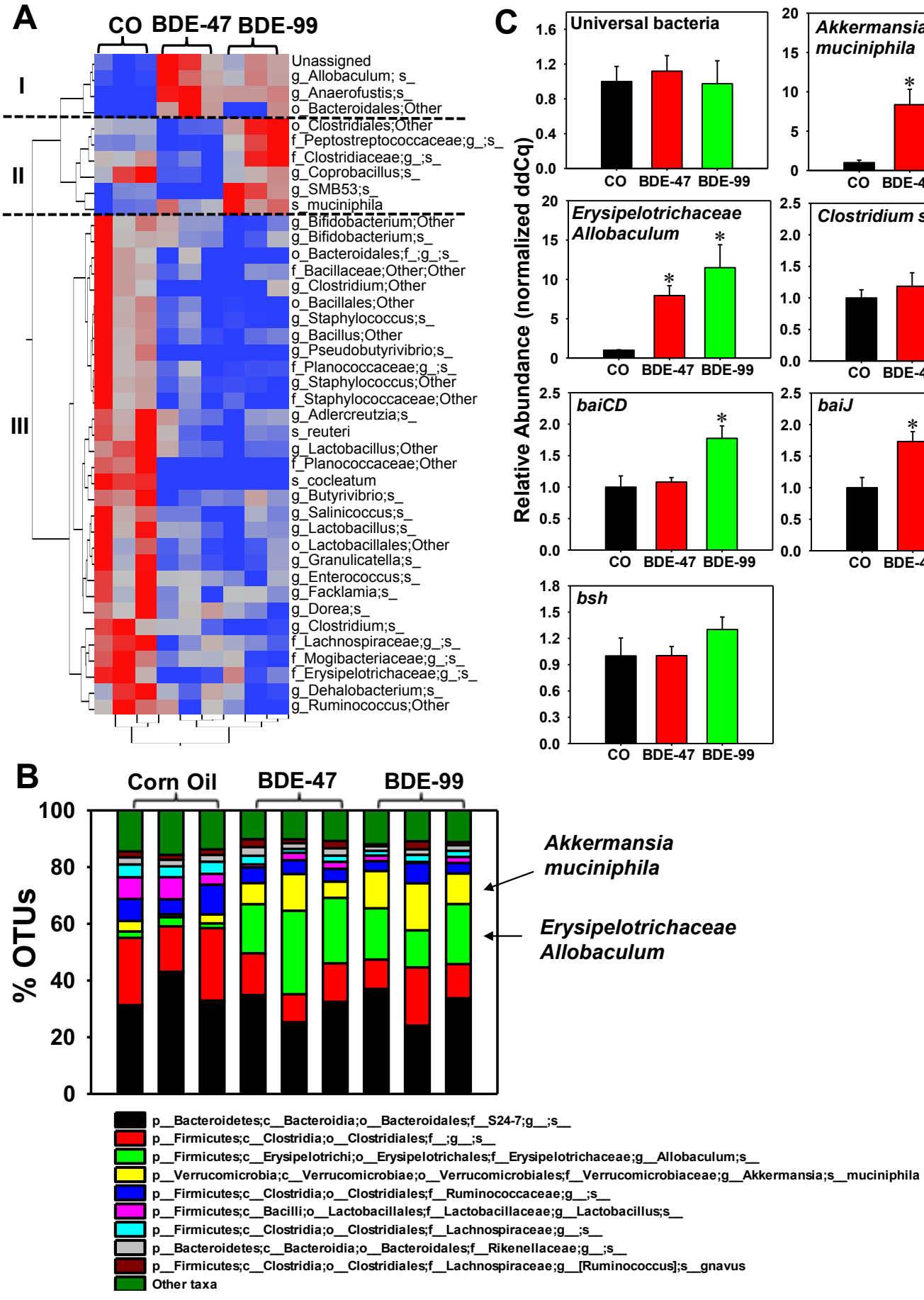
A
CO BDE-47 BDE-99
I
II
III
Unassigned
g_Allobaculum; s_
g_Anaerofustis;s_
o_Bacteroidales;Other
o_Clostridiales;Other
f_Peptostreptococcaceae;g_;s_
f_Clostridiaceae;g_;s_
g_Coprobacillus;s_
g_SMB53;s_
s_muciniphila
g_Bifidobacterium;Other
g_Bifidobacterium;s_
o_Bacteroidales;f_;g_;s_
f_Bacillaceae;Other;Other
g_Clostridium;Other
o_Bacillales;Other
g_Staphylococcus;s_
g_Bacillus;Other
g_Pseudobutyrivibrio;s_
f_Planococcaceae;g_;s_
g_Staphylococcus;Other
f_Staphylococcaceae;Other
g_Adlercreutzia;s_
s_reuteri
g_Lactobacillus;Other
f_Planococcaceae;Other
s_cocleatum
g_Butyrivibrio;s_
g_Salinicoccus;s_
g_Lactobacillus;s_
o_Lactobacillales;Other
g_Granulicatella;s_
g_Enterococcus;s_
g_Facklamia;s_
g_Dorea;s_
g_Clostridium;s_
f_Lachnospiraceae;g_;s_
f_Mogibacteriaceae;g_;s_
f_Erysipelotrichaceae;g_;s_
g_Dehalobacterium;s_
g_Ruminococcus;Other
C
Relative Abundance (normalized ddCq)
Universal bacteria
Akkermansia muciniphila
Erysipelotrichaceae Allobaculum
Clostridium scindens
baiCD
baiJ
bsh
CO BDE-47 BDE-99
B
Corn Oil BDE-47 BDE-99
% OTUs
Akkermansia muciniphila
Erysipelotrichaceae Allobaculum
p__Bacteroidetes;c__Bacteroidia;o__Bacteroidales;f__S24-7;g__;s__
p__Firmicutes;c__Clostridia;o__Clostridiales;f__;g__;s__
p__Firmicutes;c__Erysipelotrichi;o__Erysipelotrichales;f__Erysipelotrichaceae;g__Allobaculum;s__
p__Verrucomicrobia;c__Verrucomicrobiae;o__Verrucomicrobiales;f__Verrucomicrobiaceae;g__Akkermansia;s__muciniphila
p__Firmicutes;c__Clostridia;o__Clostridiales;f__Ruminococcaceae;g__;s__
p__Firmicutes;c__Bacilli;o__Lactobacillales;f__Lactobacillaceae;g__Lactobacillus;s__
p__Firmicutes;c__Clostridia;o__Clostridiales;f__Lachnospiraceae;g__;s__
p__Bacteroidetes;c__Bacteroidia;o__Bacteroidales;f__Rikenellaceae;g__;s__
p__Firmicutes;c__Clostridia;o__Clostridiales;f__Lachnospiraceae;g__[Ruminococcus];s__gnavus
Other taxa

Figure 4

A. Bacterial specific pathways

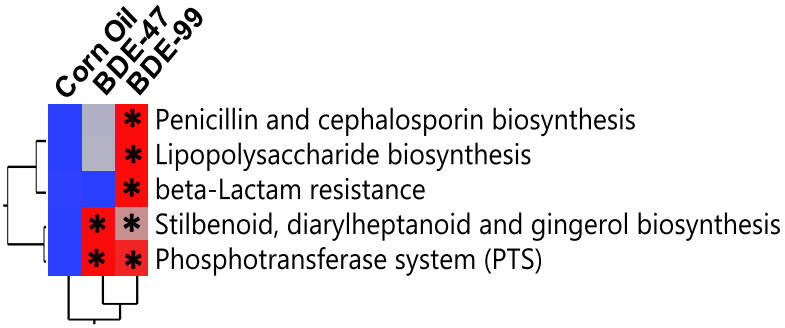

B. Xenobiotic biodegradation and metabolism

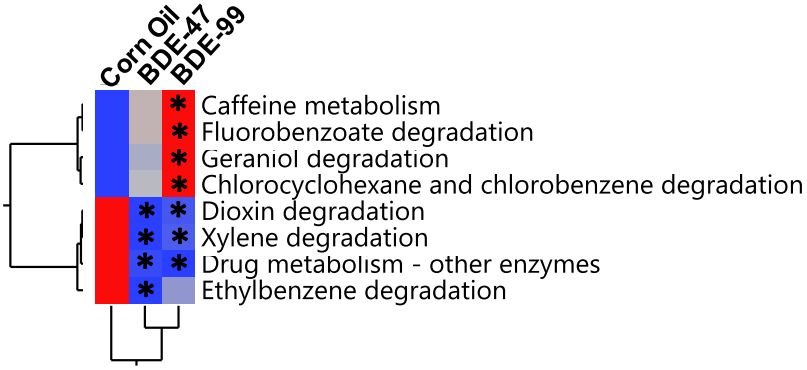

C. Cellular processes and signaling

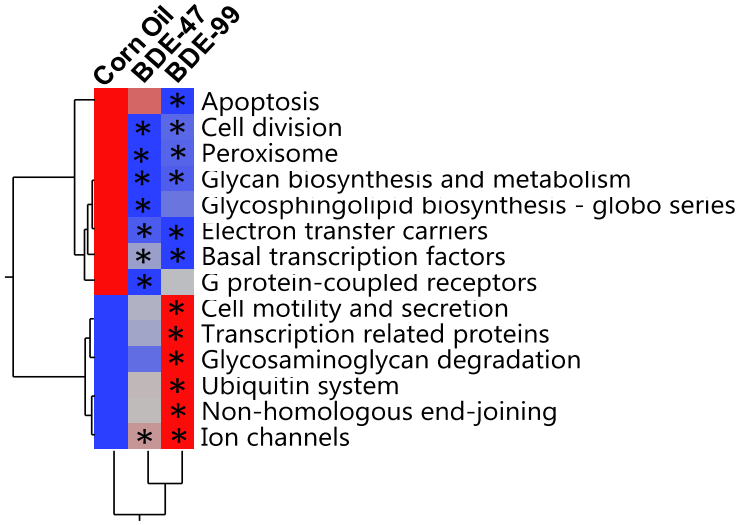

D. Intermediary metabolism

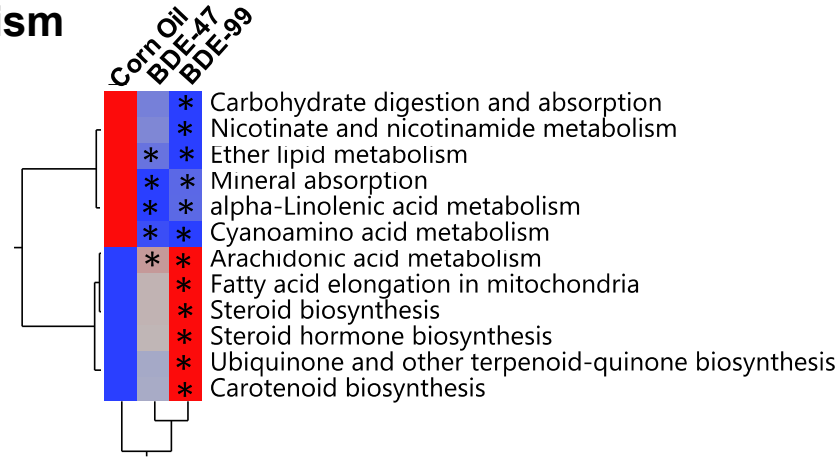

Figure 5

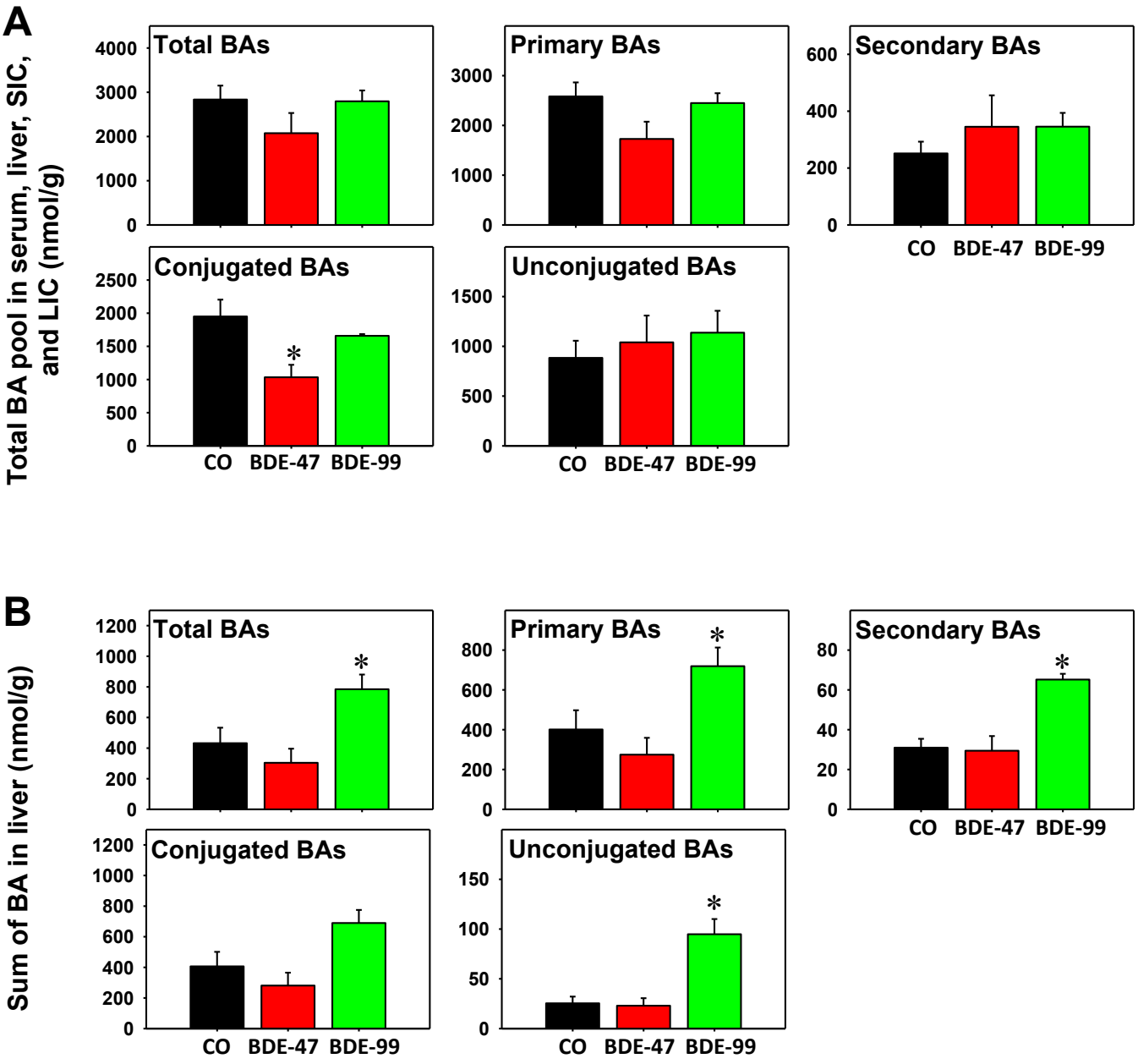
A
Total BA pool in serum, liver, SIC, and LIC (nmol/g)
Total BAs
Primary BAs
Secondary BAs
Conjugated BAs
Unconjugated BAs
CO
BDE-47
BDE-99
B
Sum of BA in liver (nmol/g)
Total BAs
Primary BAs
Secondary BAs
Conjugated BAs
Unconjugated BAs
CO
BDE-47
BDE-99

Figure 6

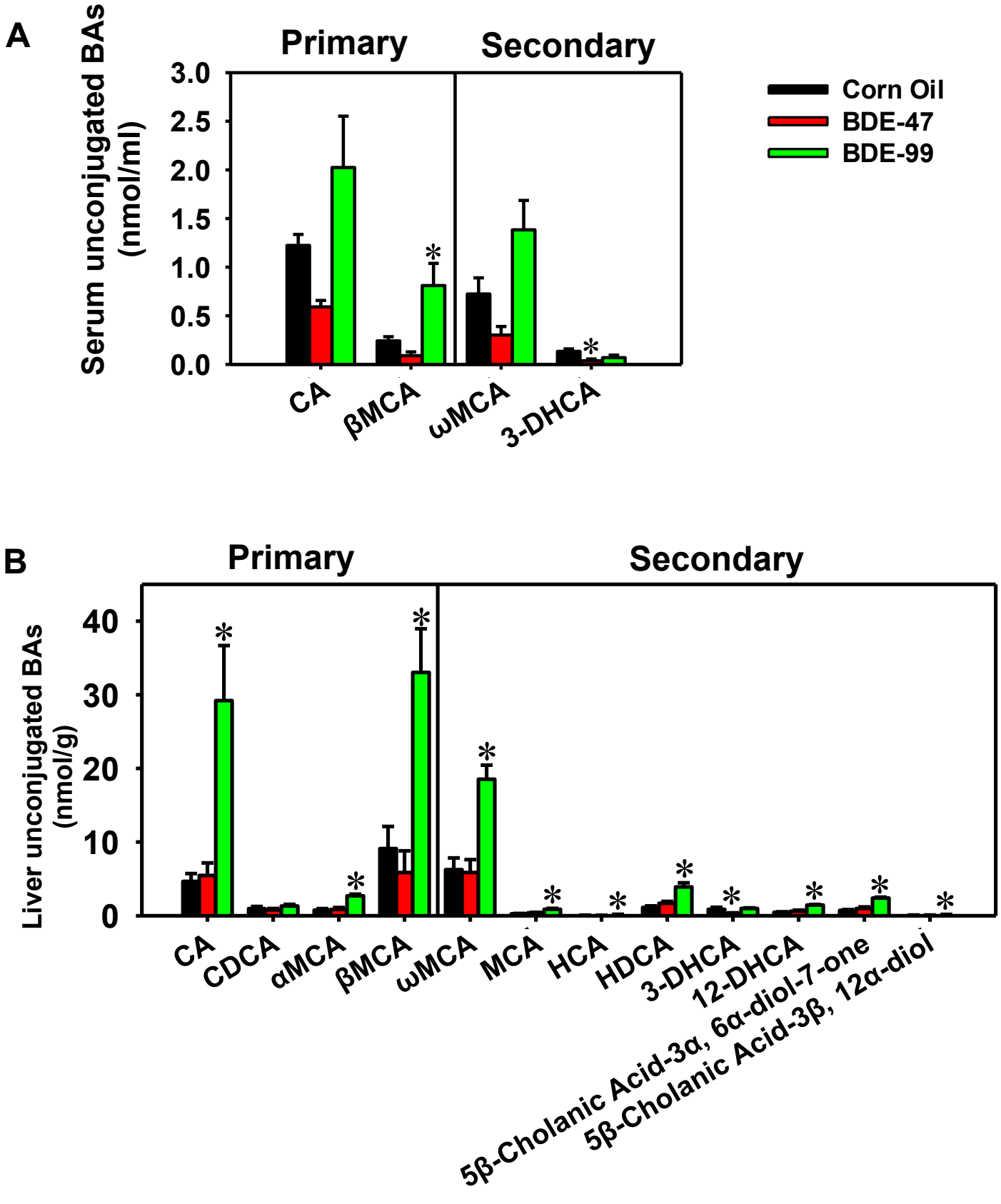
A
Primary
Secondary
Serum unconjugated BAs (nmol/ml)
3.0
2.5
2.0
1.5
1.0
0.5
0.0
Corn Oil
BDE-47
BDE-99
CA
βMCA
ωMCA
3-DHCA
B
Primary
Secondary
Liver unconjugated BAs (nmol/g)
40
30
20
10
0
CA
CDCA
αMCA
βMCA
ωMCA
MCA
HCA
HDCA
3-DHCA
12-DHCA
5β-Cholanic Acid-3α, 6α-diol-7-one
5β-Cholanic Acid-3β, 12α-diol

Figure 7

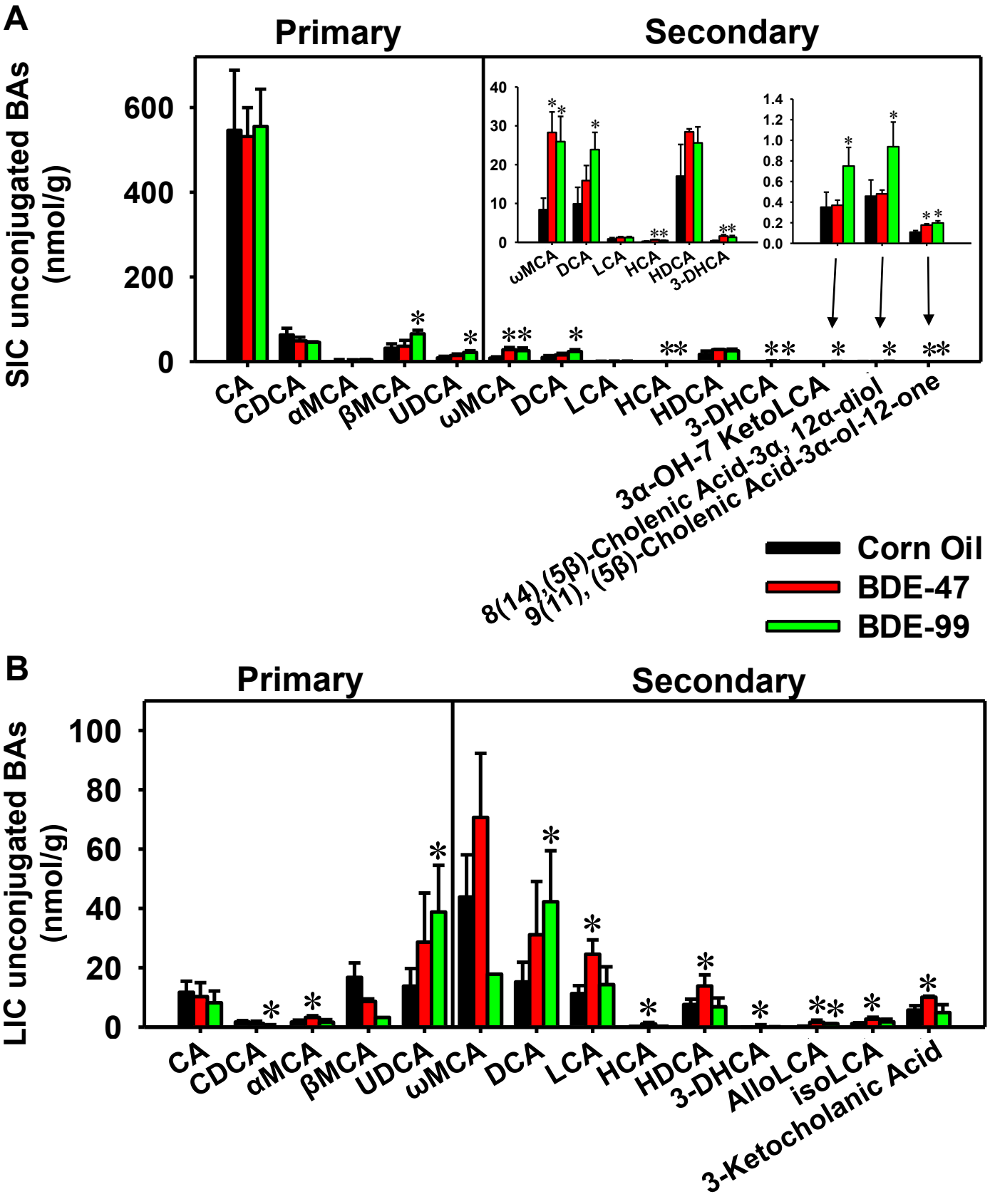
A
Primary
Secondary
SIC unconjugated BAs (nmol/g)
600
400
200
0
40
30
20
10
0
1.4
1.2
1.0
0.8
0.6
0.4
0.2
0.0
ωMCA
DCA
LCA
HCA
HDCA
3-DHCA
CA
CDCA
αMCA
βMCA
UDCA
ωMCA
DCA
LCA
HCA
HDCA
3-DHCA
3α-OH-7 KetoLCA
8(14),(5β)-Cholenic Acid-3α, 12α-diol
9(11), (5β)-Cholenic Acid-3α-ol-12-one
Corn Oil
BDE-47
BDE-99
B
Primary
Secondary
LIC unconjugated BAs (nmol/g)
100
80
60
40
20
0
CA
CDCA
αMCA
βMCA
UDCA
ωMCA
DCA
LCA
HCA
HDCA
3-DHCA
AlloLCA
isoLCA
3-Ketocholanic Acid

Figure 8

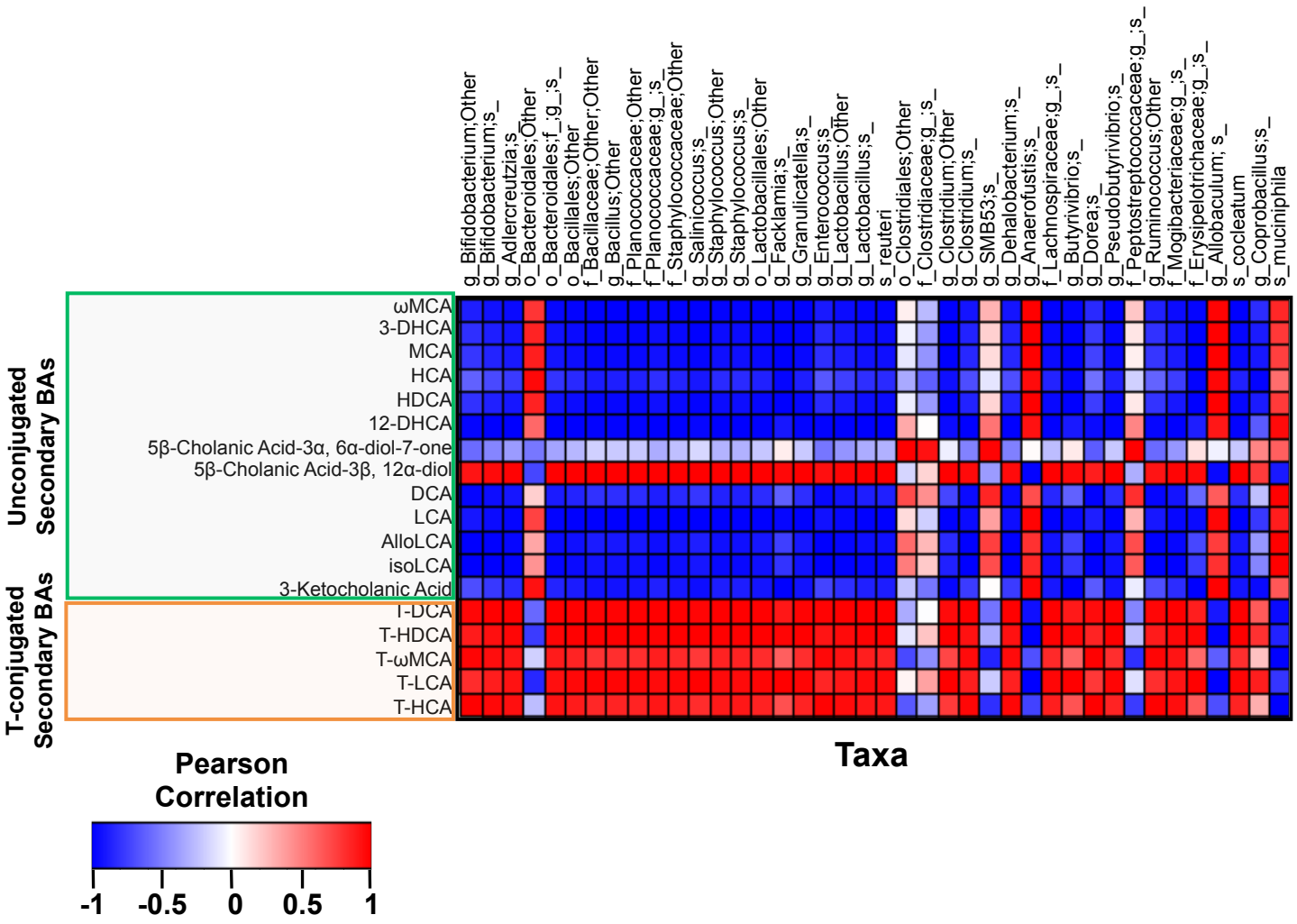
g_Bifidobacterium;Other
g_Bifidobacterium;s_
g_Adlercreutzia;s
o_Bacteroidales;Other
o_Bacteroidales;f_;g_;s_
o_Bacillales;Other
f_Bacillaceae;Other;Other
g_Bacillus;Other
f_Planococcaceae;Other
f_Planococcaceae;g_;s_
f_Staphylococcaceae;Other
g_Salinicoccus;s_
g_Staphylococcus;Other
g_Staphylococcus;s_
o_Lactobacillales;Other
g_Facklamia;s_
g_Granulicatella;s_
g_Enterococcus;s
g_Lactobacillus;Other
g_Lactobacillus;s_
s_reuteri
o_Clostridiales;Other
f_Clostridiaceae;g_;s_
g_Clostridium;Other
g_Clostridium;s_
g_SMB53;s_
g_Dehalobacterium;s_
g_Anaerofustis;s_
f_Lachnospiraceae;g_;s_
g_Butyrivibrio;s_
g_Dorea;s_
g_Pseudobutyrivibrio;s_
f_Peptostreptococcaceae;g_;s_
g_Ruminococcus;Other
f_Mogibacteriaceae;g_;s_
f_Erysipelotrichaceae;g_;s_
g_Allobaculum; s_
s_cocleatum
g_Coprobacillus;s_
s_muciniphila
Unconjugated Secondary BAs
ωMCA
3-DHCA
MCA
HCA
HDCA
12-DHCA
5β-Cholanic Acid-3α, 6α-diol-7-one
5β-Cholanic Acid-3β, 12α-diol
DCA
LCA
AlloLCA
isoLCA
3-Ketocholanic Acid
T-conjugated Secondary BAs
T-DCA
T-HDCA
T-ωMCA
T-LCA
T-HCA
Taxa
Pearson Correlation
-1
-0.5
0
0.5
1

Figure 9

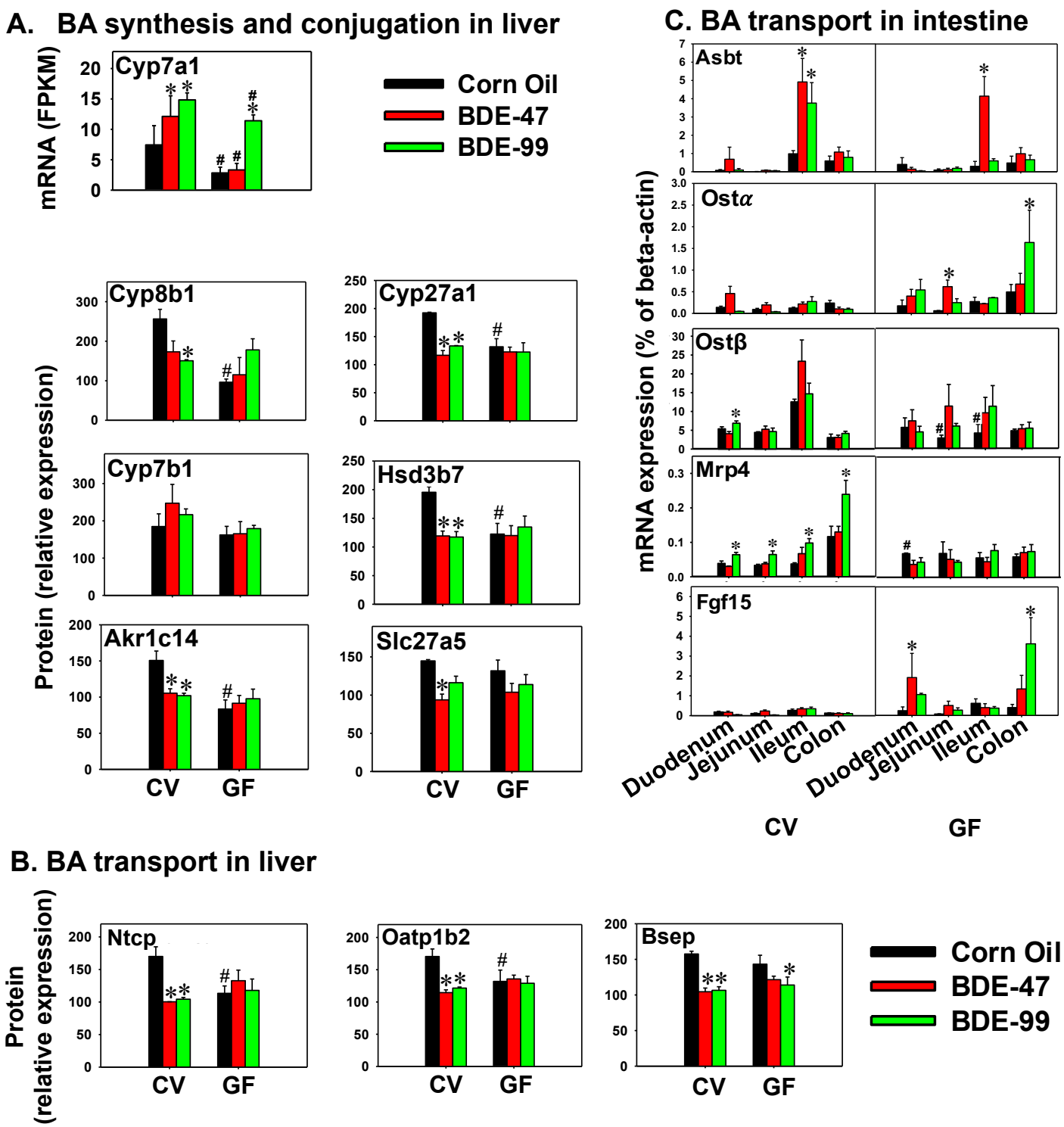
A. BA synthesis and conjugation in liver
mRNA (FPKM)
Cyp7a1
Corn Oil
BDE-47
BDE-99
Protein (relative expression)
Cyp8b1
Cyp27a1
Cyp7b1
Hsd3b7
Akr1c14
Slc27a5
CV
GF
C. BA transport in intestine
mRNA expression (% of beta-actin)
Asbt
Ostα
Ostβ
Mrp4
Fgf15
Duodenum
Jejunum
Ileum
Colon
CV
GF
B. BA transport in liver
Protein (relative expression)
Ntcp
Oatp1b2
Bsep
Corn Oil
BDE-47
BDE-99

Figure 10

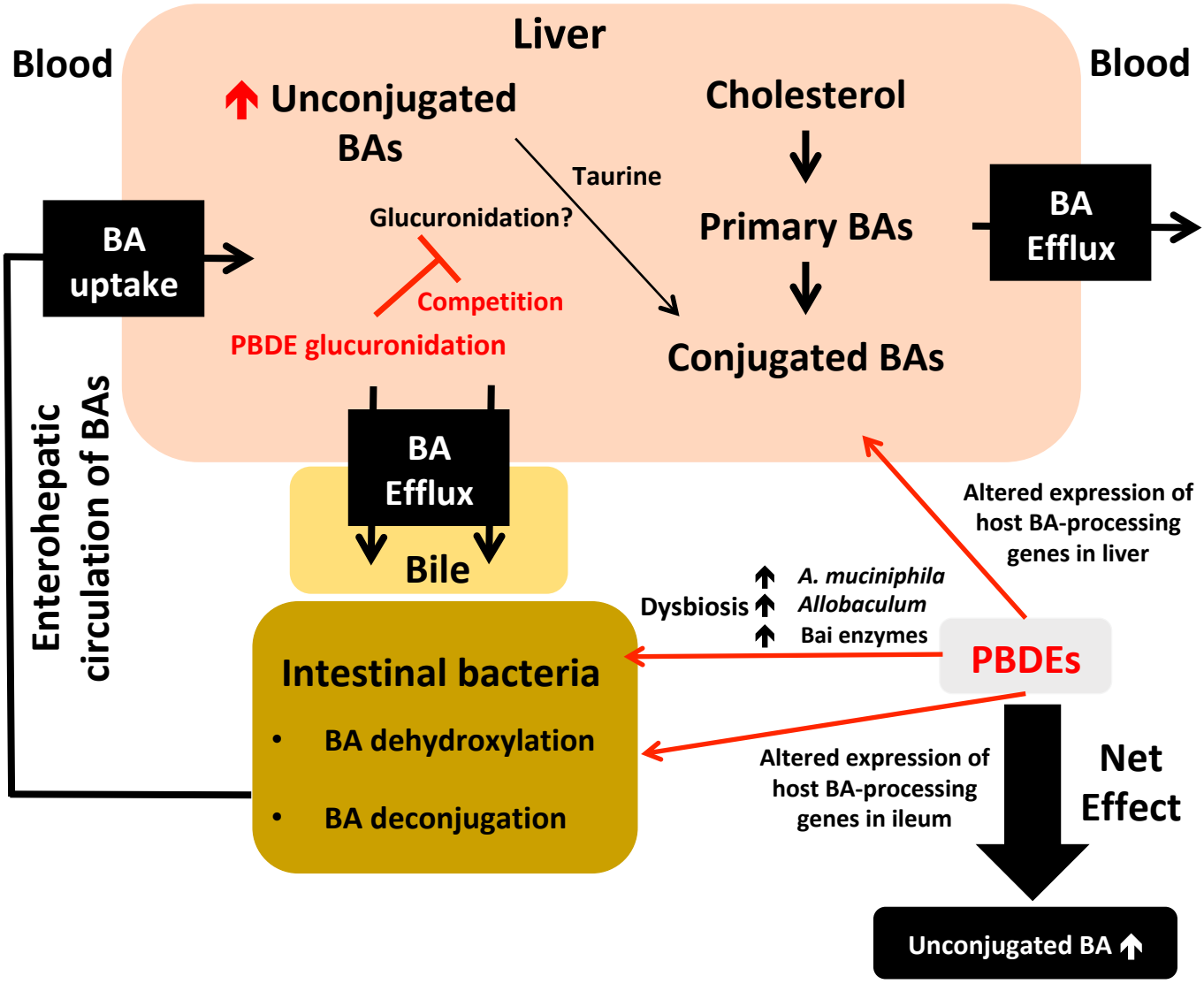
Liver
Blood
Blood
Unconjugated BAs
Cholesterol
Taurine
Primary BAs
BA Efflux
BA uptake
Glucuronidation?
Competition
PBDE glucuronidation
Conjugated BAs
BA Efflux
Bile
Enterohepatic circulation of BAs
Altered expression of host BA-processing genes in liver
Dysbiosis
A. muciniphila
Allobaculum
Bai enzymes
PBDEs
Intestinal bacteria
BA dehydroxylation
BA deconjugation
Altered expression of host BA-processing genes in ileum
Net Effect
Unconjugated BA

PBDEs Altered Gut Microbiome and Bile Acid Homeostasis in Male C57BL/6 Mice

Cindy Yanfei Li, Joseph L. Dempsey, Dongfang Wang, Soowan Lee, Kris M. Weigel, Qiang Fei, Deepak Kumar Bhatt, Bhagwat Prasad, Daniel Raftery, Haiwei Gu, and Julia Yue Cui

Department of Environmental and Occupational Health Sciences, University of Washington, Seattle, WA 98105, USA (CYF, JLD, KMW, SL, and JYC); Northwest Metabolomics Research Center, Department of Anesthesiology and Pain Medicine, University of Washington, 850 Republican St., Seattle, WA 98109, USA (DW, QF, and DR); Arizona Metabolomics Laboratory, Center for Metabolic and Vascular Biology, School of Nutrition and Health Promotion, College of Health Solutions, Arizona State University, Phoenix, AZ 85004, USA (HG); Department of Pharmaceutics, University of Washington, Seattle, WA 98105, USA (DKB, BP); Department of Laboratorial Science and Technology, School of Public Health, Peking University, Beijing 100191, P. R. China (DF); Department of Chemistry, Jilin University, Changchun, Jilin Province 130061, P. R. China (QF).

Drug Metabolism and Disposition

SUPPLEMENTAL MATERIALS - Figure Legend and Tables

Supplemental Figure 1. Differentially regulated taxa at phylum level by BDE-47 and BDE-99 compared with corn oil-treated group. Bacterial 16S rRNA sequencing was performed in large intestinal content of CV mice as described in MATERIALS AND METHODS.

Supplemental Figure 2. Concentrations of conjugated primary and secondary BAs in serum (**A**) and liver (**B**) of CV mice treated with corn oil, BDE-47 (100 μmol/kg) or BDE-99 (100 μmol/kg). BAs were quantified by LC-MS/MS as described in MATERIALS AND METHODS. Data are presented as mean ± S.E. n= 3 per group. Asterisks (*) represent statistically significant differences as compared to corn oil-treated group by ANOVA (Duncan's post hoc test, $p<0.05$).

Supplemental Figure 3. Concentrations of conjugated primary and secondary BAs in small intestinal content (SIC) (**A**) and large intestinal content (LIC) (**B**) of CV mice treated with corn oil, BDE-47 (100 μmol/kg) or BDE-99 (100 μmol/kg). BAs were quantified by LC-MS/MS as described in MATERIALS AND METHODS. Data are presented as mean ± S.E. n= 3 per group. Asterisks (*) represent statistically significant differences as compared to corn oil-treated group by ANOVA (Duncan's post hoc test, $p<0.05$).

Supplemental Figure 4. Bar chart (**A**) illustrating the percentage of individual BAs in serum across all six groups. The top 16 BAs in each group were plotted and all other detected BAs were summed together. Pie charts (**B**) showing the percentage of individual BAs in serum for each group for CV and GF mice exposed to corn oil, BDE-47 (100 μmol/kg), or BDE-99 (100 μmol/kg).

Supplemental Figure 5. Bar chart (**A**) illustrating the percentage of individual BAs in liver across all six groups The top 16 BAs in each group were plotted and all other detected BAs were summed together. Pie charts (**B**) showing the percentage of individual BAs in serum for each group for CV and GF mice exposed to corn oil, BDE-47 (100 μmol/kg), or BDE-99 (100 μmol/kg).

Supplemental Figure 6. Bar chart (**A**) illustrating the percentage of individual BAs in SIC across all six groups The top 16 BAs in each group were plotted and all other detected BAs were summed together. Pie charts (**B**) showing the percentage of individual BAs in serum for each group for CV and GF mice exposed to corn oil, BDE-47 (100 μmol/kg), or BDE-99 (100 μmol/kg).

Supplemental Figure 7. Bar chart (**A**) illustrating the percentage of individual BAs in LIC across all six groups The top 16 BAs in each group were plotted and all other detected BAs were summed together. Pie charts (**B**) showing the percentage of individual BAs in serum for each group for CV and GF mice exposed to corn oil, BDE-47 (100 μmol/kg), or BDE-99 (100 μmol/kg).

Supplemental Figure 8. Expression of other BA-processing genes in liver. Asterisks (*) represent statistically significant differences between corn oil- and PBDE-treated groups within CV or GF mouse colonies; pounds (#) represent statistically significant differences between CV and GF mice under the same treatment (Cuffdiff, $p<0.05$).

Supplemental Table 1. Primer sequences specific for bacterial cDNA and intestinal mRNA.

Target	Genes	Forward Primer (5'-3')	Reverse Primer (5'-3')
Bacterial DNA	*Universal bacteria*	GTGSTGCAYGGYTGTCGTCA	ACGTCRTCCMCACCTTCCTC
	Akkermansia muciniphila	TCCATTTGGTCCAGCAATTT	CGTGCGCCACTAGAGAATTA
	Clostridium scindens	TGACCGCGATCACAACTTT	GGCGCTTCGTTCGACTT
	Erysipelotrichaceae allobaculum	AGCGTTATCCGGAATGATTG	CCGCTACACATGGAGTTC
		CACGTAGTTAGCCGTGAC	GTAACACGTAGGGAACCTG
		CAGGAGAGGGCGGTGGAA	TTCGTGCCTCAGCGTCAG
		TCCTCGCCGGGTACCATC	TGAGCAAAGAGGAGGCATC
	baiCD	CAGCCCRCAGATGTTCTTTG	GCATGGAATTCWACTGCYTC
	baiJ	TCAGGACGTGGAGGCGATCCA	TACRTGATACTGGTAGCTCCA
	bsh	ATGGGCGGACTAGGATTACC	TGCCACTCTCTGTCTGCATC
Host mRNA	β-actin	GGCCAACCGTGAAAAGATGA	CAGCCTGGATGGCTACGTACA
	Asbt	ACAGCCTGGGTTTCTTCCTG	GGGGGAGAAGGAGAGCTGTA
	Ostα	TTGTGATCAACCGCATTTGT	CTCCTCAAGCCTCCAGTGTC
	Ostβ	ATCCTGGCAAACAGAAATCG	GGCCAAGTCTGGTTTCTCTG
	Mrp4	GCAAAGCCCATGTACCATCT	ACCACGGCTAACAACTCACC
	Fgf15	AGAACAGCTCCAGGACCAGA	TCCATGCTGTCACTCTCCAG

Supplemental Table 2. Bile acids quantified and normalized to corresponding internal standards.

BA names	Abbreviations	Compartment quantified	IS used for normalization
12-Dehydrocholic Acid	12-DHCA	Liver, Content	CA-D4
3,12-Diketocholanic Acid		Content	DCA-D4
3,6-Diketocholanic Acid		Content	DCA-D4
3,7-Diketocholanic Acid		Content	DCA-D4
3-Dehydrocholic Acid	3-DHCA	Serum, Liver, Content	CA-D4
3-Ketocholanic Acid		Content	LCA-D4
3α,12α,23-Nordeoxycholic Acid			DCA-D4
3α-Hydroxy-12 Ketolithocholic Acid	3α-OH-12 KetoLCA	Content	LCA-D4
3α-Hydroxy-6,7-DiketoCholanic Acid			CA-D4
3α-Hydroxy-7 Ketolithocholic Acid	3α-OH-7 KetoLCA	Content	DCA-D4
3α-Hydroxy-7,12-DiketoCholanic Acid			CA-D4
5-Cholenic acid-3β-ol			LCA-D4
5α-Cholanic Acid-3, 6-dione		Content	DCA-D4
5α-Cholanic Acid-3α-ol-6-one		Content	DCA-D4
5β-Cholanic Acid-3α, 6α-diol-7-one		Liver, Content	DCA-D4
5β-Cholanic Acid-3β, 12α-diol		Liver, Content	DCA-D4
8(14),(5β)-Cholenic Acid-3α, 12α-diol		Content	DCA-D4
9(11), (5β)-Cholenic Acid-3α-ol-12-one		Content	DCA-D4
Allolithocholic Acid	AlloLCA	Content	LCA-D4
Chenodeoxycholic Acid	CDCA	Liver, Content	DCA-D4
Cholic Acid	CA	Serum, Liver, Content	CA-D4
Dehydrocholic acid	DHCA		CA-D4
Deoxycholic Acid	DCA	Content	DCA-D4
Glycochenodeoxycholic Acid	G-CDCA	Serum, Liver, Content	GCDCA-D4
Glycocholic Acid	G-CA	Serum, Liver, Content	GCA-D4
Glycodehydrocholic Acid	G-DHCA	Content	GCA-D4
Glycodeoxycholic Acid	D-DCA	Content	GCDCA-D4
Glycohyocholic Acid	G-HCA		GCA-D4
Glycohyodeoxycholic Acid	G-HDCA	Content	GCDCA-D4
Glycolithocholic Acid	G-LCA		LCA-D4
Glyco-ursocholanic Acid			GCDCA-D4
Glycoursodeoxycholic Acid	G-UDCA	Content	GCDCA-D4
Hyocholic Acid	HCA	Liver, Content	CA-D4
Hyodeoxycholic Acid	HDCA	Liver, Content	DCA-D4
Isodeoxycholic Acid			DCA-D4
Isolithocholic Acid	IsoLCA	Content	LCA-D4
Lithocholenic Acid		Content	LCA-D4
Lithocholic Acid	LCA	Content	LCA-D4
Murocholic Acid	MCA	Liver	DCA-D4
Taurochenodeoxycholic Acid	T-CDCA	Liver	GCDCA-D4
Taurocholic Acid	T-CA	Serum, Liver, Content	GCA-D4
Taurodehydrocholic Acid	T-DHCA		GCA-D4
Taurodeoxycholic Acid	T-DCA	Serum, Liver, Content	GCDCA-D4
Taurohyocholic Acid	T-HCA	Liver, Content	GCA-D4
Taurohyodeoxycholic Acid	T-HDCA	Serum, Liver, Content	GCDCA-D4
Taurolithocholic Acid	T-LCA	Liver, Content	LCA-D4
Tauro-ursocholanic Acid			GCA-D4
Tauroursodeoxycholic Acid	T-UDCA	Serum, Liver, Content	GCDCA-D4
Tauro-α+Tauro-β Muricholic Acid	T-α/βMCA	Serum, Liver, Content	GCA-D4
Tauro-ω Muricholic Acid	T-ωMCA	Liver, Content	GCA-D4
Ursocholanic Acid			LCA-D4
Ursodeoxycholic Acid	UDCA	Content	DCA-D4
α-Muricholic Acid	αMCA	Liver, Content	CA-D4
β-Muricholic Acid	βMCA	Serum, Liver, Content	CA-D4
ω-Muricholic Acid	ωMCA	Liver, Content	CA-D4

Supplemental Table 3 – Optimized LC-MS/MS parameters for analysis of surrogate peptides of mouse enzymes and transporter proteins that are involved in BA homeostasis.
(DP- declustering potential, CE- Collision energy and RT-retention time)

Protein	Peptide sequence	Light/Heavy	Parent ion (m/z)	Daughter ion (m/z)	DP (V)	CE (eV)	RT (min)
Cyp8b1	FVYSLLGPR	Light	526.3	805.457	59.5	20.8	15.71
			526.3	642.393	59.5	20.8	15.71
			526.3	442.277	59.5	20.8	15.71
		Heavy	531.305	815.465	59.5	20.8	15.71
			531.305	652.402	59.5	20.8	15.71
			531.305	452.286	59.5	20.8	15.71
			531.305	723.408	59.5	20.8	15.71
Cyp27a1	AQLQETGPDGVR	Light	635.823	958.459	67.5	24.7	9.4
			635.823	830.4	67.5	24.7	9.4
			635.823	600.31	67.5	24.7	9.4
		Heavy	640.827	968.467	67.5	24.7	9.4
			640.827	840.409	67.5	24.7	9.4
			640.827	610.318	67.5	24.7	9.4
	EADNPGILHPFGSVPFGYGVR	Light	743.708	900.483	75.3	31	17.2
			743.708	851.957	75.3	31	17.2
			743.708	766.904	75.3	31	17.2
		Heavy	747.044	905.487	75.3	31	17.2
			747.044	856.961	75.3	31	17.2
			747.044	771.908	75.3	31	17.2
Cyp7b1	MFLGIQHPDSAVSFR	Light	568.956	787.41	62.6	21.5	14.9
			568.956	713.875	62.6	21.5	14.9
			568.956	657.333	62.6	21.5	14.9
		Heavy	572.292	792.414	62.6	21.5	14.9
			572.292	718.88	62.6	21.5	14.9
			572.292	662.338	62.6	21.5	14.9
Akr1c14	HFDSAYLYQIEEEVGQAIR	Light	756.703	834.378	76.3	31.8	19.7
			756.703	997.441	76.3	31.8	19.7
		Heavy	760.039	834.378	76.3	31.8	19.7
			760.039	997.441	76.3	31.8	19.7
Hsd3b7	TIQWVQAMEGSAR	Light	738.867	948.457	75	28.5	15.4
			738.867	849.388	75	28.5	15.4
		Heavy	743.871	958.465	75	28.5	15.4
			743.871	859.397	75	28.5	15.4
Slc27a5	SWLPAYATPHFIR	Light	520.277	643.356	59	18.9	16.4
			520.277	586.814	59	18.9	16.4
		Heavy	523.613	648.36	59	18.9	16.4
			523.613	591.818	59	18.9	16.4
	QGFCIPVEPGKPGLLLTK	Light	652.033	811.471	68.7	26.1	15.7
			652.033	674.914	68.7	26.1	15.7
			652.033	512.332	68.7	26.1	15.7
		Heavy	654.04	814.481	68.7	26.1	15.7
			654.04	677.924	68.7	26.1	15.7
			654.04	515.342	68.7	26.1	15.7

Supplemental Table 4. 16S rRNA sequencing reads for bacterial samples from LIC of CV mice treated with corn oil, BDE-47 (100 μmol/kg), or BDE-99 (100 μmol/kg), n=3 per group.

Samples	Total Number of Sequence Reads
Corn Oil_1	117299
Corn Oil_2	104804
Corn Oil_3	124805
BDE-47_1	104760
BDE-47_2	100873
BDE-47_3	99396
BDE-99_1	89378
BDE-99_2	100445
BDE-99_3	96781
Total	938541
Average	104282
SE	3574

Supplemental Table 5. The average value of total, conjugated or unconjugated bile acids in serum, liver, SIC and LIC of CV and GF mice treated with corn oil, BDE-47 or BDE-99.

Bile Acids		CV			GF		
		Corn Oil	BDE-47	BDE-99	Corn Oil	BDE-47	BDE-99
Serum (nmol/mL)	Total	4.58	2.40	3.87	30.29	36.62	15.35
	Conjugated	4.56	2.39	3.83	30.29	36.61	15.34
	Unconjugated	0.02	0.01	0.04	0.00	0.00	0.01
Liver (nmol/g)	Total	432.13	304.08	784.50	2016.42	1628.95	780.46
	Conjugated	406.71	281.07	689.69	1840.53	1456.18	692.02
	Unconjugated	25.42	23.01	94.81	175.88	172.77	88.44
SIC (nmol/g)	Total	2134.30	1251.18	1589.41	6833.88	7321.12	7792.59
	Conjugated	1431.80	527.04	801.83	6832.03	7319.06	7788.74
	Unconjugated	702.50	724.14	787.58	1.85	2.06	3.85
LIC (nmol/g)	Total	261.70	975.94	414.36	882.74	660.49	876.67
	Conjugated	107.74	737.90	255.10	881.41	659.01	874.70
	Unconjugated	153.96	238.05	159.27	1.33	1.48	1.97

Supplemental Figure 1. Bacterial composition at Phylum level

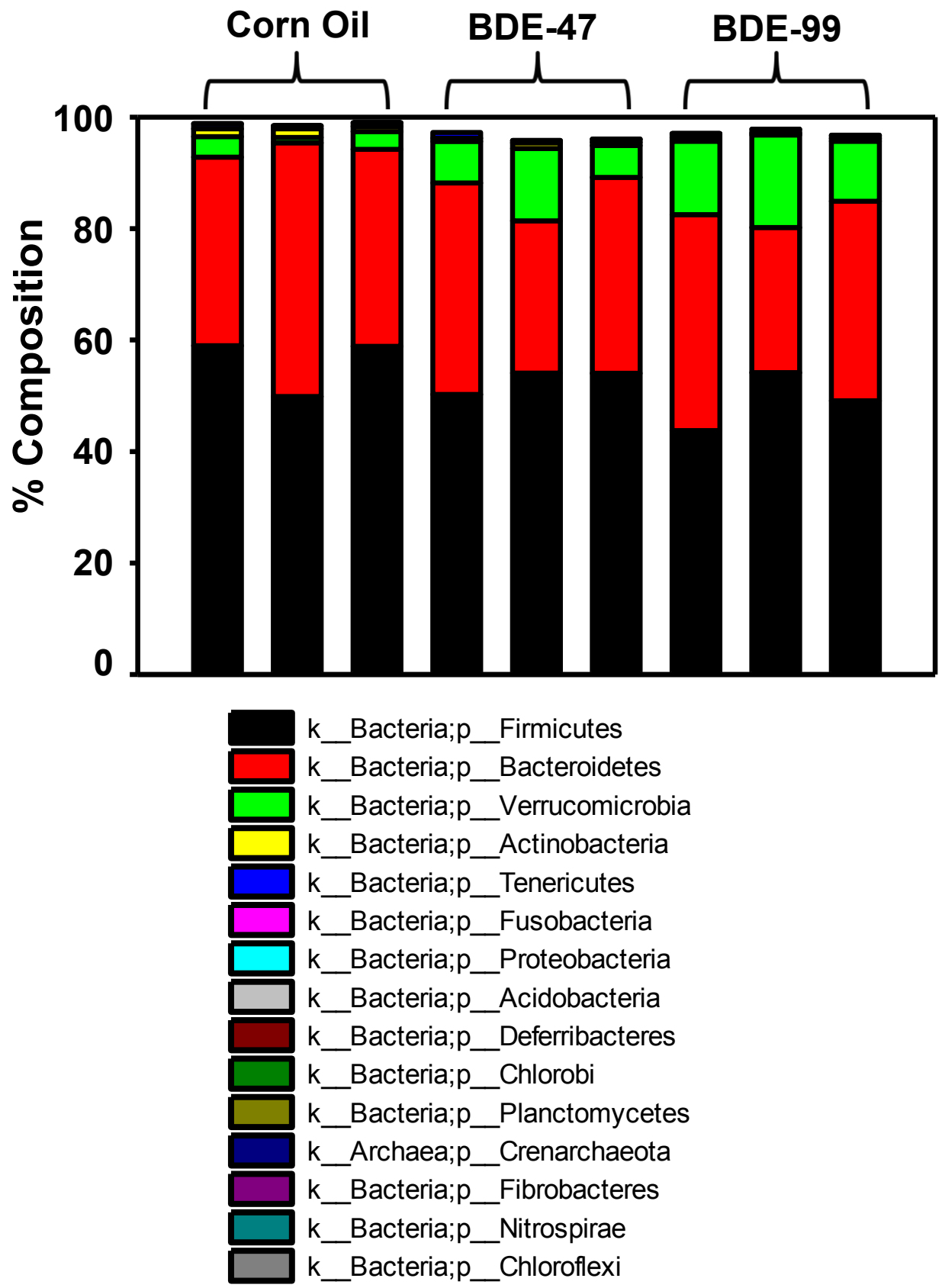

Supplemental Figure 2. Serum and liver conjugated BAs in CV mice

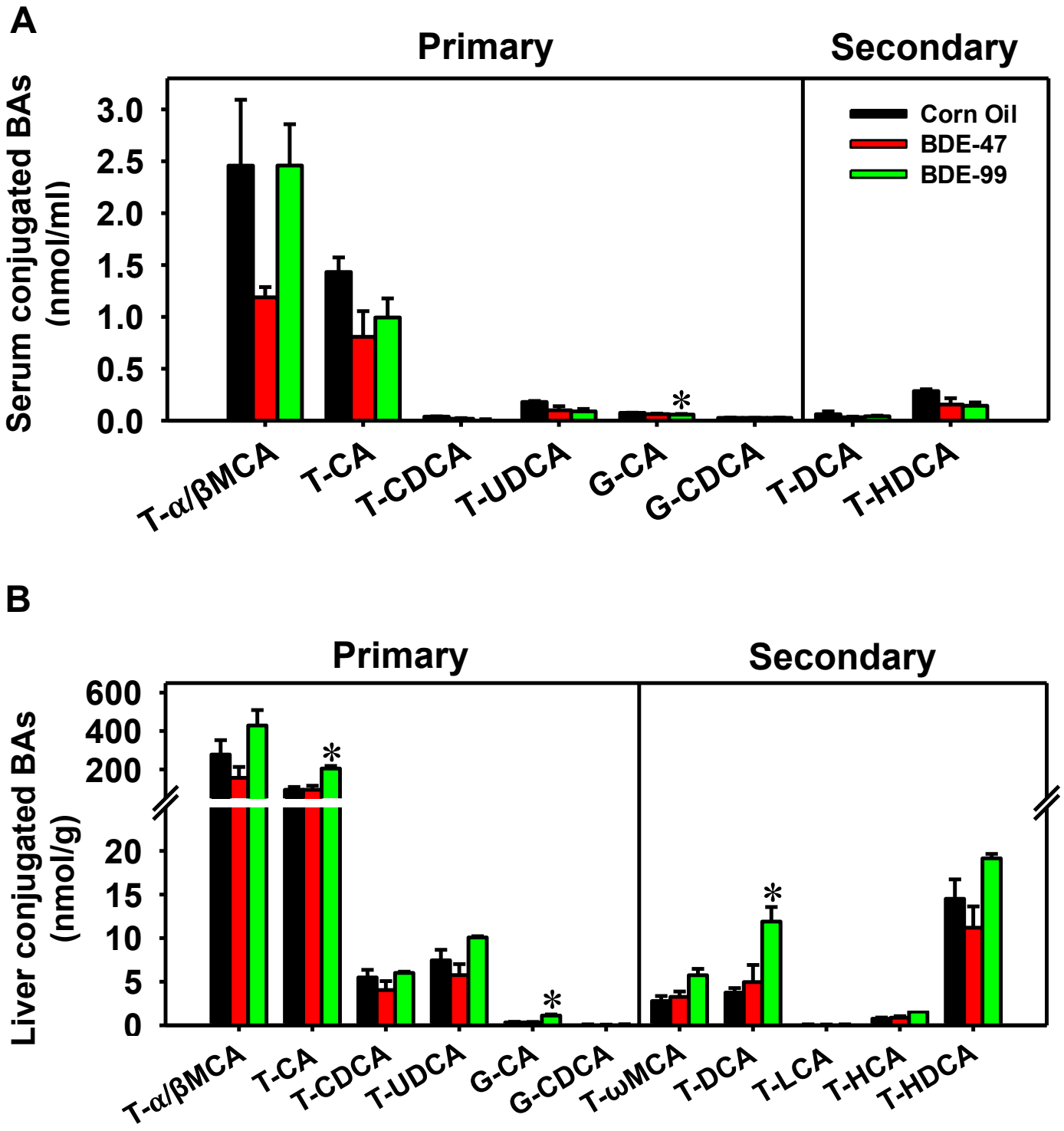

Supplemental Figure 3. SIC and LIC conjugated BAs in CV mice

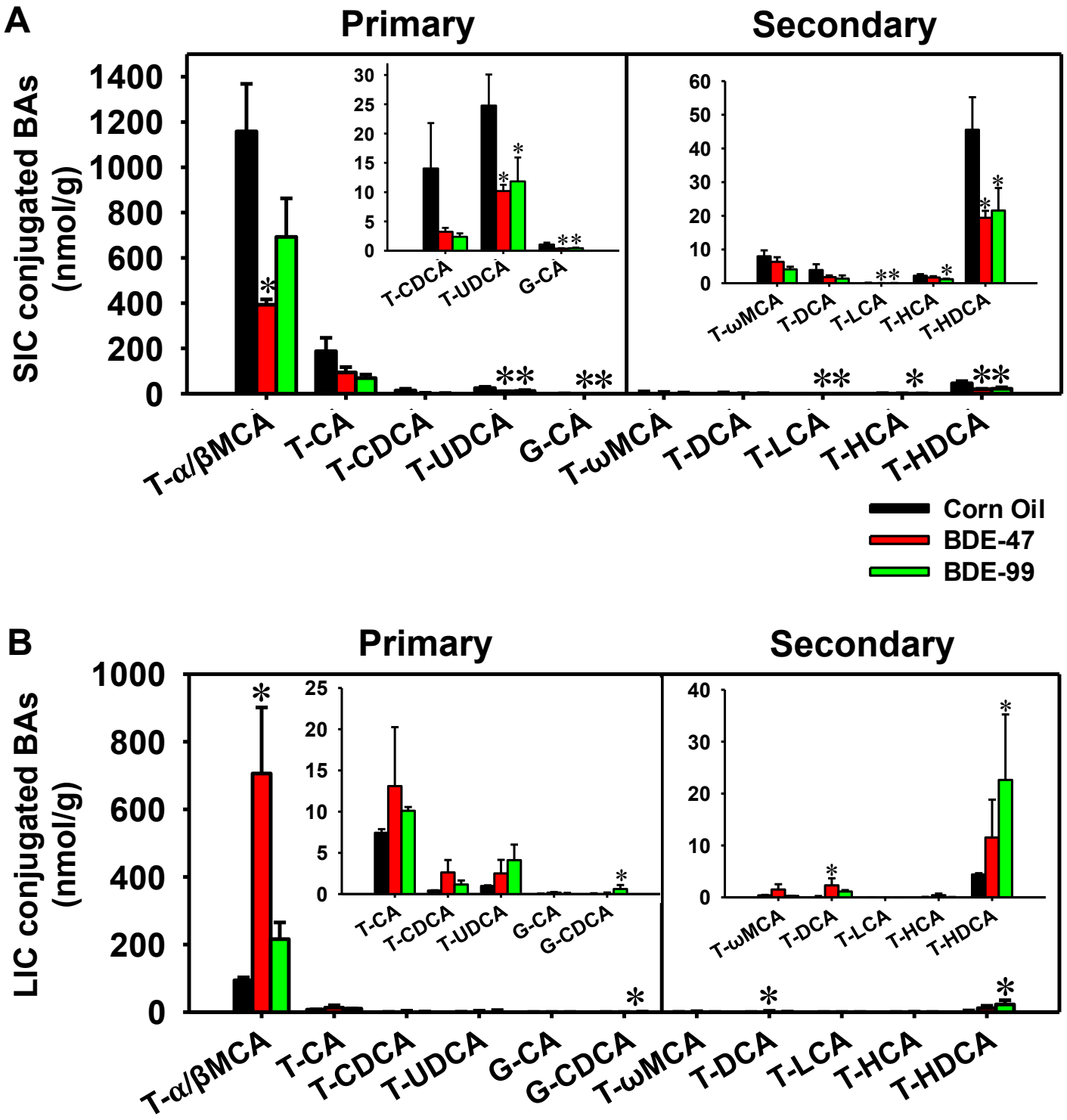

Supplemental Figure 4

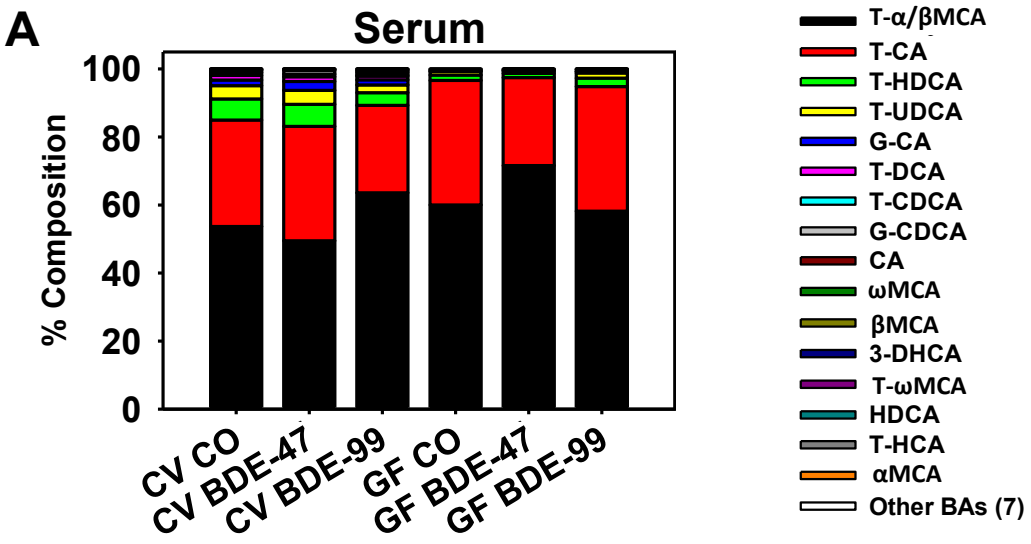

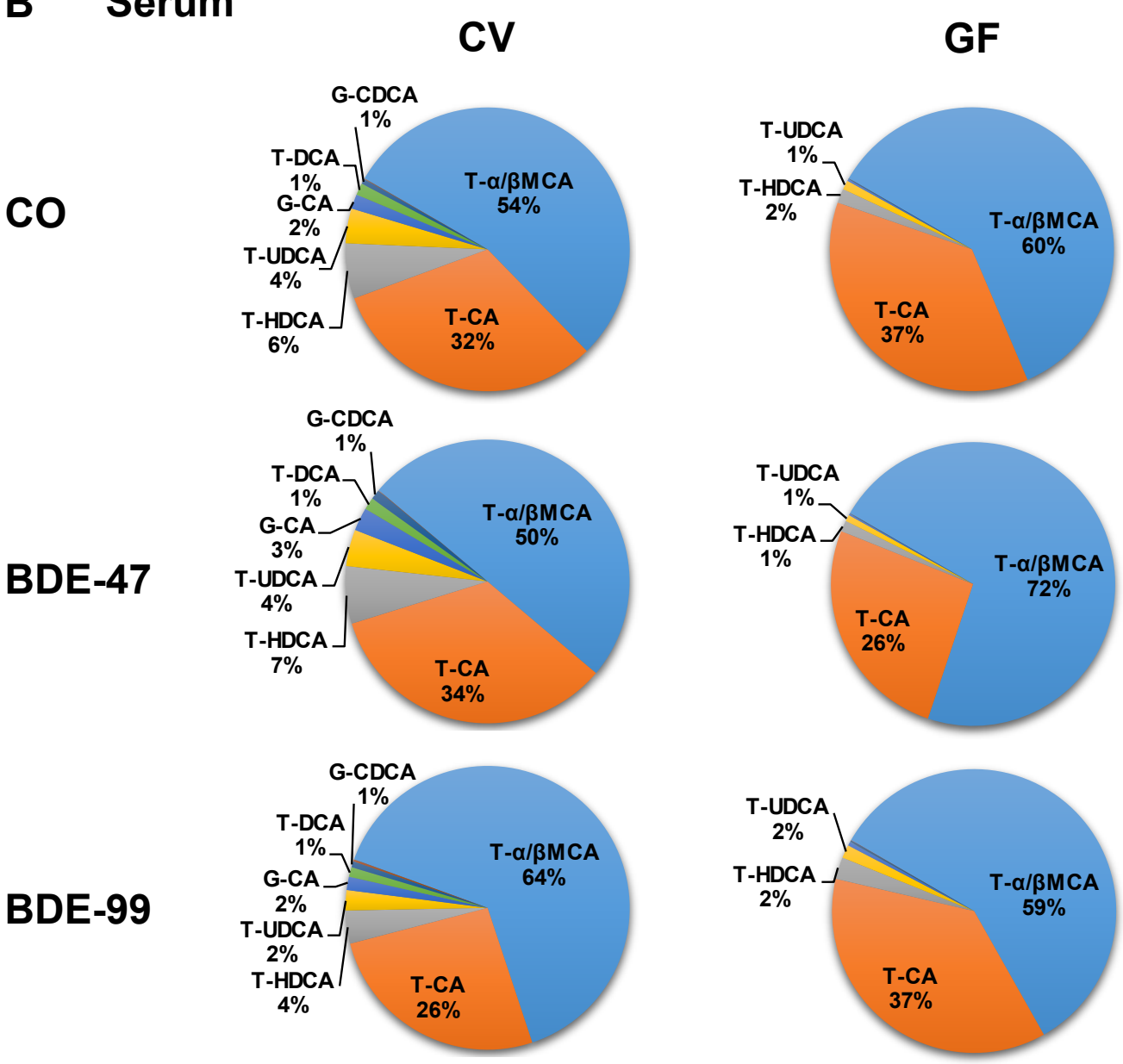

Supplemental Figure 5

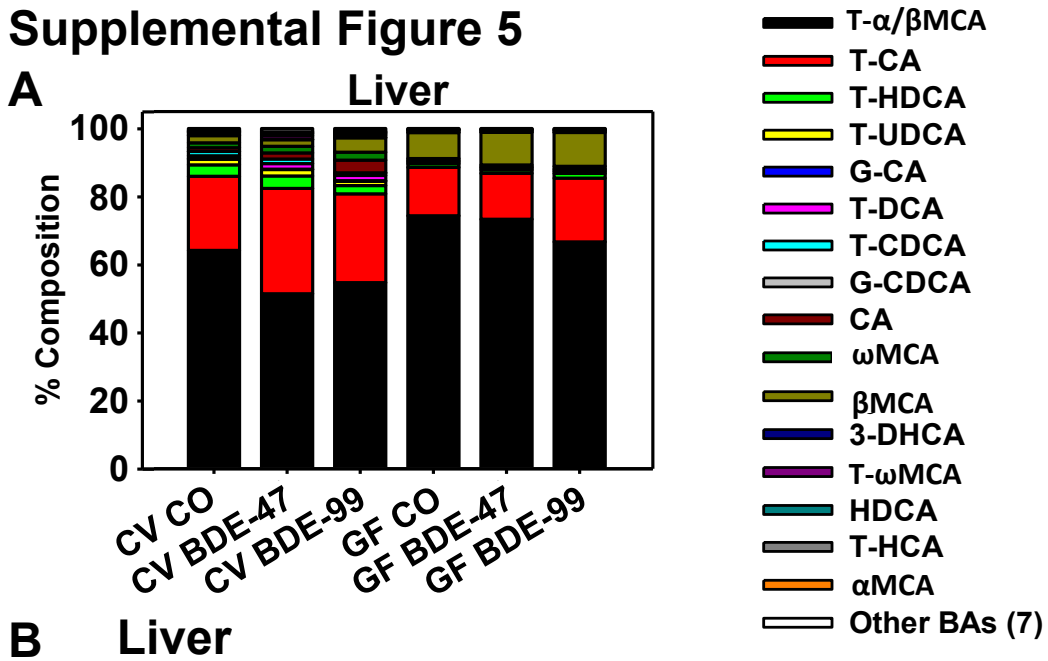

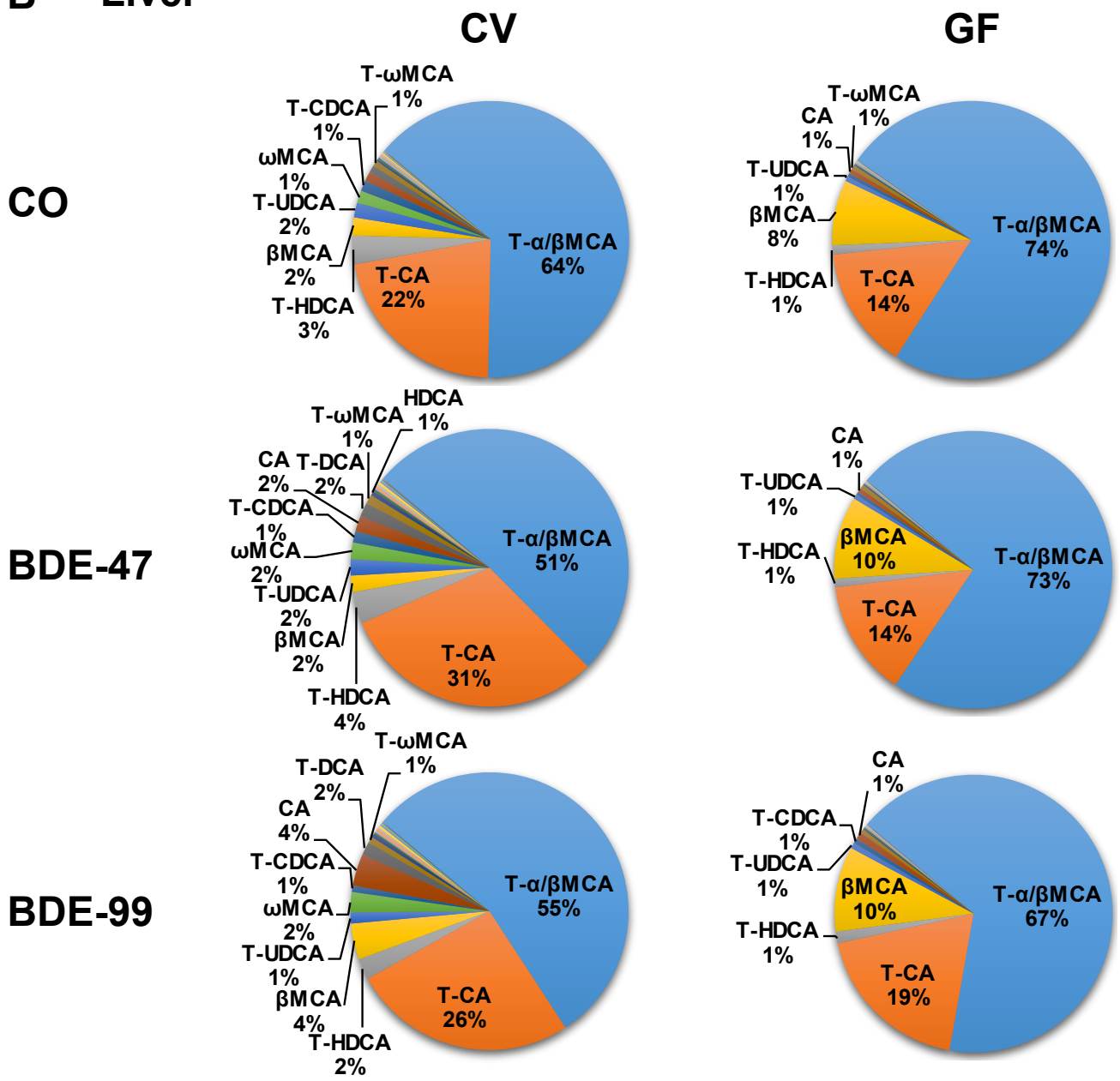

Supplemental Figure 6

A

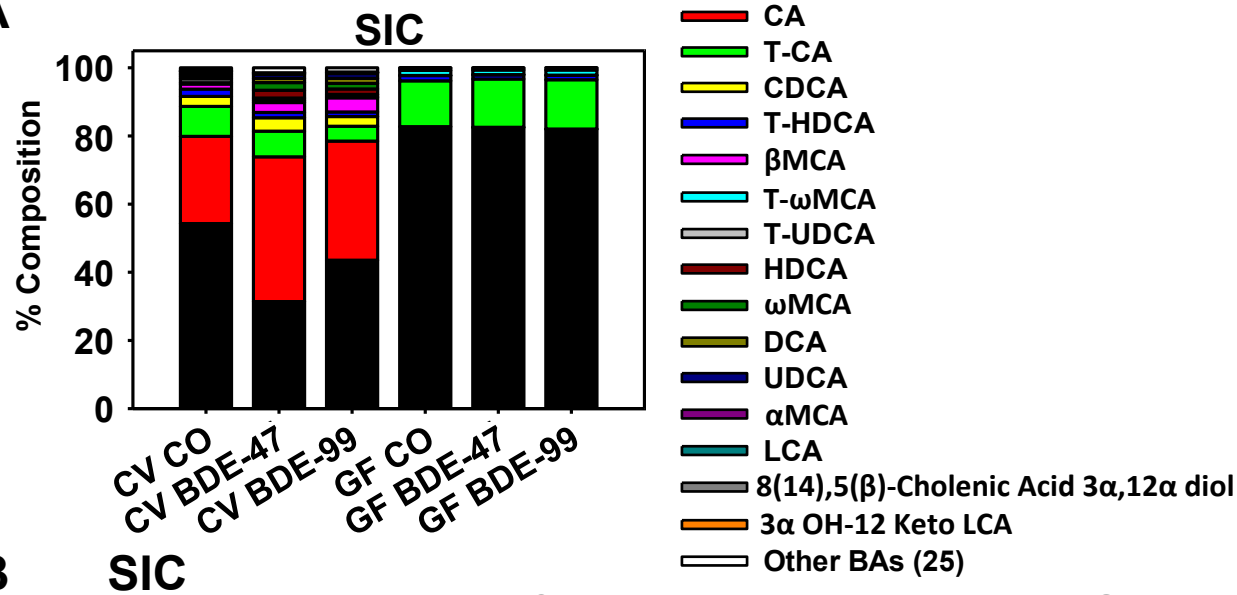

B SIC

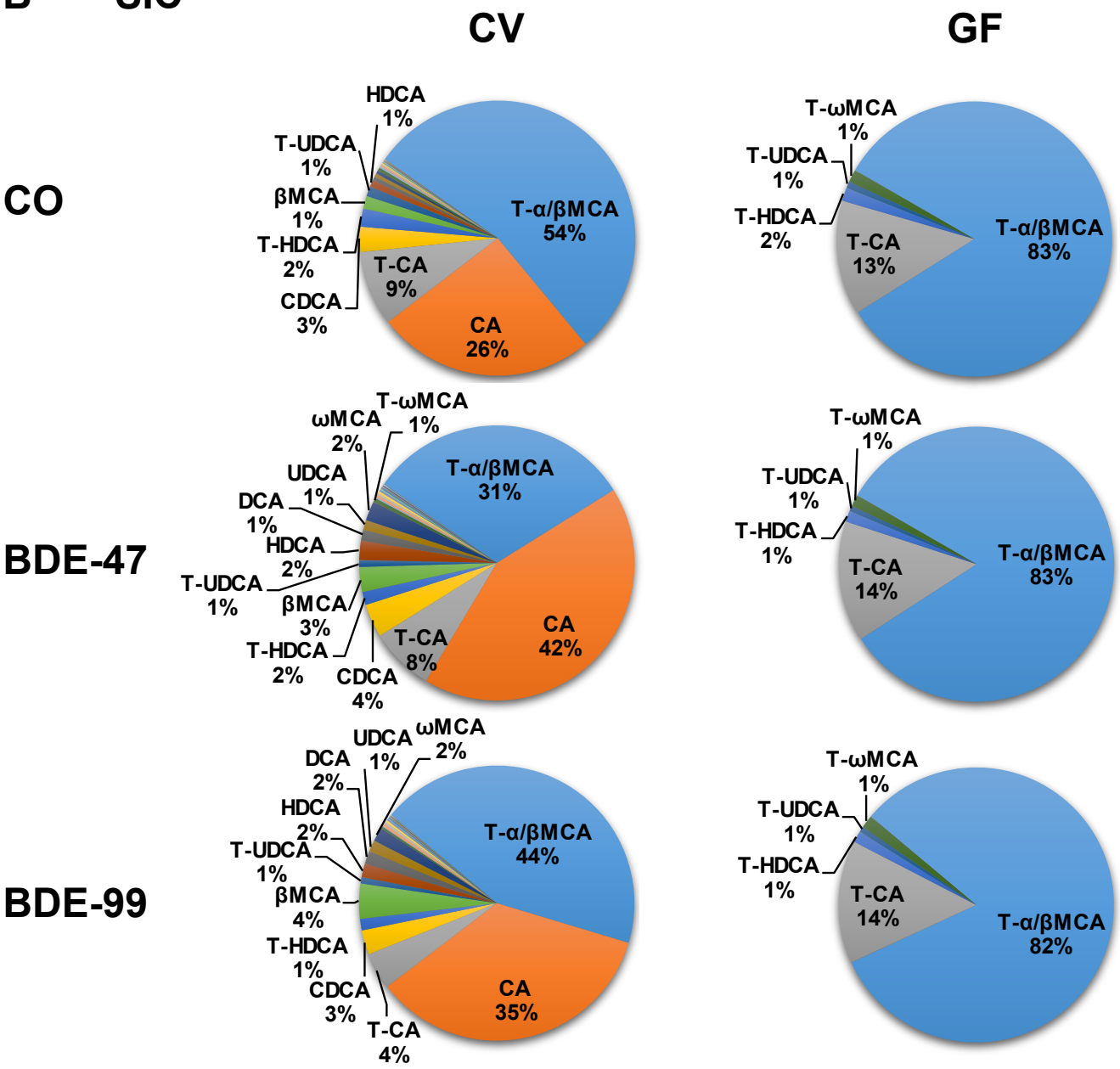

Supplemental Figure 7

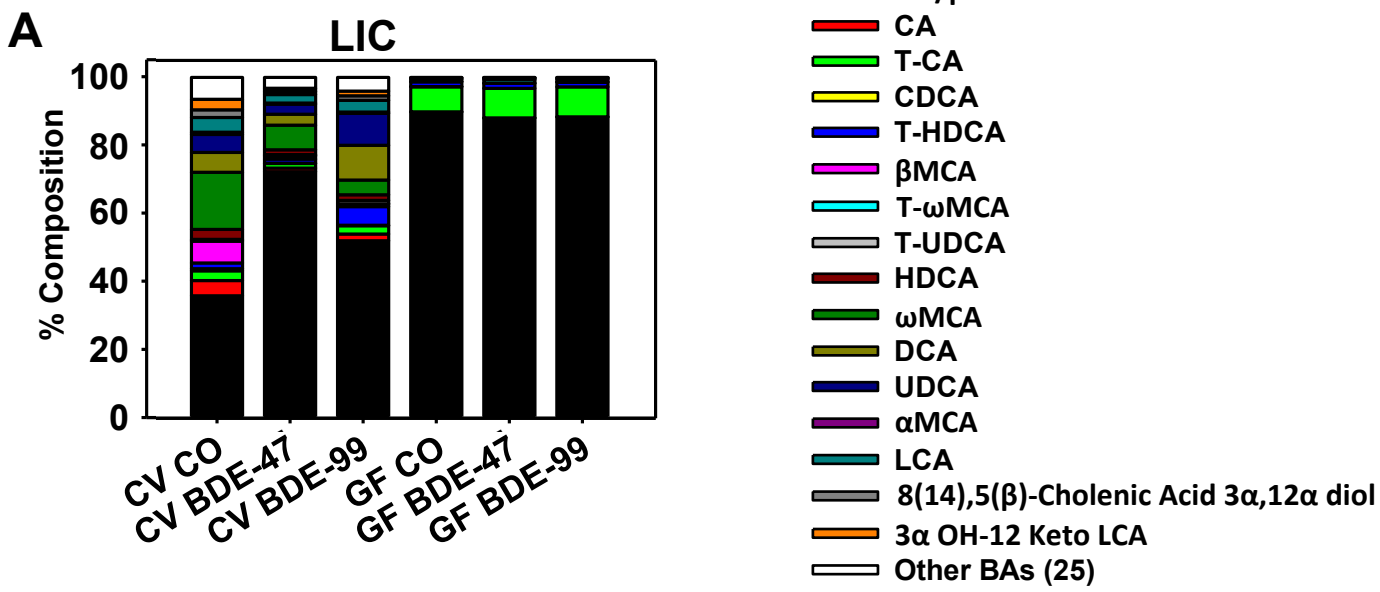

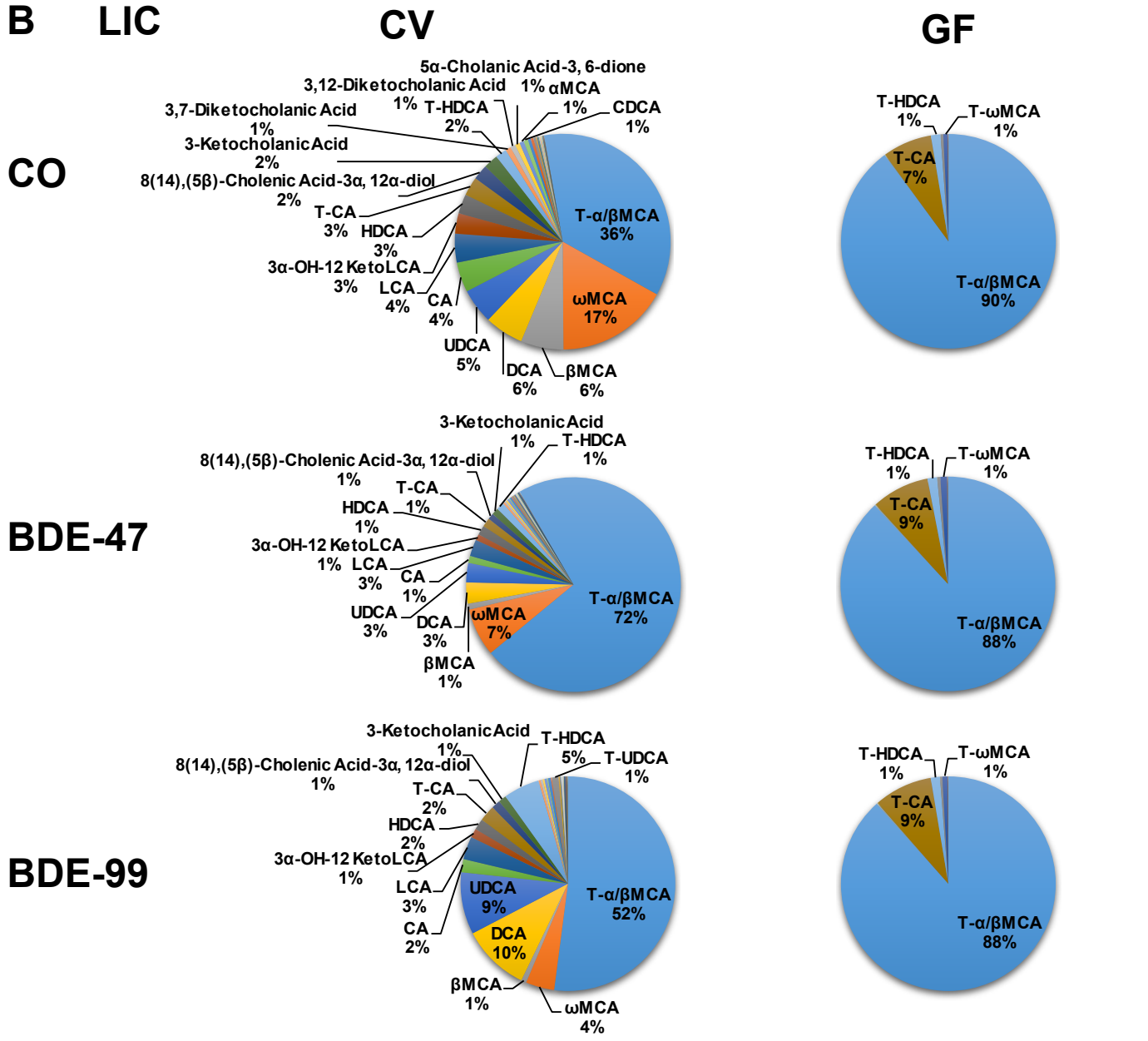

Supplemental Figure 8

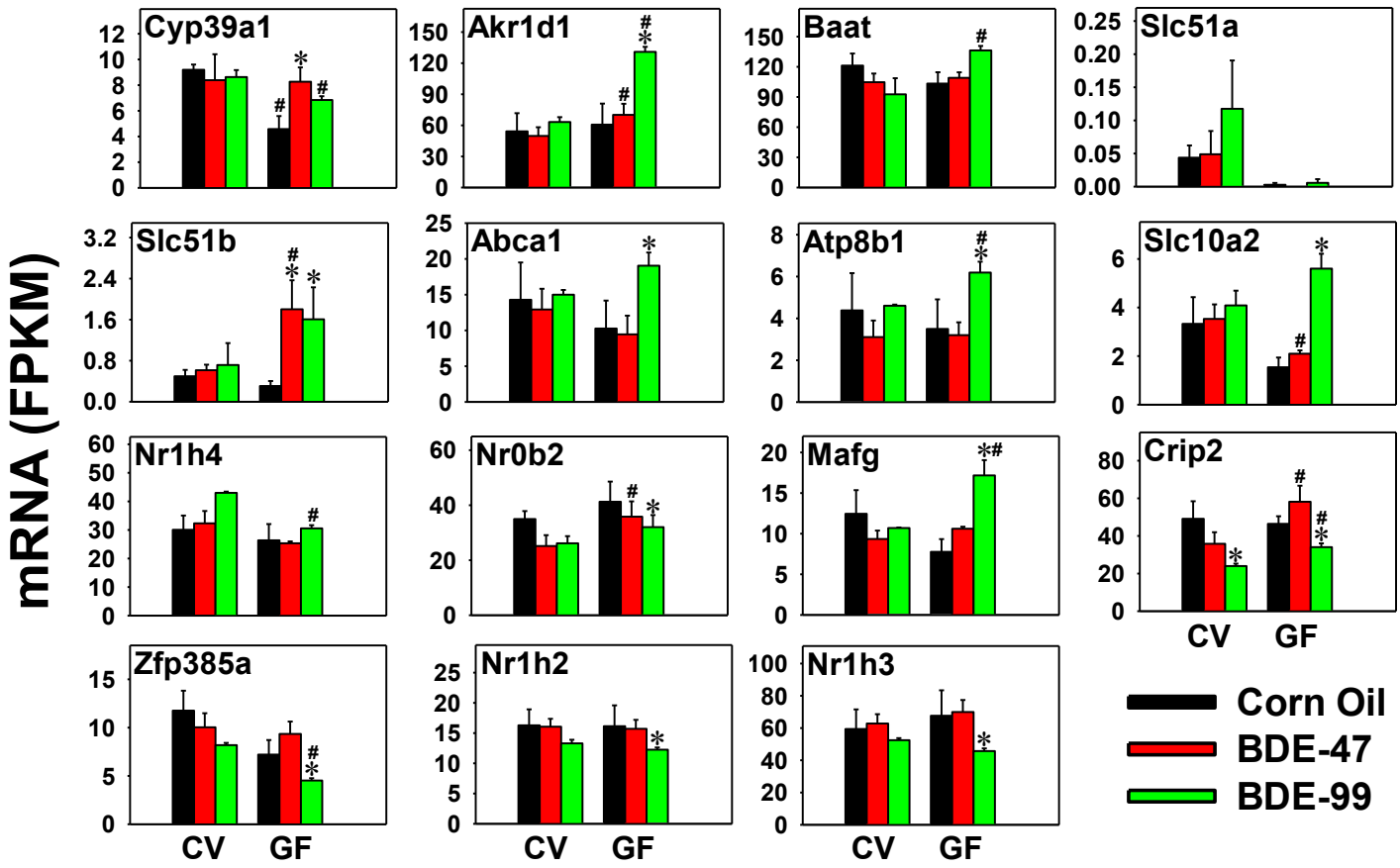

Supplemental Figure 1. Bacterial composition at Phylum level

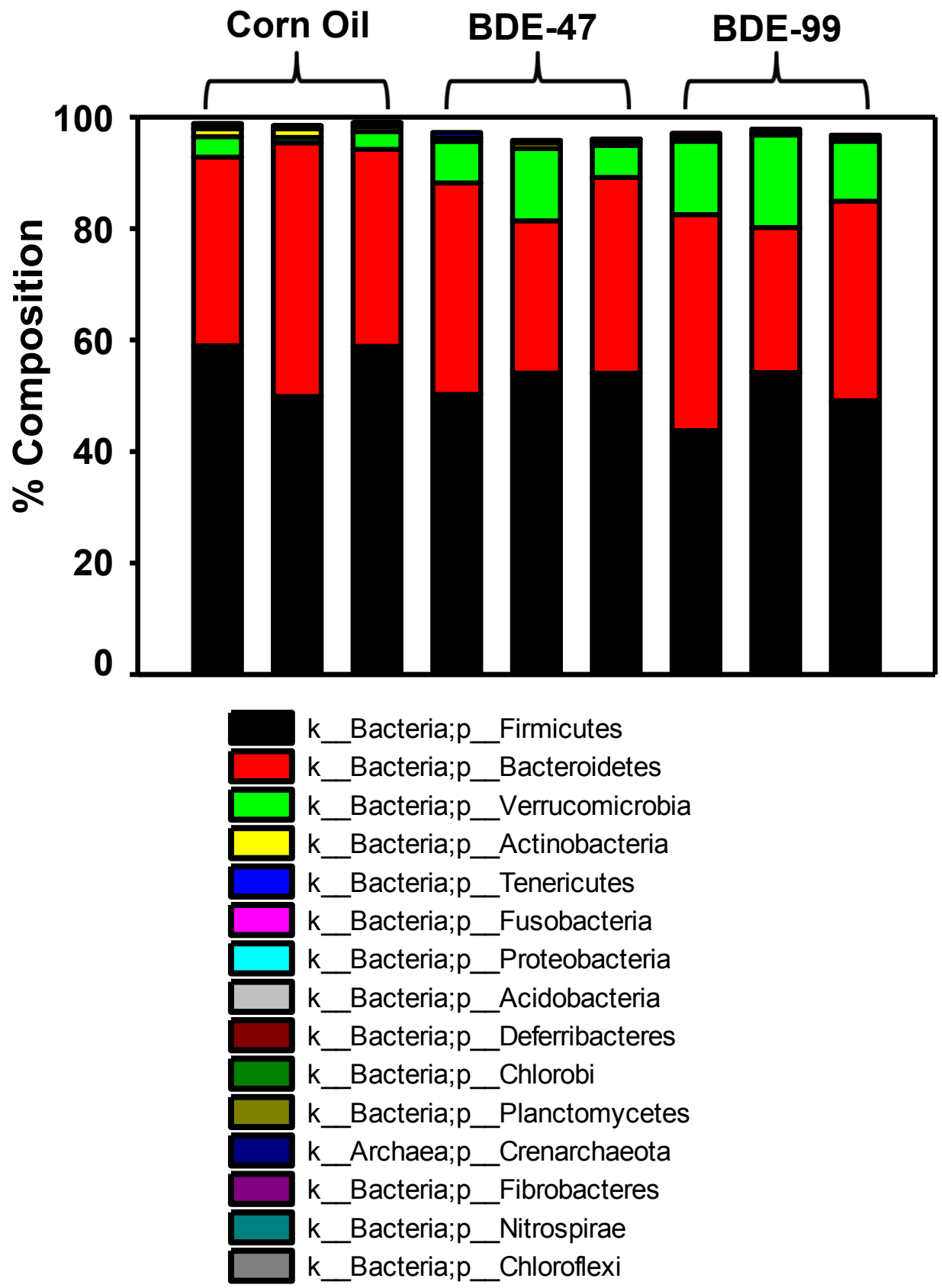

Supplemental Figure 2. Serum and liver conjugated BAs in CV mice

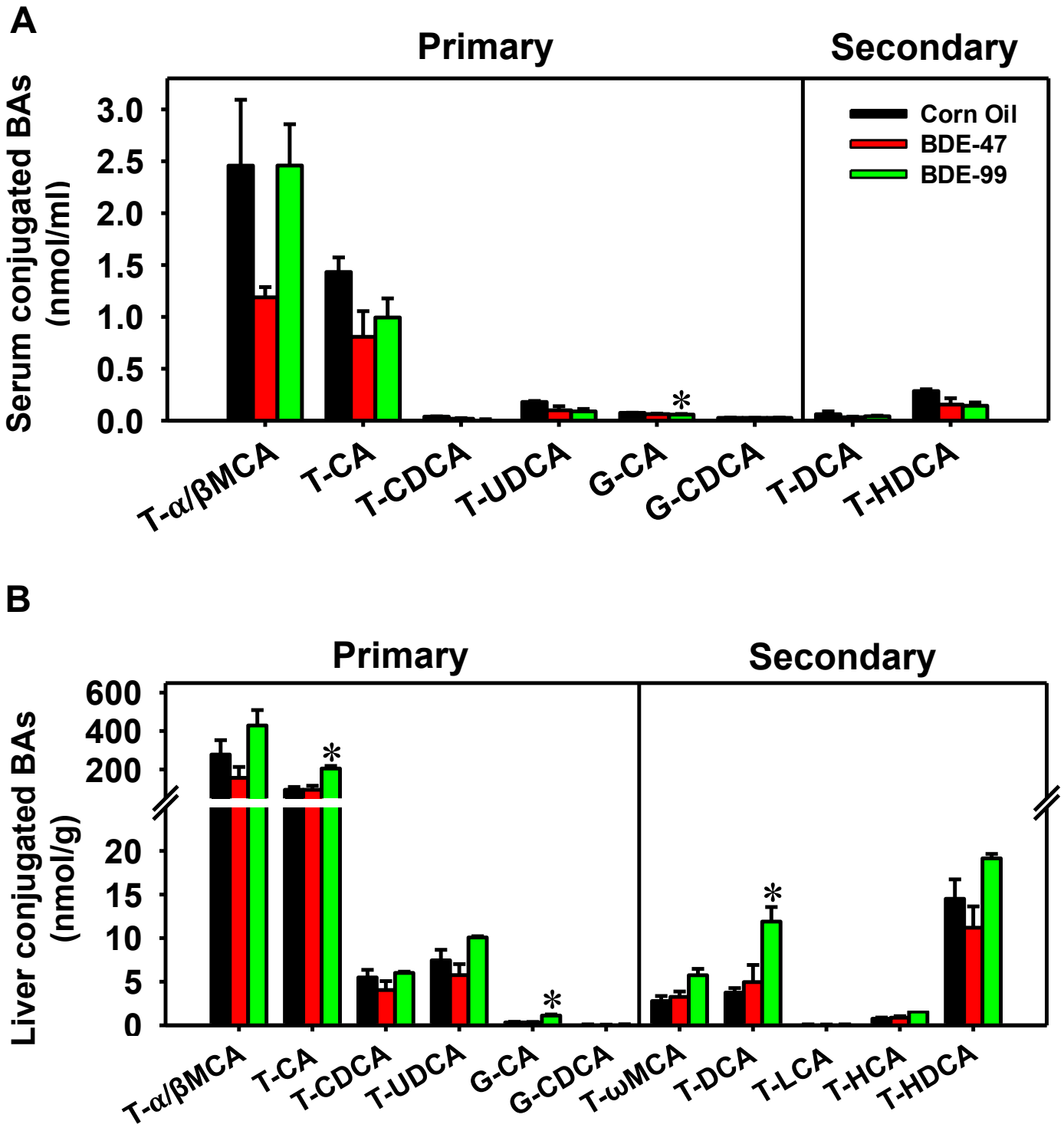

Supplemental Figure 3. SIC and LIC conjugated BAs in CV mice

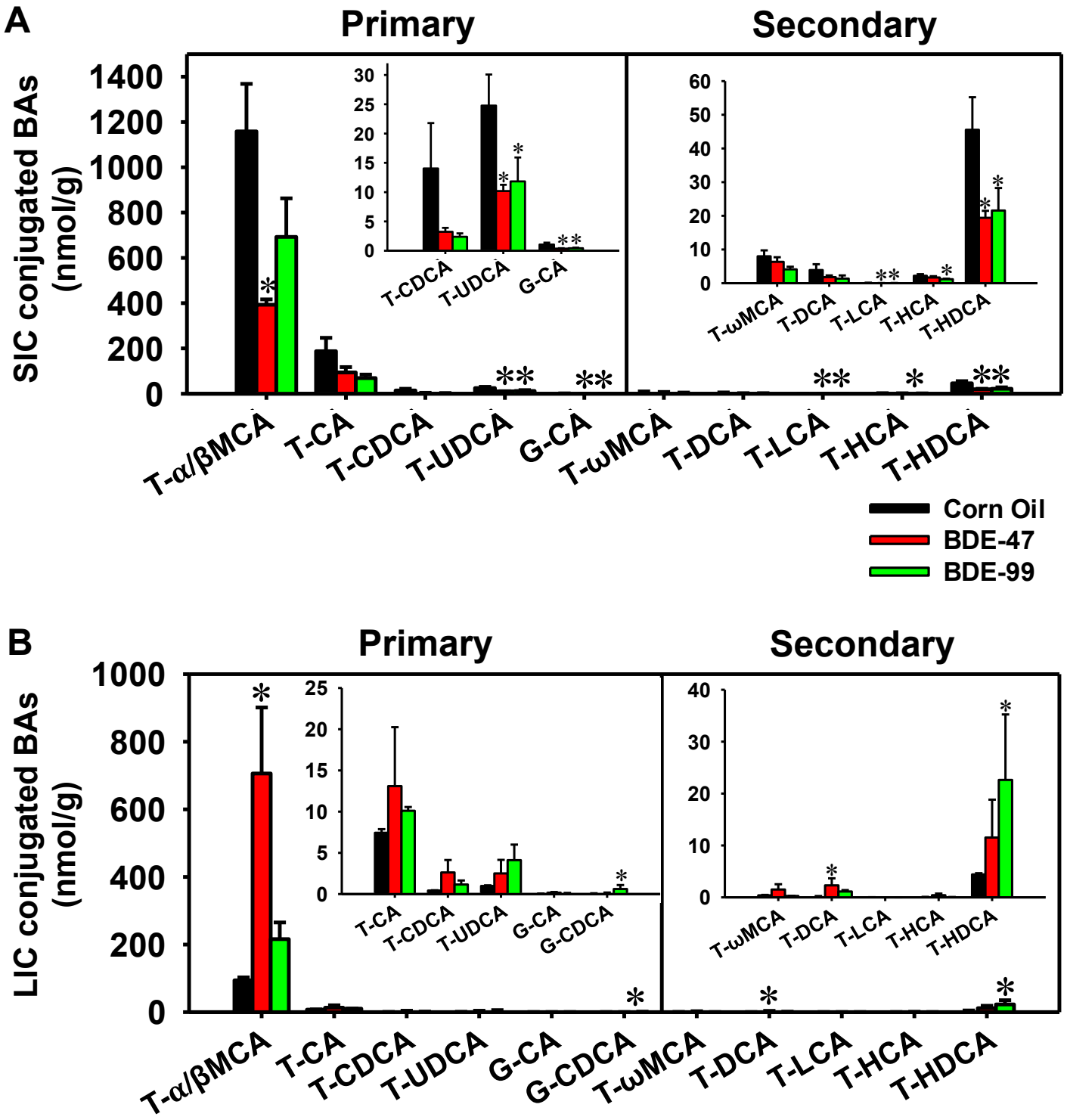

Supplemental Figure 4

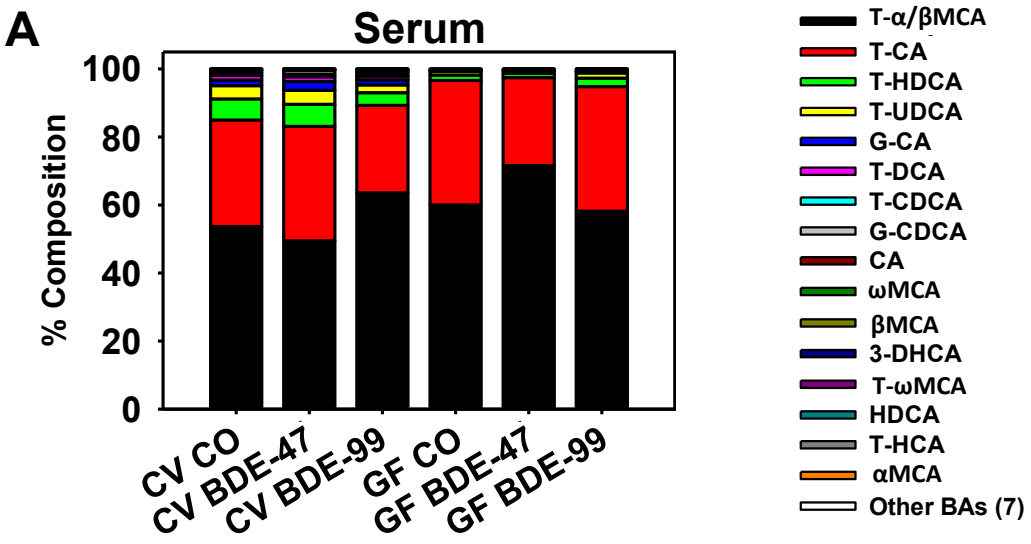

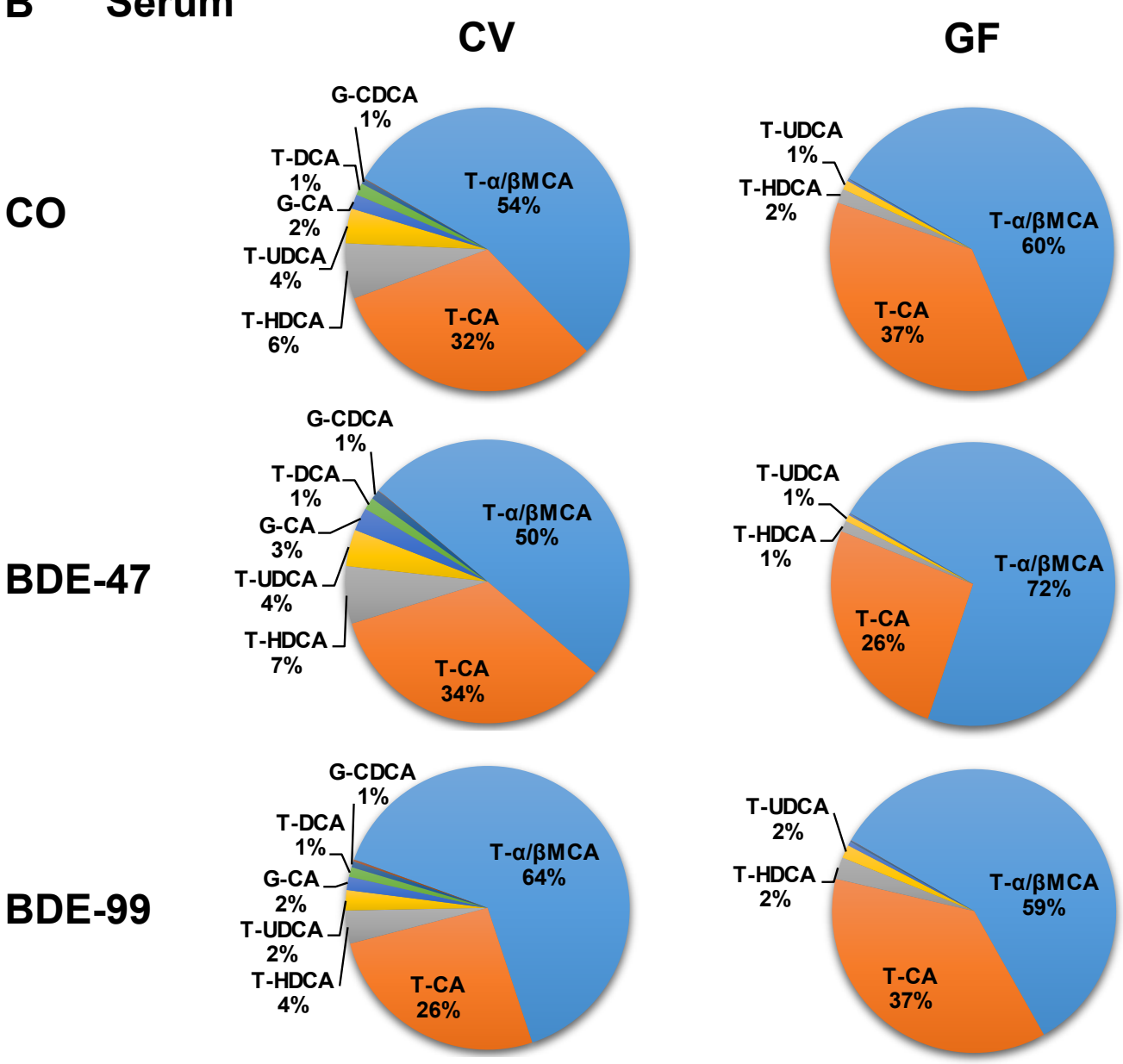

Supplemental Figure 5

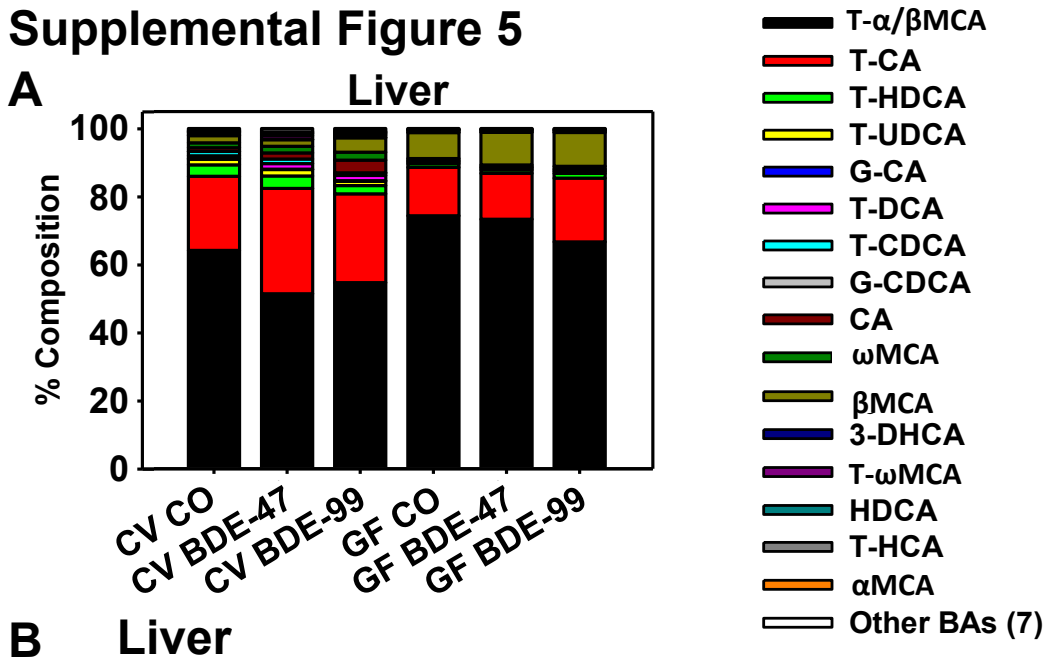

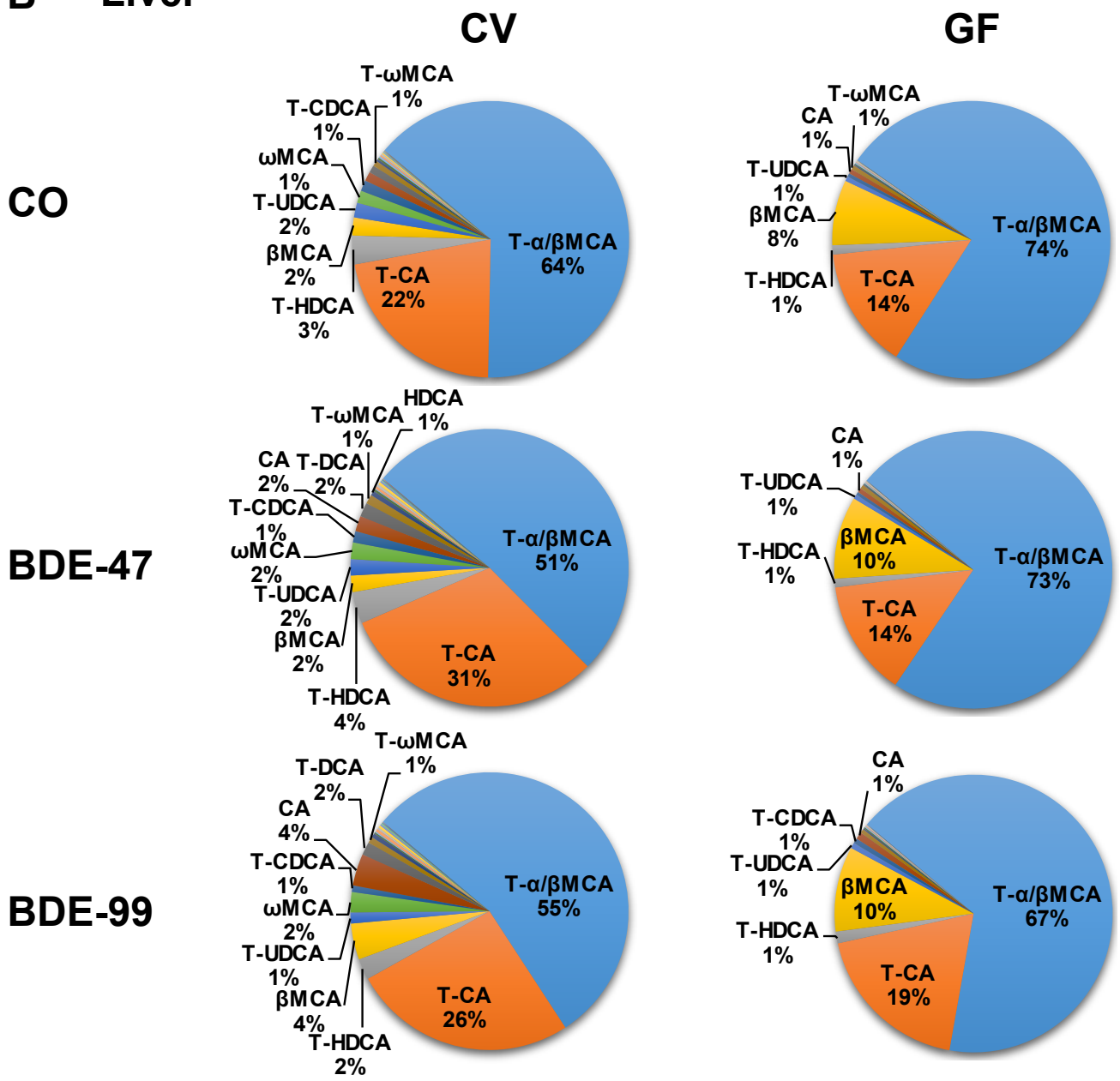

Supplemental Figure 6

A

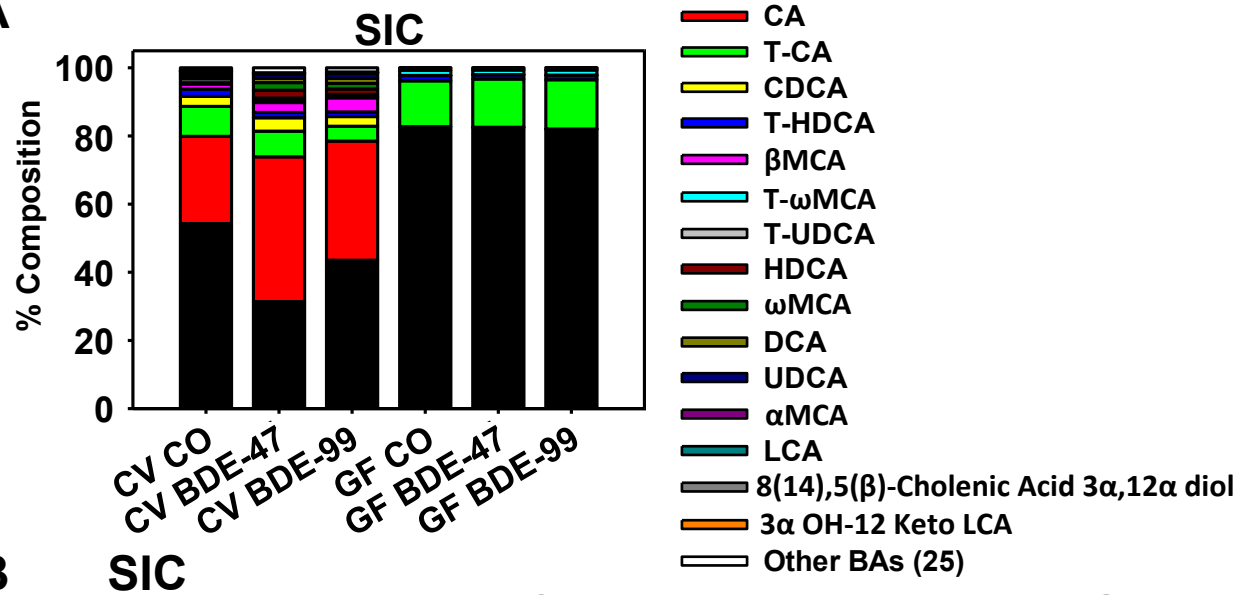

B SIC

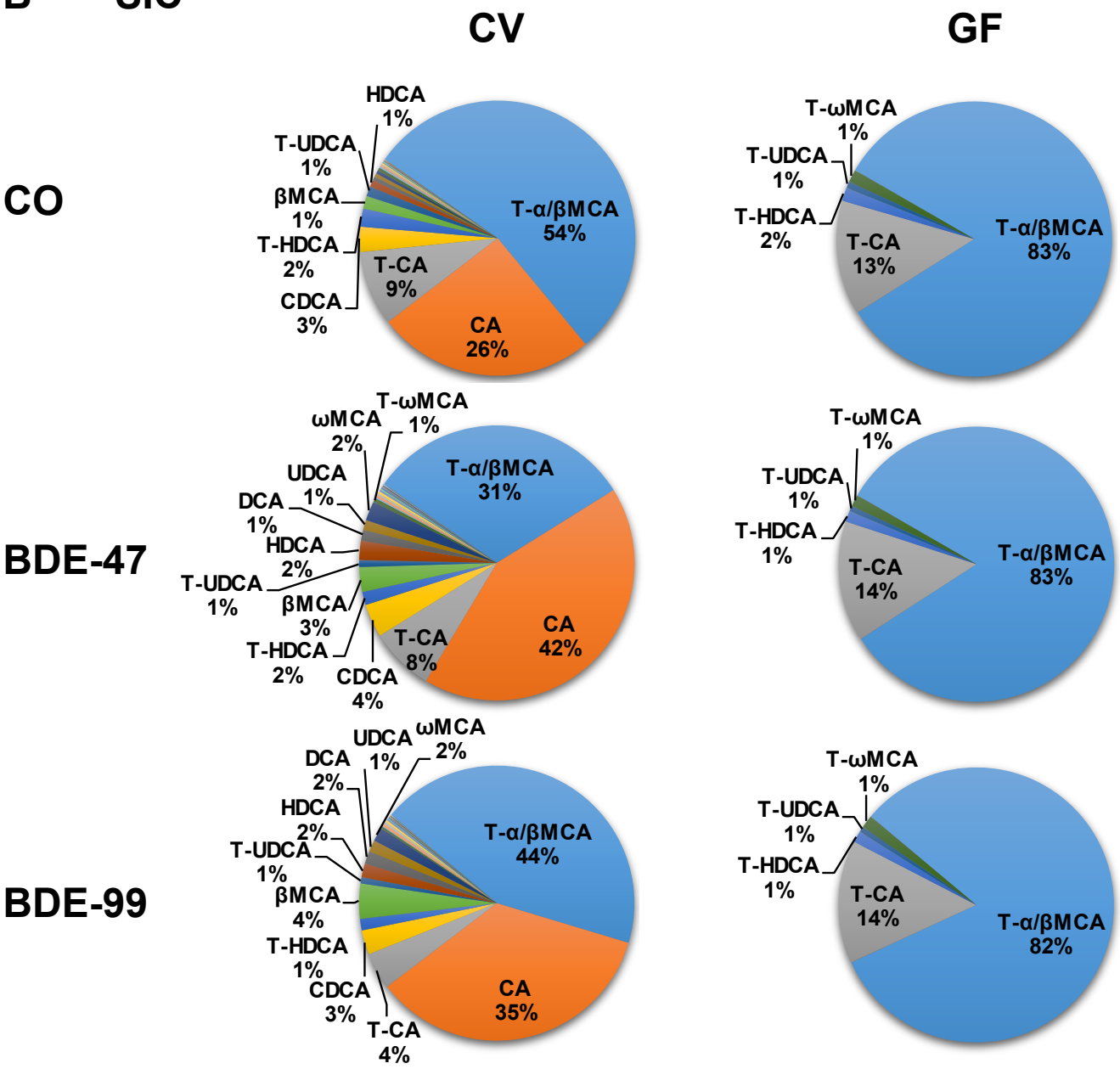

Supplemental Figure 7

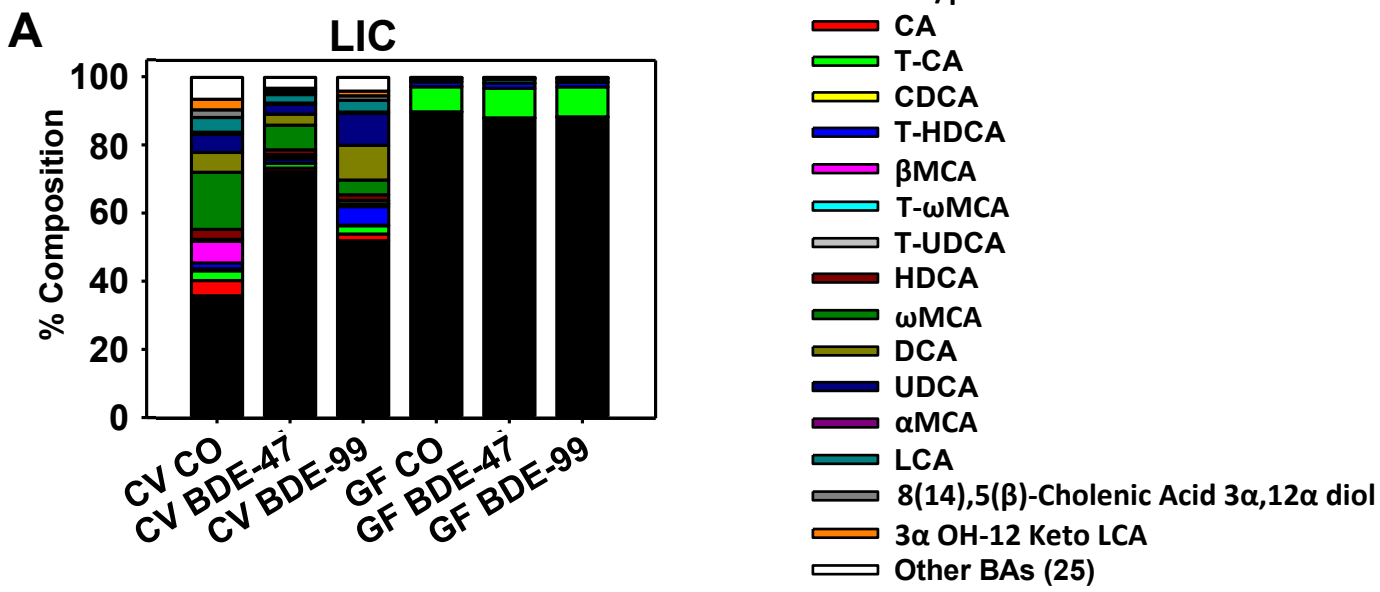

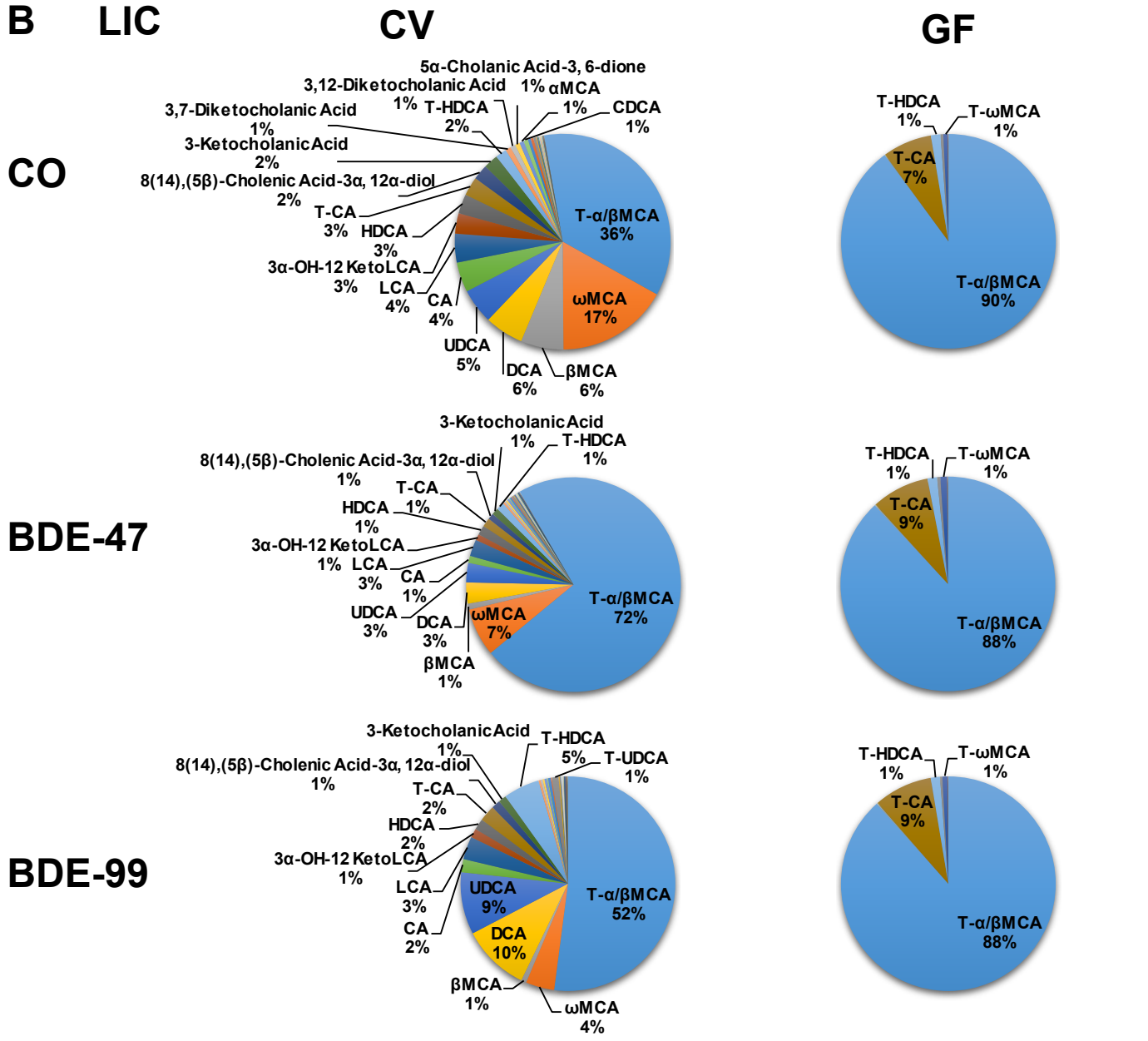

Supplemental Figure 8